

AD\_\_\_\_\_

Award Number: DAMD17-00-1-0443

TITLE: A Multileaf Collimator for Modulated Electron Radiation  
Therapy for Breast Cancer

PRINCIPAL INVESTIGATOR: Steve B. Jiang, Ph.D.

CONTRACTING ORGANIZATION: Stanford University  
Stanford, California 94305-5401

REPORT DATE: April 2001

TYPE OF REPORT: Annual

PREPARED FOR: U.S. Army Medical Research and Materiel Command  
Fort Detrick, Maryland 21702-5012

DISTRIBUTION STATEMENT: Approved for public release;  
Distribution unlimited

The views, opinions and/or findings contained in this report are those of the author(s) and should not be construed as an official Department of the Army position, policy or decision unless so designated by other documentation.

20010925 170

**REPORT DOCUMENTATION PAGE**Form Approved  
OMB No. 074-0188

Public reporting burden for this collection of information is estimated to average 1 hour per response, including the time for reviewing instructions, searching existing data sources, gathering and maintaining the data needed, and completing and reviewing this collection of information. Send comments regarding this burden estimate or any other aspect of this collection of information, including suggestions for reducing this burden to Washington Headquarters Services, Directorate for Information Operations and Reports, 1215 Jefferson Davis Highway, Suite 1204, Arlington, VA 22202-4302, and to the Office of Management and Budget, Paperwork Reduction Project (0704-0188), Washington, DC 20503

<b>1. AGENCY USE ONLY (Leave blank)</b>		<b>2. REPORT DATE</b> April 2001	<b>3. REPORT TYPE AND DATES COVERED</b> Annual (01 Apr 00 - 31 Mar 01)	
<b>4. TITLE AND SUBTITLE</b> A Multileaf Collimator for Modulated Electron Radiation Therapy for Breast Cancer			<b>5. FUNDING NUMBERS</b> DAMD17-00-1-0443	
<b>6. AUTHOR(S)</b> Chang Ming Ma, Ph.D. (on behalf of Steve B. Jiang, Ph.D.)				
<b>7. PERFORMING ORGANIZATION NAME(S) AND ADDRESS(ES)</b> Stanford University Stanford, California 94305  e-mail: cma@Reyes.stanford.edu			<b>8. PERFORMING ORGANIZATION REPORT NUMBER</b>	
<b>9. SPONSORING / MONITORING AGENCY NAME(S) AND ADDRESS(ES)</b> U.S. Army Medical Research and Materiel Command Fort Detrick, Maryland 21702-5012			<b>10. SPONSORING / MONITORING AGENCY REPORT NUMBER</b>	
<b>11. SUPPLEMENTARY NOTES</b>				
<b>12a. DISTRIBUTION / AVAILABILITY STATEMENT</b> Approved for public release distribution unlimited				<b>12b. DISTRIBUTION CODE</b>
<b>13. ABSTRACT (Maximum 200 Words)</b>  In this project, we investigate a prototype electron multileaf collimator (eMLC) for energy- and intensity-modulated electron radiotherapy (MERT) for breast cancer to deliver dose distributions that closely match the target volume and minimize the dose to critical normal structures. We have worked on the following tasks: (1) to design an eMLC using Monte Carlo simulations, (2) to manufacture an eMLC for MERT beam delivery, (3) to develop software tools for MERT beam delivery with an eMLC, and (4) to perform experimental evaluations of the prototype eMLC. During the first year research, we have established clinical criteria for MERT beam delivery, performed extensive Monte Carlo simulations of the eMLC materials and dimensions, evaluated the eMLC simulation based on the clinical criteria, and finalized the eMLC design based on our results. The results confirmed that an eMLC is superior to a conventional photon MLC and to electron cutouts for MERT beam delivery. It has better beam characteristics in terms of beam penumbra and better beam delivery efficiency. Since the principle investigator left Stanford University in Sept 2000 a replacement has been identified starting April 1 2001. Thus, the specific aim 2 scheduled for months 6 - 12 is postponed.				
<b>14. SUBJECT TERMS</b> Breast Cancer				<b>15. NUMBER OF PAGES</b> 61
				<b>16. PRICE CODE</b>
<b>17. SECURITY CLASSIFICATION OF REPORT</b> Unclassified	<b>18. SECURITY CLASSIFICATION OF THIS PAGE</b> Unclassified	<b>19. SECURITY CLASSIFICATION OF ABSTRACT</b> Unclassified	<b>20. LIMITATION OF ABSTRACT</b> Unlimited	

## Table of Contents

FRONT COVER .....	1
STANDARD FORM (SF) 298.....	2
TABLE OF CONTENTS .....	3
INTRODUCTION .....	4
BODY .....	4
KEY RESEARCH ACCOMPLISHMENTS.....	11
REPORTABLE OUTCOMES .....	12
CONCLUSIONS.....	13
REFERENCES.....	14
APPENDICES.....	16
<i>List of Figures quoted in the body of text:</i> .....	16
<i>List of manuscripts submitted with this report:</i> .....	19

## **Introduction**

This project is aimed at developing a prototype electron multileaf collimator (eMLC) for accurate beam delivery of energy- and intensity-modulated electron radiotherapy (MERT) for breast cancer treatment to deliver optimized conformal radiotherapy dose distributions that closely match the target volume and minimize the dose to critical normal structures. We proposed to use a powerful computer tool, namely Monte Carlo simulation, to design the eMLC. The advantages of using computer simulations for designing the eMLC are the short designing cycles and their cost-effectiveness. Various eMLC configurations will be investigated using the Monte Carlo simulation. The optimal configuration for the eMLC will be chosen according to the clinical requirements. Based on the optimal configuration determined by the simulation, we will manufacture a prototype eMLC. Software required for the use of eMLC will be developed, including a modified leaf sequence algorithm, a source model specifically for the eMLC, and the incorporation of eMLC effect in the inverse planning and final dose calculation processes. Extensive experiments will be conducted to evaluate the features of the prototype eMLC. For comparison, corresponding experiments using a conventional photon MLC will also be performed.

The successful completion of the project will produce a prototype eMLC and corresponding software for using the eMLC for MERT. We hypothesize that, with the eMLC, MERT will be a very effective modality for breast cancer treatment. It will increase the tumor control probability (TCP) while reducing the possibility for late effects such as lung scarring, pericarditis, and the occurrence of cancer in the contralateral breast.

## **Body**

Although photon beams have been an effective modality for breast cancer treatment in radiation therapy the following problems (or potential areas of improvement) remain: (1) the inclusion of the lung and sometimes of a small volume of the heart in the high-dose volume due to tumor location, patient size or in the case of chest-wall treatments; (2) lower dose near the skin surface due to lack of electron build-up in a photon beam; and (3) high exit or scatter dose to the normal structures such as the lung and heart, and more importantly the contralateral breast, which may be a major cause for the occurrence of secondary cancer in the contralateral breast for women under the age of 45.

Recent development of computer-controlled medical linear accelerators along with improved treatment planning techniques, may provide new solutions in the delivery and control of external beam radiation through beam-intensity modulation<sup>1-9</sup>. It is expected that using photon IMRT, the problem (1) above may be significantly improved but (2) will remain and (3) may become more serious as treatment time increases with the number of fields used (increased leakage or scattering dose). With modulated electron radiation therapy (MERT)<sup>10-15</sup>, on the other hand, problem (1) may also be significantly improved and problems (2) and (3) can be completely eliminated due to the nature of electron beams.

Recently, MERT has been exploited extensively for breast cancer treatment. In this technique, the electron beam intensity pattern, energy, and incident direction are optimized to deliver the optimal radiation dose to the patient. This technique requires a proper beam-shaping device for the intensity-modulated beam delivery. We propose to develop an electron multileaf collimator (eMLC) specifically for MERT. The eMLC will be located near the patient's skin, and have much thinner leaves and optimal shape of leaf ends and sides. We hypothesize that the quality of the electron beams and thus the clinical effect of the MERT will be further improved if we shape the electron beams using the eMLC instead of using the conventional photon multileaf collimator (pMLC), since the pMLC was designed and optimized specifically for photon beams, not for electron beams.

In the first stage of the research, we will design the eMLC using Monte Carlo computer simulations. The EGS4/BEAM/DOSXYZ Monte Carlo system<sup>16-22</sup> will be commissioned for eMLC simulation. A large number of eMLCs with various leaf materials and leaf geometric configurations will be simulated using this Monte Carlo system. The criteria for evaluating competing eMLCs will be established, which include the beam penumbra, flatness and leakage, and leaf weight, size and manufacturing cost. We will find the optimal eMLC leaf material and geometric configuration according to the evaluation criteria.

In the second stage of the research, we will manufacture a prototype eMLC based on the information obtained from the Monte Carlo simulation. A manually driven eMLC will be machined, which should be sufficient for our current study.

In the third stage of the research, we will develop software specifically for the use of eMLC. The electron pencil beam shaped by the eMLC will be calculated using the Monte Carlo method and used in the inverse planning process. We will modify and optimize an existing photon leaf sequence

algorithm for MERT beam delivery using the eMLC. The eMLC will be characterized and incorporated into a multiple-source beam model in order to perform fast Monte Carlo simulations. The effect of the eMLC will be taken into account when performing the final dose calculation using the optimized intensity patterns.

In the fourth stage of the research, the prototype eMLC will be evaluated experimentally. The electron beam intensity patterns delivered by the eMLC will be measured in air using a beam imaging system (BIS) and film. The delivered MERT dose distributions in water will be measured using film, ion chamber, TLD and diode. For comparison, measurements will also be performed for the same treatment plan delivered by a pMLC.

The MERT technique with a specially designed eMLC for beam shaping will be a very promising modality for breast cancer treatment. The successful completion of the project will produce necessary hardware and software for the use of the eMLC for MERT to improve the target dose uniformity and conformity and reduce dose to the lung, heart and contralateral breast.

This project has 4 specific aims: (1) To design an eMLC using Monte Carlo beam simulations, (2) To manufacture an eMLC, (3) To develop software tools for eMLC beam delivery for MERT, and (4) To evaluate the eMLC for MERT treatment of breast cancer.

We report on the research accomplishments associated with the tasks outlined in the approved "Statement of Work" below for our research between Apr 1, 2000 and Mar 31 2001. Since the Principle Investigator, Steve B. Jiang, left Stanford University in September 2000 a replacement has been appointed, who has started on April 1 2001. Thus, the activities in Task 2 have been postponed by about 6 months.

#### 1. Establish evaluation criteria according to the clinical requirements

An essential requirement for MERT is to deliver, both accurately and efficiently, small-field electron beams (beamlets) of different energies and intensities. Traditionally, electron beams are shaped using a cutout and different energies at treatment depths may be achieved using variable incident energies. However, it would be very time consuming to make cutouts for MERT beam delivery and the treatment time would become unacceptably long for routine applications. Bolus can be used for missing tissue compensation and/or limited depth modulation. However, 3D bolus requires

sophisticated techniques to build and it does not provide intensity modulation. As to the existing photon MLC (pMLC), although electron beam collimation can be achieved in some helium-filled, scanned beam systems<sup>10-13,23</sup>, there are some key limitations on accurate beam delivery with commonly accessible clinical accelerators. It is found that a source to surface distance (SSD) of 70 cm is necessary to provide a clinically acceptable field using the pMLC in a Varian Clinac 2100C linear accelerator. Beams collimated by a pMLC were found to be inferior to applicator fields in penumbra and uniformity. Monte Carlo simulations showed that the beam penumbra can be reduced significantly by either replacing the treatment head air with helium, together with a helium filled balloon between the accelerator and the patient or moving the MLC at least 11 cm towards the patient, or both<sup>13</sup>. According to the accelerator engineers, however, it is extremely difficult (if not impossible) to replace the air in an accelerator head with helium without major changes in the accelerator design. Therefore, an electron specific MLC has been proposed, which is located at the same level as a Cerrobend cutout, about 40 cm closer to the patient than the pMLC<sup>24</sup>. An eMLC will be as accurate as a cutout in field shaping, and as efficient as a pMLC for intensity modulation. It is generally believed that one of the reasons for the low use of electron beams in small cancer clinics is the extra manpower required to make customized cutouts for every patient. If so, the development of an eMLC will not only meet the needs for MERT but provide an efficient and effective device for beam shaping for conventional electron therapy.

## 2. Perform Monte Carlo simulations for various EMLC materials and geometric configurations

We have performed extensive Monte Carlo simulations of electron fields collimated by 1 cm wide leaves to study the effect of material type and leaf thickness. Although the beam penumbral widths did not change significantly for leaf thicknesses smaller than 2 cm the beam intensity outside the field was affected by the leaf thickness and the atomic number of the leaf material. As shown in Fig. 1 for a 20 MeV electron beam, 1.5 cm thick zinc leaves reduced the electron fluence outside the field to about 5% of the central axis value. These electrons were mainly generated by the bremsstrahlung photons in the MLC leaves. This was confirmed by the photon fluence as shown, where 1.5 cm zinc MLC leaves resulted in about 60% higher photon fluence outside the field compared to the central axis photon fluence. Some electrons were also scattered off the leaf ends and by air. For 1.5 cm copper, 1.5 cm lead and 2 cm steel, the electron fluence was about 2.5% of the central axis value. The electron fluence was reduced to about 1.5% if the leaves were made of 1.5 cm tungsten. This was reflected by the 30% less photon fluence under the tungsten MLC leaves compared to the central axis photon fluence.

Clearly, tungsten is superior to other materials in terms of leaf leakage. If we increased the tungsten leaf thickness to 2 cm the electron fluence would be reduced to less than 1% of the central axis value and the photon leakage would be reduced to about 50% of the central axis value (not shown).

To study the overall effect of the leaf leakage, leaf scattering, air scattering and the extended source in an electron beam, we compared the dose distributions for single fields and multiple abutting fields collimated by an electron MLC with 1.5 cm thick tungsten leaves. We compared the Monte Carlo calculated dose distributions for a single 4 cm x 4 cm electron field and a multiple abutting field of the same size formed by four 1 cm x 4 cm electron fields<sup>24</sup>. For a 20 MeV electron beam, the dose at the phantom surface for the abutting field shows about 4% fluctuation compared to a single electron field. This is potentially due to the effect of leaf shape and extended source. The dose outside the field for the abutting field is about 3 times higher than that for the single field, which is mainly caused by the leaf leakage due to the longer beam-on time to deliver the four 1 cm x 4 cm fields and electron scattering off the leaf ends. This increased leakage is comparable to that for photon IMRT, where the beam-on time is generally 2.5-3.5 times longer than a conventional photon treatment. The dose at 3 cm depth shows little difference between the abutting field and the single field except for the dose near the field edges and outside the field. For a 6 MeV electron beam, the dose at the phantom surface for the abutting field is almost the same as that for the single field. The effect of leaf leakage is very small for a 6 MeV beam and the dose immediately outside the field is thought mainly due to the effect of electron scattering in the air. It seems that field abutting with 1 cm beamlets collimated by an electron MLC can provide adequate beam characteristics for MERT for the beam energies investigated. However, the dose outside the field needs to be minimized through beam energy and leaf sequence optimization.

We have also studied electron beam collimation using a photon MLC<sup>23</sup>. One of the advantages of using a photon MLC is the possibility of easily combining both photon and electron beams in the same plan. An essential requirement for matching a photon beam and an electron beam at different depths is that both beams share the same source position. Several modifications to the design of a Varian Clinac 2300CD accelerator have been proposed<sup>13</sup>, one of which was to replace the intervening air with helium. This could significantly reduce the effect of electron scattering in the air on the beam penumbra. However, filling the accelerator head with helium requires major modifications to the existing accelerator design. Also, the beam properties deteriorated significantly for energies below 6 MeV even for helium filled treatment head based on the results of our previous DOD project<sup>23</sup>.

To solve this problem, we have investigated an alternative solution - a thin leaf MLC at the electron cutout level to reduce the air scattering effect. As can be seen in Fig. 2, the unfocused pMLC leaf ends could scatter the electrons very significantly to degrade the beam characteristics near the field edges. The Varian MLC has rounded leaf ends, which are expected to have similar or worse dosimetric characteristics as the unfocused MLC studied here. Focused leaf ends could greatly improve the beam edges and provided even slightly better dose profiles inside the field for a 20 MeV electron beam compared to an electron MLC, primarily due to the reduction of electron scattering in the accelerator head (helium vs. air). The dose outside the field was slightly lower for the electron MLC than for the photon MLC. For a 6 MeV beam, an electron MLC gave slightly better surface dose profiles both inside and outside the field than the focused and unfocused photon MLC (Fig. 3). The difference in the dose profiles decreases with depth (not shown). Note that in these comparisons, we have placed the phantom surface at 20 cm below the photon MLC and 7 cm below the electron MLC to minimize the effect of electron scattering in the air or helium between the MLC and the phantom (a fair comparison for using both MLCs). It is evident that an electron MLC will have similar dosimetric characteristics as a photon MLC with focused leaf ends but without the need to replace the air in the accelerator head with helium.

### 3. Evaluate the simulation results using the criteria

We have evaluated the Monte Carlo results using the established clinical criteria. The three important factors are beam delivery accuracy (beam penumbra), beam delivery efficiency (treatment time) and cost-effectiveness. An electron MLC is more accurate than a photon MLC for MERT beam delivery. It has smaller beam penumbra for small beamlet delivery compared to a photon MLC for the currently available clinical accelerators such as the Varian Clinac accelerators. A photon MLC also require the air in the treatment head to be replaced by He to reduce electron scattering effects but it is very difficult for some accelerators if not impossible because of the accelerator configuration. An eMLC is more efficient than electron cutouts for MERT beam delivery. A MERT treatment will require many cutouts for a single treatment which will take much longer time to deliver. In the long run the eMLC based MERT beam delivery will be more economical than using the cutouts.

### 4. Finalize the design based on the optimal leaf material and geometric configuration

Based on our Monte Carlo simulation results<sup>23,24</sup>, we will develop a manually-set eMLC for this project. Since our primary goal is to study the eMLC physical characteristics, the major concerns are

the MLC leaf shape and material. The mechanical construction of the eMLC will be done in our machine shop, where the previous eMLC was built. The eMLC will be directly installed on a 25cm x 25cm electron applicator for a Varian Clinac 2100C accelerator. The applicator will be donated by Varian Medical systems with technical support for mechanical and electrical modifications for the installation. The mechanical characteristics of the eMLC are listed in the table below:

Leaf material	Tungsten alloy
Leaf width	0.5 cm (nominal) projected at 100 cm SSD, leaves will travel in the x direction
Leaf length	20 cm, installed on a carriage movable along x direction
Leaf thickness	1.5 cm
Leaf end shape	Straight edge (unfocused)
Leaf side shape	Straight edge (unfocused) and/or side surface focused to a virtual source position
Leaf location	The bottom of the leaves will be at about 95 cm SSD
Field size	Maximum 25 cm by 25 cm defined at 100 cm SSD

These parameters are determined based on our investigation results<sup>23,24</sup>. We have chosen a 0.5cm leaf width because thinner leaves will not provide effective beamlet collimation, especially for energies below 12 MeV while wider leaves will deteriorate spatial resolution in the y direction (across the leaves). The MLC leaf length is chosen to keep the overall dimension and weight low. The leaves will be installed on a movable carriage to compensate the limited leaf travel in the x direction. The 1.5cm thickness is considered to be optimal for tungsten leaves in terms of leaf leakage (about 1.5% for 20 MeV electrons) and end scatter. Thicker leaves will further reduce leaf leakage but will degrade beamlet penumbra. Straight leaf ends will ensure minimum interleaf leakage when a leaf pair is closed. The effective leaf position and the penumbral change for off-axis positions will be investigated. Focused leaf sides will give slightly better beamlet penumbra in the y direction than unfocused leaf sides. We will evaluate both to determine the optimal design. For equal leaf width projected at 100cm SSD, the actual leaf width will vary depending on the off-axis position. For easy construction (therefore low cost), the actual leaf width can be made the same for a nominal 0.5cm leaf width. The effective leaf positions in the y direction will be determined experimentally and used in the beamlet dose calculation and treatment optimization. The maximum field size provided by the eMLC will be 25cm x 25cm at 100cm SSD.

##### 5. Develop a prototype manual set eMLC

We have made a prototype manual set eMLC to test the Monte Carlo simulations and for the experimental work scheduled for this project. The eMLC consists of 30 steel leaf pairs, which were made using conventional steel bars for convenience and cost-effectiveness (Tungsten leaves are difficult to machine and cost too much for this project). Each leaf is 0.476 cm wide (about 0.5 cm wide projected at 100 cm SSD), 20 cm long and 2.54 cm thick with straight edges and ends. The leaves were mounted on a steel frame attached to the bottom scraper of a 25 cm x 25 cm electron applicator on a Varian Clinac 2100C (Varian Medical Systems, Palo Alto, CA). The leaves can slide in the steel frame and the leaf positions can be easily set using a pre-cut cardboard for a beam segment. The field shape is maintained by tightening screws from the side. The largest radiation field available using the electron MLC was 15.7 cm x 15.7 cm projected at 100 cm SSD. We are discussing with Varian Medical Systems about the possibility of contributing an electron applicator specially used for this study. Since the cost of an electron applicator is well beyond the budget of this project, their contributions are very important to the development of the eMLC. We will be able to make changes to the existing electron applicator so that the eMLC can be placed right above the bottom scraper by removing the electrical device attached to the applicator. Further modifications to the eMLC and the applicator are expected for the task 2 activities.

### **Key Research Accomplishments**

We have accomplished the following tasks:

- *Establish clinical criteria for MERT beam delivery:* The requirements for MERT beam delivery are accuracy, efficiency and cost-effectiveness.
- *Perform Monte Carlo simulations to investigate eMLC parameters:* We have investigated different materials and dimensions for the prototype electron MLC and compared the results with a photon MLC and electron cutouts.
- *Evaluate eMLC parameters based on clinical criteria:* We have evaluated the Monte Carlo results based on the clinical criteria. It is concluded that an eMLC is superior to a pMLC and electron cutouts. An eMLC is more accurate (small beam penumbra) than a pMLC and more efficient and cost-effective than electron cutouts.
- *Develop an eMLC for experimental MERT beam delivery study:* We have finalized the eMLC

parameters for the prototype eMLC for MERT beam delivery. We have made a manual set eMLC based on the project budget and our current linear accelerator.

## **Reportable Outcomes**

*Peer-reviewed papers resulting from or supported in part by this grant:*

- C.M. Ma, T. Pawlicki, M.C. Lee, S.B. Jiang, J.S. Li, J. Deng, E. Mok, B. Yi, G. Luxton and A.L. Boyer, Energy- and intensity-modulated electron beams for radiotherapy, *Phys. Med. Biol.* (2000) 45: 2293-2311
- S.B. Jiang, A. Kapur and C.M. Ma, Electron beam modelling and commissioning for Monte Carlo treatment planning, *Med. Phys.* (2000) 27:180-191
- M. C. Lee, S. B. Jiang and C.M. Ma, Monte Carlo and Experimental Investigations of Multileaf Collimated Electron Beams for Modulated Electron Radiotherapy, *Med. Phys.* (2000) 27: 2708-18

*Meeting abstracts resulting from or supported in part by this grant:*

- C.M. Ma, JS Li, T Pawlicki, SB Jiang and J Deng, MCDOSE – a Monte Carlo dose calculation tool for radiation therapy treatment planning, *Proc. of the XIII International Conference on the Use of Computer in Radiation Therapy (ICCR)*, Eds: W Schlegel and T Bortfeld (Springer-Verlag, Heidelberg) 2000. 123-125
- C.M. Ma, T Pawlicki, MC Lee, SB Jiang, JS Li, J Deng, E Mok and AL Boyer, Modulated electron beams for treatment of breast cancer, Oral presentation at the XIII International Conference on the Use of Computer in Radiation Therapy (ICCR), Heidelberg, Germany, May 22 - 25, 2000. Proceedings to be published at the meeting.
- C.M. Ma, Monte Carlo methods in electron beams treatment planning, invited talk at the 41st Annual Meeting of the *American Association of Physicists in Medicine*, Nashville, TN, July 24-29, 1999. *Med. Phys.*, 26(1999 AAPM Annual Meeting Program) 1999.
- J. Deng, S.B. Jiang, T. Pawlicki, J. Li and C.M. Ma, Electron beam commissioning for Monte Carlo dose calculation, *ICCR 2000*.
- C.M. Ma, T Pawlicki, SB Jiang, JS Li, Deng, D Findley, E Mok and AL Boyer, Implementation of a Monte Carlo dose calculation module in the FOCUS treatment planning system, *CMS' FOCUS 2000 User's Symposium*, St. Louis, MO, April 10-11, 2000.
- J. S. Li, T. Pawlicki, J. Deng, S.B. Jiang, A. Kapur, E. Mok and C.M. Ma, Clinical validation of a Monte Carlo dose calculation code for radiotherapy treatment planning (abstract), *Med. Phys.* 26, 1083

- J. S. Li, T. Pawlicki, J. Deng, S.B.Jiang and C.M. Ma, Simulation of Beam Modifiers for Monte Carlo Treatment Planning, submitted to ICCR 2000
- S. B. Jiang, A. Kapur, and C.M. Ma, Electron beam modeling and commissioning for Monte Carlo treatment planning, Med. Phys. 26, 1084 (1999) (abstract), AAPM Annual Meeting (Nashville).

*Funding applied for based on work resulting from or supported in part by this grant:*

Modulated Electron Radiation Therapy

NIH: R01 Principle Investigator: C-M Charlie Ma, Ph.D. (April 1, 2001)

## **Conclusions**

We have made significant progress during our first-year investigation. We have successfully performed the tasks scheduled in the "Statement of Work". We have established clinical criteria for MERT beam delivery. We have performed extensive Monte Carlo simulations of the electron MLC leaf materials and dimensions and evaluated the MLC leaf parameters based on the clinical criteria. We have proposed a set of parameters for the prototype manual set electron MLC for MERT beam delivery study.

"So what?"

Our first year results have provided evidence to support the hypothesis of this proposal that by using a specially designed multi-leaf collimator for electron beams energy- and intensity-modulated electron beams may be optimized to significantly improve the dose uniformity in the target volume, to reduce the dose to the critical structures nearby and therefore reduce the late effects associated with breast cancer radiotherapy. Further studies as scheduled in the "Statement of Work" are needed to manufacture an eMLC and to investigate treatment plans for realistic breast cases generated using different beam modalities. We shall be able to finally determine the degree of feasibility of using MERT to improve breast cancer treatment.

## References

1. R Boesecke, G Becker, K Alandt, *et al.* Modification of a three-dimensional treatment planning system for the use of multileaf collimators in conformation radiotherapy. *Radioth. and Oncol.* 21:261-268, 1991.
2. AL Boyer, TG Ochran, CE Nyerick and TJ Waldron. Clinical dosimetry for implementation of a multileaf collimator. *Med. Phys.* 19:1255-1261, 1992.
3. A Brahme. Optimal setting of multileaf collimators in stationary beam radiation therapy. *Strahlenther. Onkol.* 164:343-350, 1988.
4. DJ Convery and M E Rosenbloom. The generation of intensity-modulated fields for conformal radiotherapy by dynamic collimation. *Phys. Med. Biol.*, 37:1359-1374, 1992.
5. WD Powlis, A Smith, E Cheng, *et al.* Initiation of multileaf collimator conformal radiation therapy. *Int. J. Radiat. Oncol. Biol. Phys.* 25:171-179, 1993.
6. JM Galvin, X Chen, and RM Smith. Combining multileaf fields to modulate fluence distributions. *Int. J. Radiat. Oncol. Biol. Phys.* 27:697-705, 1993.
7. T Bortfeld, A L Boyer, W Schlegel, D L Kahler, and T J Waldron. Realization and verification of three-dimensional conformation radiotherapy with modulated fields. *Int. J. Radiat. Oncol. Biol. Phys.* 30:899-908, 1994.
8. CX Yu, M J Symons, MN Du, AA Martinez, and J Wong. A method for implementing dynamic photon beam intensity modulation using independent jaws and multileaf collimator. *Phys. Med. Biol.*, 40:769-787, 1995.
9. R Mohan, X Wang, A Jackson, T Bortfeld, A L Boyer, G J Kutcher, S A Leibel, Z Fuks, and CC Ling. The potential and limitations of the inverse radiotherapy technique. *Radiotherapy and Oncology*, 32: 0232-248, 1994.
10. S Hyodynmaa, A Gastafsson and A Brame. Optimisation of conformal electron beam therapy using energy- and fluence-modulated beams, *Med. Phys.*, 23: 659-666, 1996.
11. EP Lief, A Larsson and JL Humm. Electron dose profile shaping by modulation of a scanning elementary beam, *Med. Phys.*, 23: 33-44, 1996.
12. B Zackrisson and M Karlsson, Matching of electron beams for conformal therapy of target volumes at moderate depths, *Radiotherapy and Oncology*, 39: 261-270, 1996.
13. MG Karlsson, M Karlsson, CM Ma and A Satherberg, MLC-collimated electron beams – a Monte Carlo based optimisation, *World Congress on Med. Phys.* (Nice, France) 1997 submitted
14. AAPM TG-21, A protocol for the determination of absorbed dose from high-energy photons and

- electrons, *Med. Phys.*, 10: 741, 1983.
15. C-M Ma, E Mok, A Kapur and D Findley, Improvement of small-field electron beam dosimetry by Monte Carlo simulations *Proc. XIIIth ICCR* (Salt Lake City, Utah) 159-162, 1997.
  16. R. Nelson, H Hirayama and DWO Rogers. *The EGS4 code system*, Stanford Linear Accelerator Center Report SLAC-265 (SLAC, Stanford, CA) 1985.
  17. DWO Rogers, BA Faddegon, GX Ding, CM Ma, J Wei and TR Mackie, BEAM: a Monte Carlo code to simulate radiotherapy treatment units, *Med. Phys.* 22:503-525, 1995.
  18. A Kapur, C-M Ma, E Mok, D Findley, Characterization of small field electron beams for radiotherapy by Monte Carlo simulations, *Proc. XIIIth ICCR* (Salt Lake City, Utah) 157-158, 1997.
  19. C-M Ma , BA Faddegon, DWO Rogers and TR Mackie, Accurate characterization of the Monte Carlo calculated electron beams for radiotherapy, *Med. Phys.*, 24:401-417, 1997.
  20. C.-M. Ma, E. Mok, A. Kapur, T. Pawlicki, D. Findley, S. Brain, K. Forster and A.L. Boyer, Clinical implementation of a Monte Carlo treatment planning system, *Med. Phys.* 26: 2133-43 (1999)
  21. C.-M. Ma and S.B. Jiang, Topical review: Monte Carlo modeling of electron beams from medical accelerators, *Phys. Med. Biol.*, (1999) 44: R167-212
  22. C-M Ma, PJ Reckwerdt, M Holmes, DWO Rogers and B Geiser, *DOSXYZ Users Manual*, national Research Council of Canada report PIRS-509B (NRCC, Ottawa, Canada) 1995.
  23. M. C. Lee, S. B. Jiang and C.M. Ma, Monte Carlo and Experimental Investigations of Multileaf Collimated Electron Beams for Modulated Electron Radiotherapy, *Med. Phys.* (2000) 27: 2708-18
  24. C.-M. Ma, T. Pawlicki, M.C. Lee, S.B. Jiang, J.S. Li, J. Deng, E. Mok, B. Yi, G. Luxton and A.L. Boyer, Energy- and intensity-modulated electron beams for radiotherapy, *Phys. Med. Biol.* (2000) 45: 2293-2311

## Appendices

### List of Figures quoted in the body of text:

Figure 1 Monte Carlo simulated electron (top) and photon (bottom) planar fluence in the penumbral region and outside the treatment field for a 20 MeV electron beam collimated by an eMLC of different leaf materials and thicknesses.

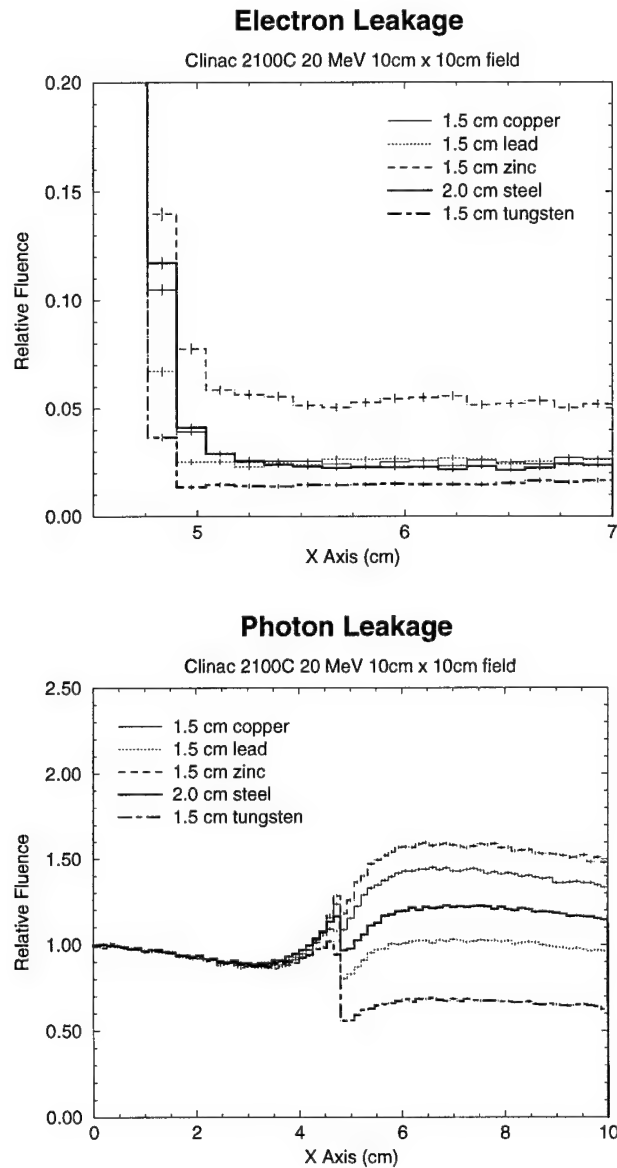


Figure 2 Monte Carlo calculated 20 MeV, 10 cm x 10 cm field electron beam profiles at 0.5 cm depth in water.

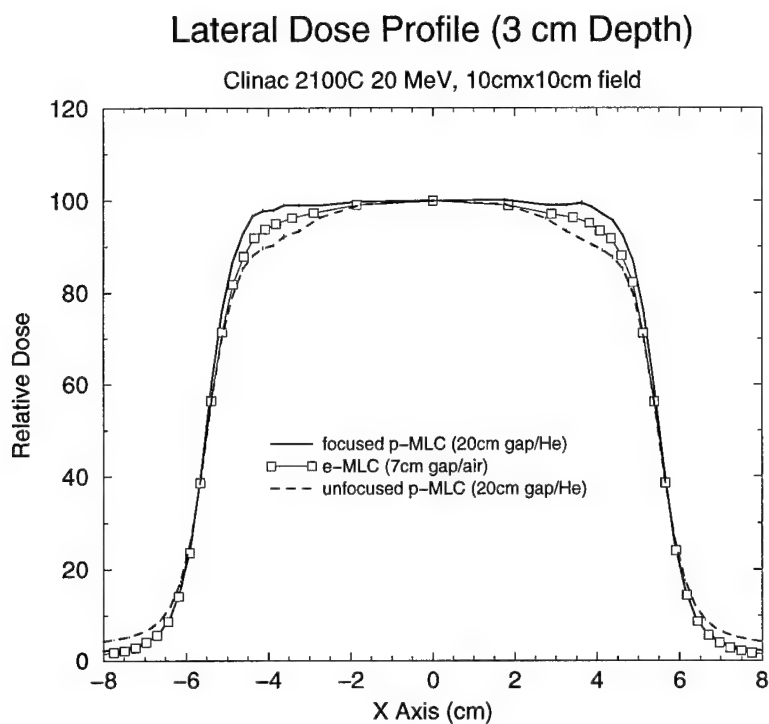
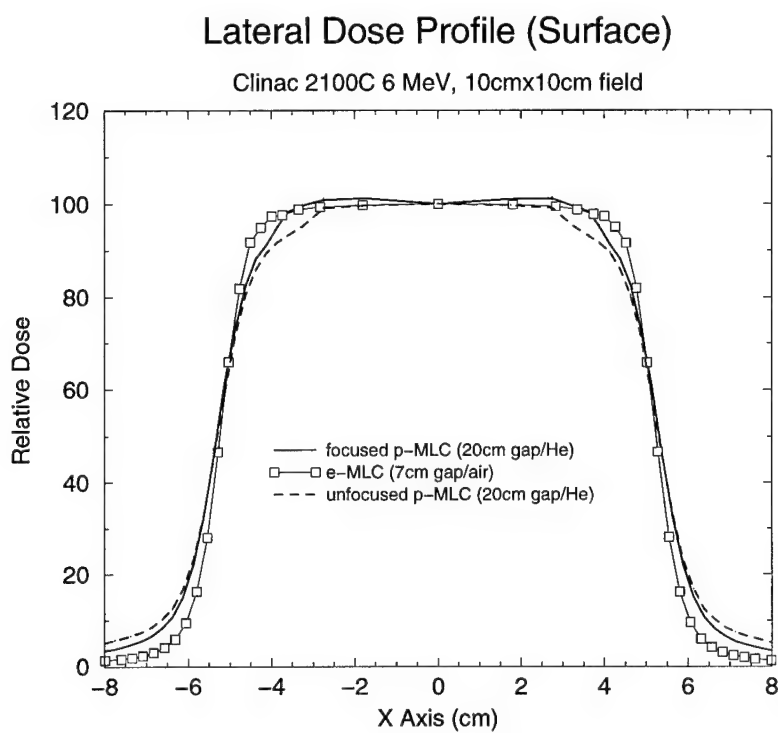


Fig. 3 Monte Carlo calculated 6 MeV, 10 cm x 10 cm field electron beam profiles at 0.5 cm depth in water calculated by Monte Carlo.



**List of manuscripts submitted with this report:**

1. C.-M. Ma, T. Pawlicki, M.C. Lee, S.B. Jiang, J.S. Li, J. Deng, E. Mok, B. Yi, G. Luxton and A.L. Boyer, Energy- and intensity-modulated electron beams for radiotherapy, *Phys. Med. Biol.* (2000) 45: 2293-2311
2. S.B.Jiang, A. Kapur and C.-M. Ma, Electron beam modelling and commissioning for Monte Carlo treatment planning, *Med. Phys.* (2000) 27:180-191
3. M. C. Lee, S. B. Jiang and C.M. Ma, Monte Carlo and Experimental Investigations of Multileaf Collimated Electron Beams for Modulated Electron Radiotherapy, *Med. Phys.* (2000) 27: 2708-18

## Energy and intensity modulated electron beams for radiotherapy

C-M Ma, T Pawlicki, M C Lee, S B Jiang, J S Li, J Deng, B Yi, E Mok and A L Boyer

Department of Radiation Oncology, Stanford University School of Medicine, Stanford, CA 94305-5304, USA

E-mail: cma@reyes.stanford.edu

Received 5 January 2000, in final form 10 April 2000

**Abstract.** This work investigates the feasibility of optimizing energy- and intensity-modulated electron beams for radiation therapy. A multileaf collimator (MLC) specially designed for modulated electron radiotherapy (MERT) was investigated both experimentally and by Monte Carlo simulations. An inverse-planning system based on Monte Carlo dose calculations was developed to optimize electron beam energy and intensity to achieve dose conformity for target volumes near the surface. The results showed that an MLC with 5 mm leaf widths could produce complex field shapes for MERT. Electron intra- and inter-leaf leakage had negligible effects on the dose distributions delivered with the MLC, even at shallow depths. Focused leaf ends reduced the electron scattering contributions to the dose compared with straight leaf ends. As anticipated, moving the MLC position toward the patient surface reduced the penumbra significantly. There were significant differences in the beamlet distributions calculated by an analytic 3-D pencil beam algorithm and the Monte Carlo method. The Monte Carlo calculated beamlet distributions were essential to the accuracy of the MERT dose distribution in cases involving large air gaps, oblique incidence and heterogeneous treatment targets (at the tissue–bone and bone–lung interfaces). To demonstrate the potential of MERT for target dose coverage and normal tissue sparing for treatment of superficial targets, treatment plans for a hypothetical treatment were compared using photon beams and MERT.

(Some figures in this article are in colour only in the electronic version; see [www.iop.org](http://www.iop.org))

### 1. Introduction

Photon beams have been an effective modality for breast cancer treatment in radiation therapy. Although such conventional treatment with tangential photon fields has been successful, the following two problems (or potential areas of improvement) remain:

- (a) The inclusion of the lung and other normal tissues, and sometimes of a small volume of the heart, in the high-dose volume due to tumour location, patient size or in the case of chest-wall treatments.
- (b) High exit or scatter dose to the normal structures such as the lung, the heart and the contralateral breast.

Advances in the state of the art of computer-controlled medical linear accelerators have recently become available that, along with newly developed treatment planning techniques, may provide significant improvements in the delivery and control of external beam radiation through beam-intensity modulation (Boesecke *et al* 1988, Brahme 1988, Convery and

Rosenbloom 1992, Leibel *et al* 1992, Webb 1992, 1997, LoSasso *et al* 1993, Powlis *et al* 1993, Chui *et al* 1994, Mageras *et al* 1994, Brewster *et al* 1995, Fraass *et al* 1995, Kutcher *et al* 1995, Mackie *et al* 1995, McShan *et al* 1995, Ling *et al* 1996, Boyer *et al* 1997). It is expected that using photon IMRT, the problem (a) above may be significantly improved but (b) may become more serious as treatment time increases with the number of fields/segments used (increased leakage or scattering dose). Using the modulated electron radiotherapy (MERT) technique (Lief *et al* 1996, Hyödynmaa *et al* 1996, Zackrisson and Karlsson 1996, Åsell *et al* 1997, Ebert and Hoban 1997, Karlsson *et al* 1998, 1999), on the other hand, problem (a) may also be significantly improved and problem (b) may almost be eliminated due to the nature of the electron beams.

In the optimization process of MERT, dose conformity along the beam direction can be achieved by modulating the electron incident energy, making use of the sharp dose fall-off feature. A drawback is its large penumbra at large depths. Traditionally, electron beams are shaped using a cutout (or blocks) and beam penetration/intensity may be modified using a bolus. However, it is time-consuming to make such beam modifiers and the treatment time would be significantly increased if such beam modifiers are used for MERT. Efforts have been made to use computer-controlled MLC for electron beam modulation. The recent results by Karlsson *et al* (1999) showed that by replacing the air in the treatment head with a low-cost, custom-made helium balloon, the beam penumbral width (20/80) was reduced from 18 to 11 mm at 80 cm SSD. The beam characteristics are affected by the position of the MLC. However, by replacing the air between the MLC and the patient with a helium balloon, the beam penumbra become almost the same as that achieved by electron beam-shaping with an electron applicator that extends to the patient skin surface (Karlsson *et al* 1999). This means that many of the techniques so far developed with computer-controlled MLC and our experience with MLC photon beam modulation can be adopted for use with MERT.

The calculation of dose distributions for electron beam radiotherapy planning is challenging because electron scattering is strongly affected by changes in density and composition in the patients. The 3D pencil beam algorithm (Hogstrom *et al* 1981) is a fast analytical algorithm which has been adopted by most treatment planning systems. However, it has limitations with small irregular electron fields and in the presence of inhomogeneities (Cygler *et al* 1987, Bielajew *et al* 1987, Mah *et al* 1989, Mackie *et al* 1994, Ma *et al* 1999). The Monte Carlo simulation has been demonstrated to be a viable option for such complex situations, and also the only way to take into account back-scattering from denser materials in a patient (e.g. bone or metal inserts) (Shortt *et al* 1986, Cygler *et al* 1987, Mackie *et al* 1994, Kawrokwaw *et al* 1996, Mohan 1997, Kapur 1999, Ma *et al* 1999). The EGS4/BEAM system was developed for the simulation of radiotherapy beams from various radiotherapy treatment units, such medical accelerators (Rogers *et al* 1995). Excellent agreement (1–3%) has been achieved between the Monte Carlo dose distributions calculated using the simulated particle phase-space data and measurements (Rogers *et al* 1995, Kapur *et al* 1998, Zhang *et al* 1999, Ma *et al* 1999). We have installed a Monte Carlo patient dose calculation tool on a clinical treatment planning system (Ma *et al* 1999) and used Monte Carlo for treatment planning and dose delivery validation. This has reduced the uncertainty of the accelerator output for small irregular field electron beams from up to 10% to about 3% (Ma *et al* 1997, Kapur *et al* 1998).

Conformal radiotherapy was initially used to limit the normal tissue dose by conforming the treatment field to the beam's-eye-view projection of the target volume (Takahashi 1965). For photon beams, the MLC was used to collimate the fields and later to modulate the beam intensity in the field (Boesecke *et al* 1988, Brahme 1988, Convery and Rosenbloom 1992, Leibel *et al* 1992, Webb 1992, 1997, LoSasso *et al* 1993, Powlis *et al* 1993, Chui *et al* 1994, Mageras *et al* 1994, Brewster *et al* 1995, Kutcher *et al* 1995, Mackie *et al* 1995,

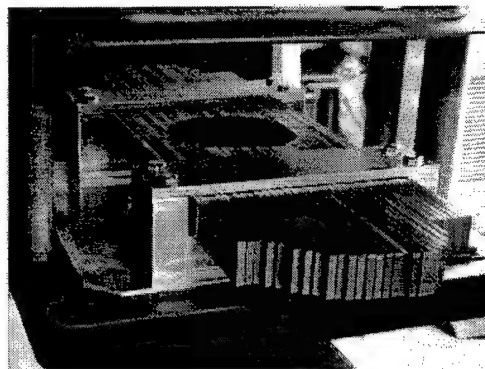


Figure 1. A prototype of an electron MLC mounted on the bottom scraper of a 25 cm  $\times$  25 cm applicator on a Varian Clinac 2100C accelerator. The MLC has 30 pairs of steel leaves and the leaf positions are fixed by the tightening screws.

McShan *et al* 1995, Ling *et al* 1996, Boyer *et al* 1997). There have been a few studies on electron conformal therapy. Tailoring dose distributions using electron beams requires substantial beam manipulation, due to their scattering characteristics. Such manipulation is already possible with radiation sources such as microtrons where preferential energy selection and magnetically scanned pencil beams are possible (Lief *et al* 1996). Both intensity- and energy/intensity-modulated electron beams have been investigated to conform the dose to the target near the surface (Lief *et al* 1996, Hyödynmaa *et al* 1996, Zackrisson and Karlsson 1996, Ebert and Hoban 1997, Karlsson *et al* 1998). More recent work has studied the combination of photon IMRT and MERT for targets at greater depth (Karlsson *et al* 1999). Using the helium-balloon technique together with a computer-controlled MLC, it may be possible to deliver a set of intensity-modulated beams with different energies and incident angles.

In this work, we investigate the feasibility of optimizing energy- and intensity-modulated electron beams for radiotherapy treatment. We report here our Monte Carlo studies of a multileaf collimator specially designed for MERT and some preliminary experimental results. We also report on the dose calculation algorithms and their effects on treatment plan optimization for MERT. We will discuss the differences in the beam characteristics between a photon MLC and an electron MLC. We will compare the dose distributions between a conventional tangential photon treatment plan and a MERT treatment plan for a hypothetical breast treatment to demonstrate the potential of MERT for target dose coverage and normal tissue sparing.

## 2. Materials and method

### 2.1. The prototype electron MLC

We have developed a prototype manual-driven electron MLC for the beam delivery for MERT. As shown in figure 1, the electron MLC consists of 30 steel leaf pairs, which were made from the off-the-shelf steel bars for convenience and cost-effectiveness. Each leaf is 0.476 cm wide, 20 cm long and 2.54 cm thick with straight edges and ends. The leaves were mounted on a steel frame, which can be attached to the bottom scraper of a 25 cm  $\times$  25 cm electron applicator on a Varian Clinac 2100C (Varian Oncology Systems, Palo Alto, CA). The leaves can slide in

the steel frame and the leaf positions can be easily set using a pre-cut cardboard for a beam segment. The field shape is maintained by tightening the screws from the side. The largest radiation field available using the electron MLC was  $15.7\text{ cm} \times 15.7\text{ cm}$  projected at 100 cm source-surface distance (SSD).

Because of the existing electronic device for inserting the electron cutout, the leaves could not be placed at the last scraper level without modifying the existing applicator geometry. Instead, the steel frame was inserted using the electron cutout mount and the leaves were placed immediately above the last scraper. This resulted in a slightly greater air gap (7 cm) between the bottom of the electron MLC leaves and the phantom surface (assuming a 97 cm SSD) compared with that of an electron cutout (5 cm for a 100 cm SSD). The projected leaf width for a 5 cm air gap is 0.5 cm, while for a 7 cm air gap the projected leaf width is 0.51 cm (e.g. for the current configuration at 97 cm SSD). Further modifications are needed to the electron applicator geometry in order to lower the electron MLC leaves. The ideal location for the MLC leaves is the last scraper since electron cutouts will no longer be needed if an electron MLC is in place.

Film measurement was performed to study the characteristics of the electron beams collimated by the electron MLC. The film was calibrated following the AAPM TG-25 recommendations (AAPM 1991) and the exposures were taken by placing film at different depths in a solid water phantom. The film was scanned using a film scanner which has a spatial resolution of about 0.15 cm.

## 2.2. The Monte Carlo beam simulation

We have used the EGS4 (Nelson *et al* 1985) user code BEAM for the accelerator head simulation. Detailed descriptions of the software can be found in Rogers *et al* (1995). A detailed description of the clinical implementation of the Monte Carlo method at the Stanford Medical Center was given in a previous publication (Ma *et al* 1999).

For this work, we have used the previously simulated Monte Carlo beam data for 6, 12 and 20 MeV electron beams from a Varian Clinac 2100C linear accelerator and for 6 MV photon beams from a 2300CD accelerator (Varian Oncology Systems, Palo Alto, CA). The dimensions and materials for the accelerator components were incorporated according to the manufacturer's specifications. Electron beams emerging from the vacuum exit window were assumed to be monoenergetic and monodirectional with a beam radius of 0.1–0.2 cm (Kapur *et al* 1998). The energy cutoffs for electron transport in the accelerator simulation (ECUT and AE) were 700 keV (kinetic + rest mass) and for photon transport (PCUT and AP) 10 keV. The electron transport step length was confined such that the maximum fractional energy loss per electron step is 4% (i.e. ESTEPE = 0.04). The ICRU recommended compositions and stopping power values were used for the materials in the accelerator simulations (ICRU 1984). The phase-space data were scored at a plane either immediately above the photon MLC or above the lowest scraper. The number of particles was about 2–30 million in an electron beam file and about 50 million in a photon file.

Field shaping by the photon MLC or electron MLC was further simulated using the BEAM component module MLC. MLC could simulate either straight or 'double focused' leaf edges and ends. In this work, we have simulated electron beams collimated by a photon MLC with both straight and double focused MLC leaf shapes. The leaves were 7.5 cm thick and made of tungsten. The leaf center was 49 cm from the isocentre. The intervening air in the accelerator and between the MLC and the isocentre was in some cases replaced with helium to investigate the effect of electron scattering in the air. In the simulations of the electron beams collimated by an electron MLC, the leaves were placed on the bottom scraper of a  $25\text{ cm} \times 25\text{ cm}$  applicator

with a 7 cm air gap between the bottom surface of the MLC and the isocentre. Tungsten leaves of 1.5 cm thickness with straight edges and ends were used in all the simulations and the phase space data were used in the subsequent dose calculations except for the leaf leakage study where different leaf materials and thicknesses were investigated for the electron MLC.

### 2.3. The Monte Carlo dose calculation

The EGS4 user code, MCDOSE (Ma *et al* 1999), was used in this work for the dose calculations. MCDOSE was designed for dose calculations in a 3D rectilinear voxel geometry. Voxel dimensions were completely variable in all three directions. Every voxel (volume element) could be assigned to a different material. The cross-section data for the materials used were available in a pre-processed PEGS4 cross-section data file. The mass density of the material in a MCDOSE calculation was varied based on the patient's CT data although the density effect corrections for the stopping powers of the material remain unchanged (Ma *et al* 1999). The voxel dimensions and materials were defined in a MCDOSE input file together with the transport parameters such as the energy cutoffs (ECUT and PCUT), the maximum fractional energy loss per electron step (ESTEPE), and the parameters required by PRESTA (Bielajew and Rogers 1987). Several variance reduction techniques have been implemented in the MCDOSE code to improve the calculation efficiency. These include photon interaction forcing, particle splitting, Russian roulette, electron range rejection and region rejection, particle track displacement and rotation, and correlated sampling. Detailed descriptions of these techniques have been given elsewhere (Rogers and Bielajew 1990, Ma and Nahum 1993, Rogers *et al* 1995, Kawrakow *et al* 1996, Keall and Hoban 1996, Ma *et al* 1999).

For patient dose calculations, the simulation phantom was built from the patient's CT data with up to  $128 \times 128 \times 128$  voxels (uniform in any dimension). The side of a voxel varied from 0.2 to 0.4 cm. A separate program was developed to convert the patient's CT data from the FOCUS treatment planning system (Computerized Medical Systems, St Louis, MO) to desired dimensions, material types and densities. The organ contours were also obtained for dose calculation and analysis. The phase-space data obtained from a BEAM simulation were used as a source input with variable source positions and beam incident angles. To simulate the dose distribution of a finite size beamlet used by the inverse planning process, particles were transported to the MLC plane and only those within the beamlet area ( $= 1 \text{ cm} \times 1 \text{ cm}$  projected at 100 cm SSD) were allowed to go through. This ignored the bremsstrahlung photon leakage and electron scattering by the leaf ends in the optimization process (the effect was corrected in the final dose calculation, as discussed below). After optimization, a leaf sequence was generated using a modified 'step and shoot' algorithm based on our early work (Ma *et al* 1998). The final MERT dose distribution was computed based on an intensity map (a 2D distribution of particle weighting factors) reconstructed from the leaf sequence. The bremsstrahlung leaf leakage effect was included in the intensity map using the leaf sequence and pre-calculated leaf leakage data for 1.5 cm thick tungsten leaves. MCDOSE produced data files that contained geometry specifications such as the number of voxels in all the three directions and their boundaries as well as the dose values and the associated ( $1\sigma$ ) statistical uncertainties in the individual voxels and organs (structures). The EGS4 transport parameters were ECUT = AE = 700 keV, PCUT = AP = 10 keV and ESTEPE = 0.04. The number of particle histories simulated ranged from 2 million to 30 million for a MERT treatment. The  $1\sigma$  statistical uncertainty in the dose was generally 2% or smaller of the  $D_{\text{max}}$  value. The CPU time required for a MERT simulation was about 1–3 h on a Pentium III 450 MHz PC with the variance reduction option switched on.

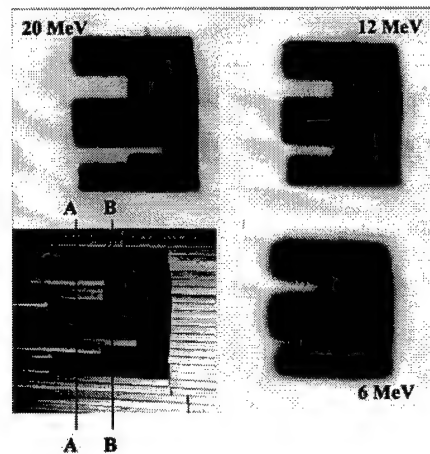


Figure 2. Beam intensity distributions measured by film on the surface of a solid water phantom for 6, 12 and 20 MeV electrons. The MLC leaf positions for the electron fields are also shown (bottom left).

#### 2.4. The optimization process

The treatment planning optimization system used in this work is a home-developed system based on the work by Jiang (1998). First, the planner inputs the patient geometry and defines the treatment setup, such as the beam energy, number and orientations of beams, etc. The target volume and the critical structures are defined by the clinician. A reference monitor unit is assigned to each open rectangular beam and the dose deposition coefficients, which are defined as the dose contribution from a beamlet to a point, are calculated using the MCDOSE code.

Second, using the calculated dose deposition coefficients as input, the optimal intensity profile for each beam is achieved using a gradient method to minimize the objective function. For the target area, a quadratic form of objective function is specified. In addition, two target dose-uniformity constraints are used to ensure a uniform target dose distribution and to distinguish the clinical importance of cold and hot spots. For the critical structures, maximum-dose constraint and several levels of dose-volume constraints are assigned to each structure. For each objective function and constraint, an importance weight relative to the target objective function is assigned. All the constraints are mathematically transformed to the penalty functions of quadratic forms. The augmented objective function, which should be minimized, is a combination of the original objective functions and all penalty functions. The results of the optimization process are the intensity profiles for the individual fields (different incident energies and gantry angles). The same optimizer has been used for photon beam optimization with the Monte Carlo method and a finite-size pencil beam algorithm (Jiang 1998, Jiang *et al* 1999, Pawlicki *et al* 1999).

### 3. Results and discussion

#### 3.1. Characteristics of electron beams collimated by an electron MLC

Figure 2 shows the electron fields collimated by the prototype electron MLC for 6, 12 and 20 MeV electron beams on a Varian Clinac 2100C machine. For convenience, a photo showing

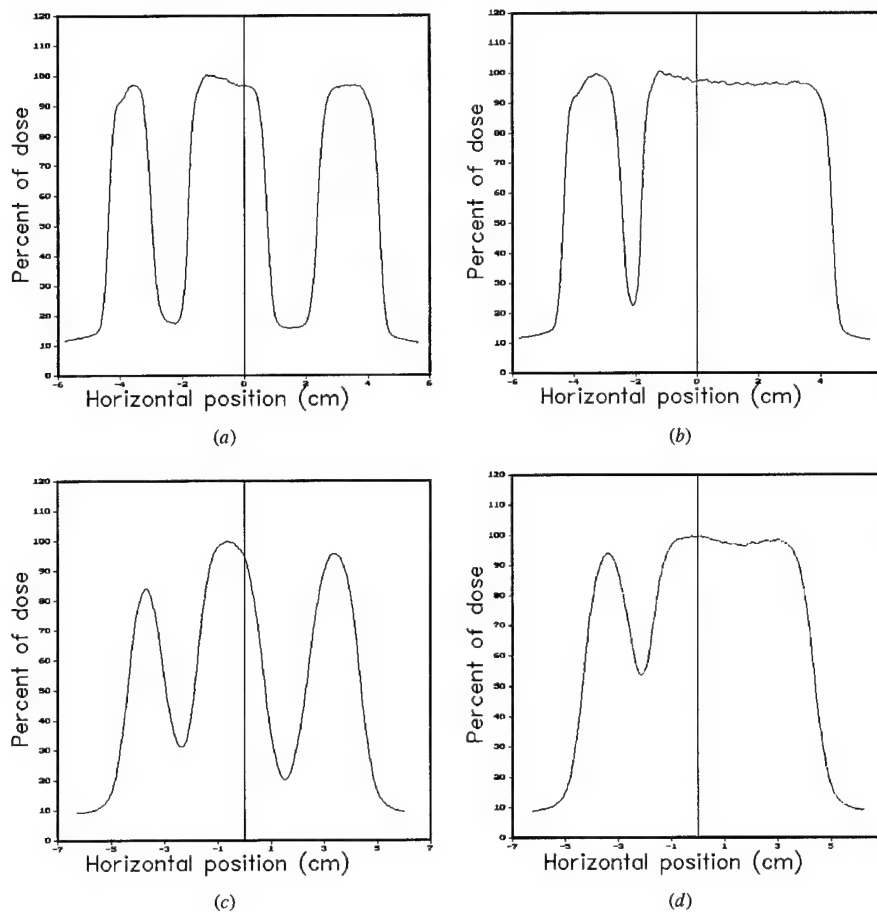


Figure 3. Beam profiles measured by film on the surface of a solid water phantom for the 6 MeV and 20 MeV electron fields shown in figure 2: (a) 20 MeV along A-A; (b) 20 MeV along B-B; (c) 6 MeV along A-A; (d) 6 MeV along B-B.

the MLC leaf positions for the field shape is also included in figure 2. Figure 2 shows the film measurement at the surface of a solid water phantom (97 cm SSD) for 6, 12 and 20 MeV electron beams. Figure 3 shows the measured profiles on the phantom surface along A-A and B-B for the 6 MeV and 20 MeV electron fields shown in figure 2. Figure 4 shows the beam profiles at 2 cm depth in the solid water phantom. It can be seen that for a 20 MeV electron beam, 0.5 cm leaf shapes are still distinguishable on the surface but become very blurred at 2 cm depth. For a 6 MeV electron beam, however, the effect of electron scattering becomes so severe that a leaf width smaller than 1.0 cm will not result in any improvement in the spatial resolution. However, a small leaf width may have the advantage of defining the field more precisely in the direction perpendicular to the leaves.

Based on these experimental results, we further performed Monte Carlo simulations of electron fields collimated by 1 cm wide leaves to study the effect of material type and

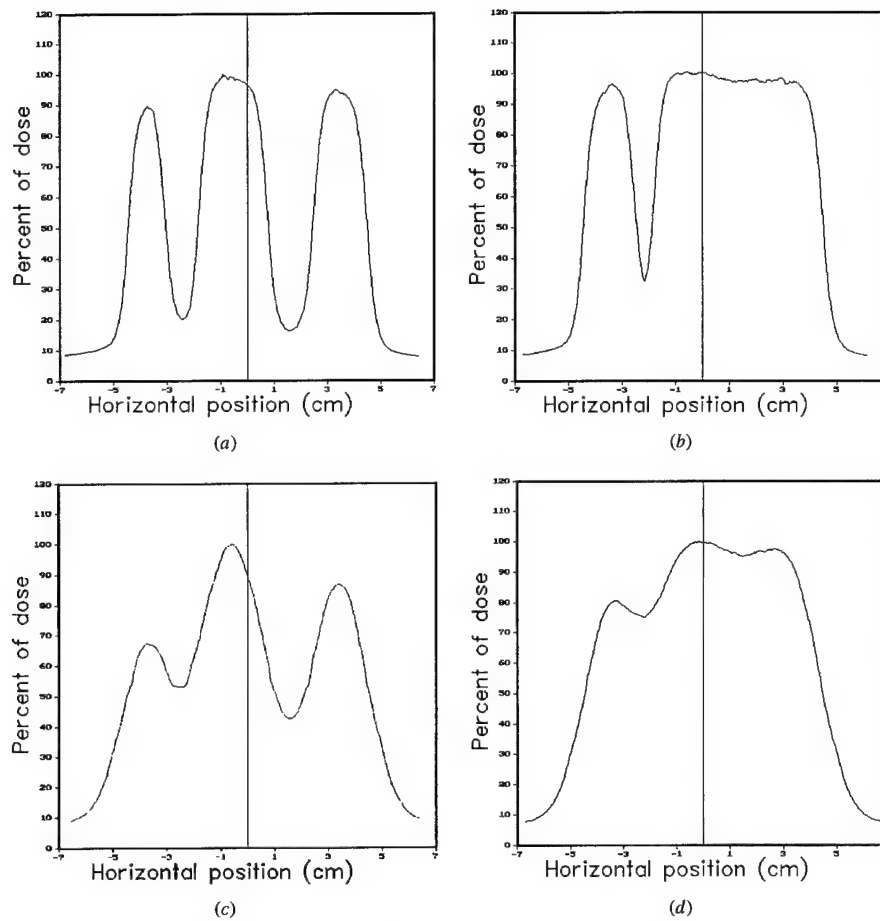
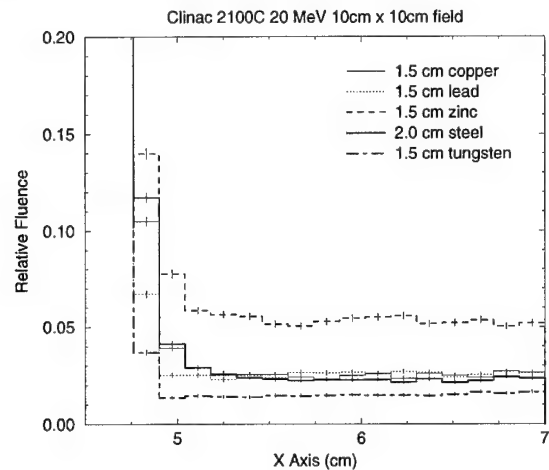
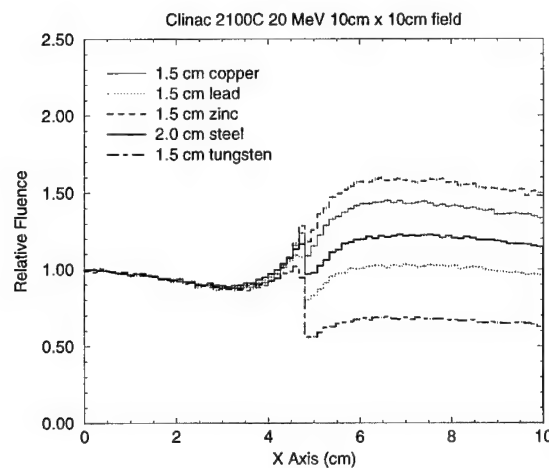


Figure 4. Beam profiles measured at 2 cm depth in a solid water phantom for the 6 MeV and 20 MeV electron fields shown in figure 2: (a) 20 MeV along A-A; (b) 20 MeV along B-B; (c) 6 MeV along A-A; and (d) 6 MeV along B-B.

leaf thickness. Although the beam penumbral widths did not change significantly for leaf thicknesses smaller than 2 cm, the beam intensity outside the field was affected by the leaf thickness and the atomic number of the leaf material. As shown in figure 5 for a 20 MeV electron beam, 1.5 cm thick zinc reduced the electron fluence outside the field to about 5% of the central axis value (figure 5(a)). These electrons were mainly generated by the bremsstrahlung photons in the MLC leaves. This was confirmed by the photon fluence as shown in figure 5(b), where 1.5 cm zinc MLC leaves resulted in about 60% higher photon fluence outside the field compared with the central axis photon fluence. Some electrons were also scattered off the leaf ends and by air. For 1.5 cm copper, 1.5 cm lead and 2 cm steel, the electron fluence was about 2.5% of the central axis value. The electron fluence was reduced to about 1.5% if the leaves were made of 1.5 cm tungsten. This was reflected by the 30% smaller photon fluence under the tungsten MLC leaves compared with the central axis photon fluence. Clearly, tungsten was superior to



(a)



(b)

Figure 5. Monte Carlo simulated electron (a) and photon (b) planar fluence in the penumbral region and outside the treatment field for a Varian Clinac 2100C 20 MeV electron beam collimated by an electron MLC of different leaf materials and thicknesses. The air gap between the electron MLC and the scoring plane is 7 cm.

other materials in terms of leaf leakage. If we increased the tungsten leaf thickness to 2 cm the electron fluence would be reduced to less than 1% of the central axis value and the photon leakage would be reduced to about 50% of the central axis value (not shown).

To study the overall effect of the leaf leakage, leaf scattering, air scattering and the extended source in an electron beam, we compared the dose distributions for single fields and multiple abutting fields collimated by an electron MLC with 1.5 cm thick tungsten leaves. Figure 6 shows the Monte Carlo calculated dose distributions for a single 4 cm  $\times$  4 cm electron field and a multiple abutting field of the same size formed by four 1 cm  $\times$  4 cm electron fields. For

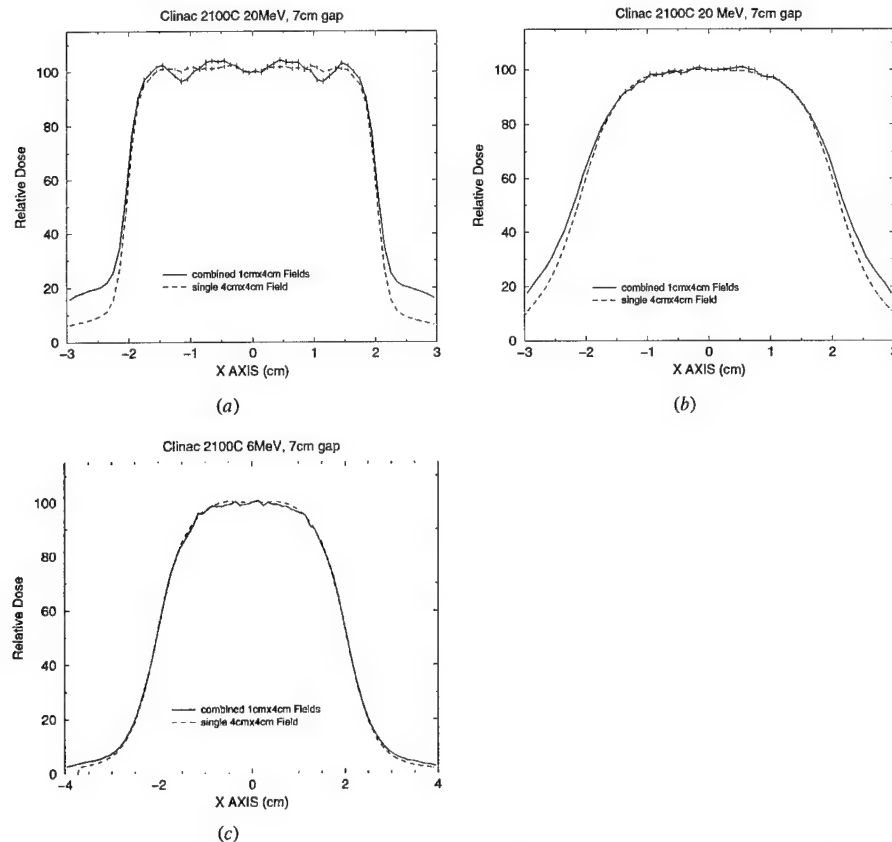


Figure 6. Monte Carlo calculated dose distributions in a water phantom for Varian Clinac 6 and 20 MeV electron beams collimated by an electron MLC of 1.5 cm thick tungsten leaves for a single 4 cm  $\times$  4 cm electron field and a 4 cm  $\times$  4 cm field formed by four 1 cm  $\times$  4 cm electron fields: (a) dose at surface for a 20 MeV beam; (b) dose at 3 cm depth for a 20 MeV beam; (c) dose at surface for a 6 MeV beam.

a 20 MeV electron beam, the dose at the phantom surface for the abutting field shows about 4% fluctuation compared with a single electron field (figure 6(a)). This is potentially due to the effect of leaf shape and extended source. The dose outside the field for the abutting field is about three times higher than that for the single field, which is mainly caused by the leaf leakage due to the longer beam-on time to deliver the four 1 cm  $\times$  4 cm fields and electron scattering off the leaf ends. The dose at 3 cm depth shows little difference between the abutting field and the single field except for the dose near the field edges and outside the field (figure 6(b)). For a 6 MeV electron beam, the dose at the phantom surface for the abutting field is almost the same as that for the single field (figure 6(c)). The dose outside the field for the abutting field is only slightly higher than that for the single field. The effect of leaf leakage is very small for a 6 MeV beam and the dose immediately outside the field is thought to be mainly due to the effect of electron scattering in the air. It seems that field abutting with 1 cm beamlets collimated by an electron MLC can provide adequate beam characteristics for MERT for the beam energies

investigated. However, the dose outside the field needs to be minimized through beam energy and leaf sequence optimization.

### 3.2. Comparisons of a photon MLC and an electron MLC

There have been studies on electron beam collimation using a photon MLC (Karlsson *et al* 1999). One of the advantages of using a photon MLC is the possibility of combining both photon and electron beams in the same plan. An essential requirement for matching a photon beam and an electron beam at different depths is that both beams share the same source position. Karlsson *et al* (1999) proposed several modifications to the design of a Varian Clinac 2300CD accelerator, one of which was to replace the intervening air with helium. This could significantly reduce the effect of electron scattering in the air on the beam penumbra. However, filling the accelerator head with helium requires major modifications to the existing accelerator design. In this work, we have investigated an alternative solution—a thin leaf MLC at the electron cutout level to reduce the air scattering effect. As can be seen in figure 7, the unfocused MLC leaf ends could scatter the electrons very significantly to degrade the beam characteristics near the field edges. The Varian MLC has rounded leaf ends, which are expected to have similar dosimetric characteristics as the unfocused MLC studied here. Focused leaf ends could greatly improve the beam edges and provided even slightly better dose profiles inside the field for a 20 MeV electron beam compared with an electron MLC (figures 7(a)–(c)), primarily due to the reduction of electron scattering in the accelerator head (helium versus air). The dose outside the field was slightly lower for the electron MLC than for the photon MLC. For a 6 MeV beam, an electron MLC gave slightly better surface dose profiles both inside and outside the field than the focused and unfocused photon MLC. However, the dose profiles became practically similar at the depth of the maximum dose and greater depths (not shown). Note that in these comparisons, we have placed the phantom surface at 20 cm below the photon MLC and 7 cm below the electron MLC to minimize the effect of electron scattering in the air or helium between the MLC and the phantom. It is evident that an electron MLC will have similar dosimetric characteristics as a photon MLC with focused leaf ends but without the need to replace the air in the accelerator head with helium.

### 3.3. Comparison of beamlet distributions

The accuracy of the beamlet distribution calculation may play an important role in the treatment planning optimization process. Ma *et al* (1999) reported significant differences in the final dose distributions of the optimized treatment plans computed by a commercial inverse treatment planning system with a finite-size pencil beam and the Monte Carlo method. Pawlicki *et al* (1999) demonstrated that inaccurate beamlet distributions may result in under-dosing in the target and over-dosing in the adjacent critical structures, and using the Monte Carlo calculated beamlets could potentially reduce the uncertainty in the photon IMRT dose distributions. This was demonstrated again by Jeraj and Keall (1999) using a Monte Carlo dose calculation based inverse planning algorithm.

It has been shown that the electron beam dose distributions calculated by the pencil beam algorithm as implemented in some commercial treatment planning systems could be fairly uncertain in the regions near material interfaces and inhomogeneities (Cygler *et al* 1987, Shortt *et al* 1986, Mackie *et al* 1994, Ma *et al* 1999). We have computed the beamlet dose distributions using the 3D pencil beam as implemented in the FOCUS treatment planning system (Computerized Medical Systems, St Louis, MO) and compared them with the Monte Carlo calculated beamlets. Figure 8 shows the dose distributions calculated using the Monte

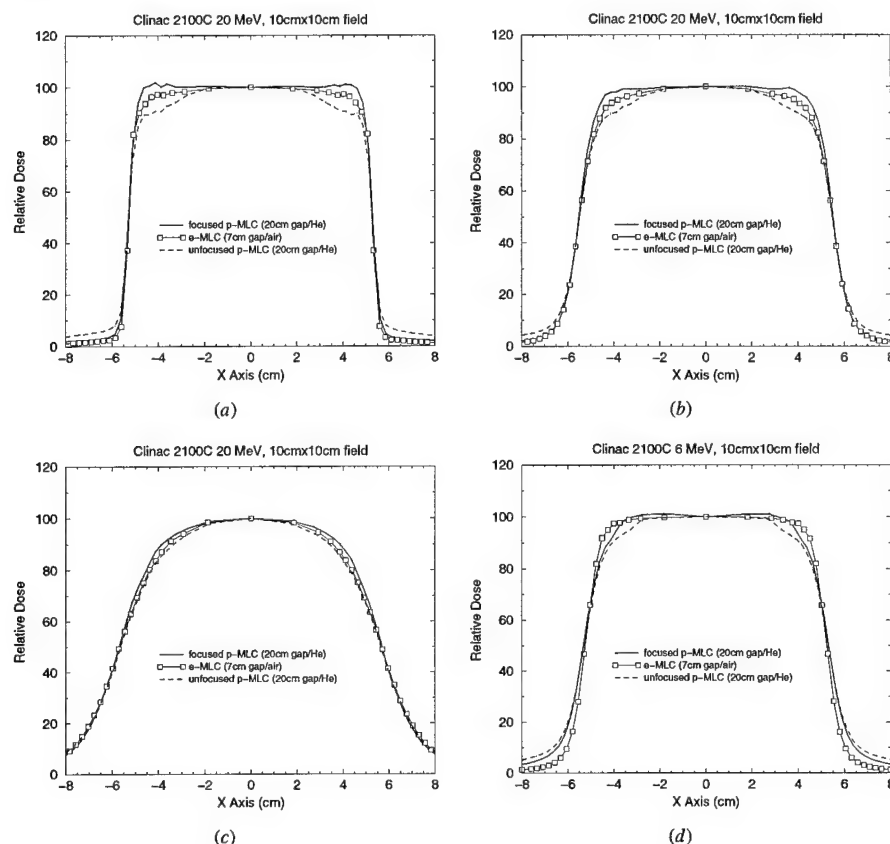


Figure 7. Monte Carlo calculated dose distributions in a water phantom for a 10 cm  $\times$  10 cm field collimated by an electron MLC with 1.5 cm thick tungsten leaves and a photon MLC with 7.5 cm thick leaves on a Varian Clinac 2100C accelerator: (a) surface dose for a 20 MeV beam; (b) dose at 3 cm depth for a 20 MeV beam; (c) dose at 6 cm depth for a 20 MeV beam; (d) surface dose for a 6 MeV beam. The electron MLC has straight leaf ends. The photon MLC has either straight or double-focused leaves.

Carlo method (a, c, e) and the FOCUS 3D pencil beam algorithm (b, d, f) for a 1 cm  $\times$  1 cm 12 MeV beamlet incident on a patient phantom built from CT data. For beamlets with normal incidence (figures 8(a) and (b)), the difference in the dose distributions in the heart was evident: the Monte Carlo calculated isodose lines varied with the heart contour while the pencil beam isodose lines remained symmetrical despite the change in material densities. Figures 8(c) and (d) show the beamlet distributions with a 10 cm air gap. The difference is clearly seen near the surface. The beamlet distributions again differed significantly in the lung for oblique incidence (figures 8(e) and (f)). The axis of the beamlet was intentionally placed to go through soft tissues and bones. The pencil beam isodose lines seemed to stretch according to the beam axis pathlength and showed no signs of electron build-down near the low-density material. These results provided enough evidence to show that to ensure the accuracy of the optimized dose distributions for MERT we should use the Monte Carlo method to compute the electron beamlets for the inverse planning process.

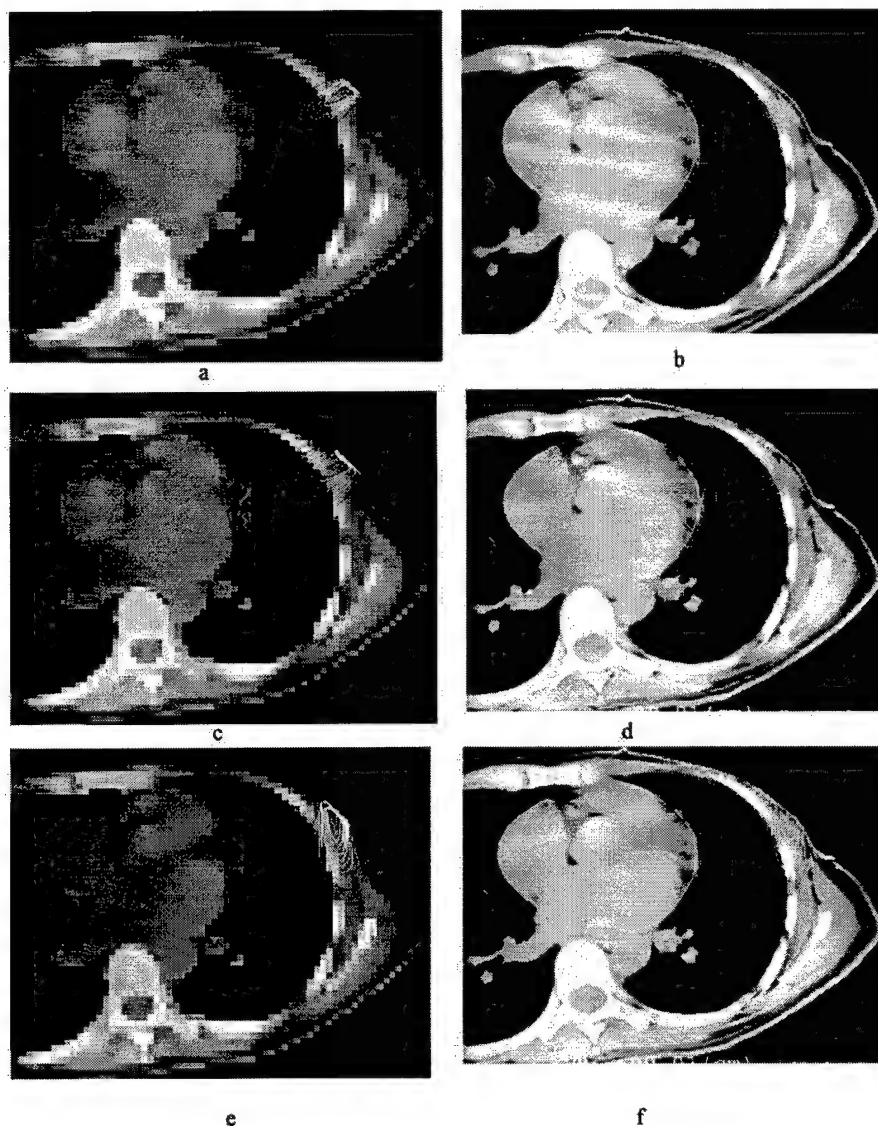


Figure 8. Dose distributions calculated using the Monte Carlo method (*a, c, e*) and the FOCUS 3D pencil beam algorithm (*b, d, f*) for a  $1\text{ cm} \times 1\text{ cm}$  12 MeV beamlet with normal incidence (*a* and *b*), normal incidence plus 10 cm air gap (*c* and *d*), and oblique incidence (*e* and *f*). The beamlet size is defined at 100 cm SSD. The isodose lines shown are 10, 20, 30, 40, 50, 60, 70, 80 and 90% of the maximum dose respectively.

### 3.4. MERT versus photons: a hypothetical treatment plan

Modulated electron radiotherapy is a general purpose technique that should be advantageous in many clinical situations. An exhaustive investigation of the specific advantages of MERT

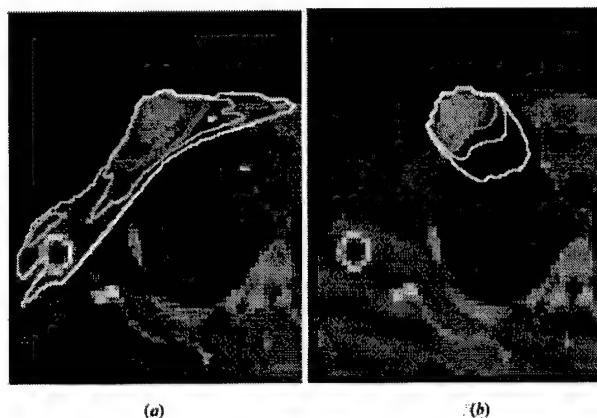


Figure 9. Treatment plans for a hypothetical breast case using tangential 6 MV photon beams (a) and MERT with 6, 12 and 20 MeV electron beams (b). Both plans were calculated using the Monte Carlo method. The isodose lines (90, 70, 50 and 30%) represented 50, 38.9, 25 and 16.7 Gy.

over traditional treatment modalities on a site by site basis is outside the scope of this work. However, to demonstrate the possibility of improving the dose homogeneity in the target and the reduction of the dose in surrounding normal tissues, we compare the dose distributions to treat a hypothetical target using tangential photon beams and MERT. The purpose of the comparison was to illustrate the concept of MERT but not to draw specific conclusions on the use of either technique. Previous investigators have used artificial phantoms and hypothetical targets to mimic different treatment sites (e.g. Hyödynmaa *et al* 1996, Åsell *et al* 1997, Ebert and Hoban 1997). We considered it to be clinically relevant to use a more realistic patient geometry (built from CT data) in our comparison, although the target definition and beam setup are somewhat arbitrary. Figure 9 shows the hypothetical treatment plan using tangential 6 MV photon beams and MERT with normally incident 6, 12 and 20 MeV electron beams. The intensity maps for each electron beam energy are shown in figure 10. The beamlet size was  $1\text{ cm} \times 1\text{ cm}$  at 100 cm at isocentre. It is worth noting here, that as a matter of practicality, it is impossible to create the intensity maps shown in figure 10 using the conventional electron cutout approach but the electron MLC is a viable alternative. The dose distributions for both plans were calculated using the Monte Carlo method. The isodose lines (90, 70, 50 and 30%) were normalized in such a way that the 90% isodose surface would receive the prescribed target dose of 50 Gy. For the photon plan, the 90% dose line also included a margin in the lung to account for the effect of patient breathing. This was not needed for the electron plan as the electron beams were incident *en face* and the electron beamlet dose distributions do not vary significantly with breathing. Figure 11 shows the dose volume histograms (DVH) for the hypothetical treatment plans shown in figure 9. The target DVH together with the right lung DVH are shown in figure 11(a) (as percentage volume) and the right lung DVH and the 'total body' (including everything inside the external contour) DVH are shown in figure 11(b) (as absolute volume).

It is clear that MERT provided better dose homogeneity in the target region than tangential photon beams. Tangential photon beams produced hot spots in the target and cold spots near the skin (figure 11(a)). MERT significantly reduced the dose to the lung relative to tangential photon beams; the maximum dose to the lung was reduced from 50 Gy for a tangential treatment to 35 Gy for MERT (figure 11(a)). However, MERT increased the volume of the lung that

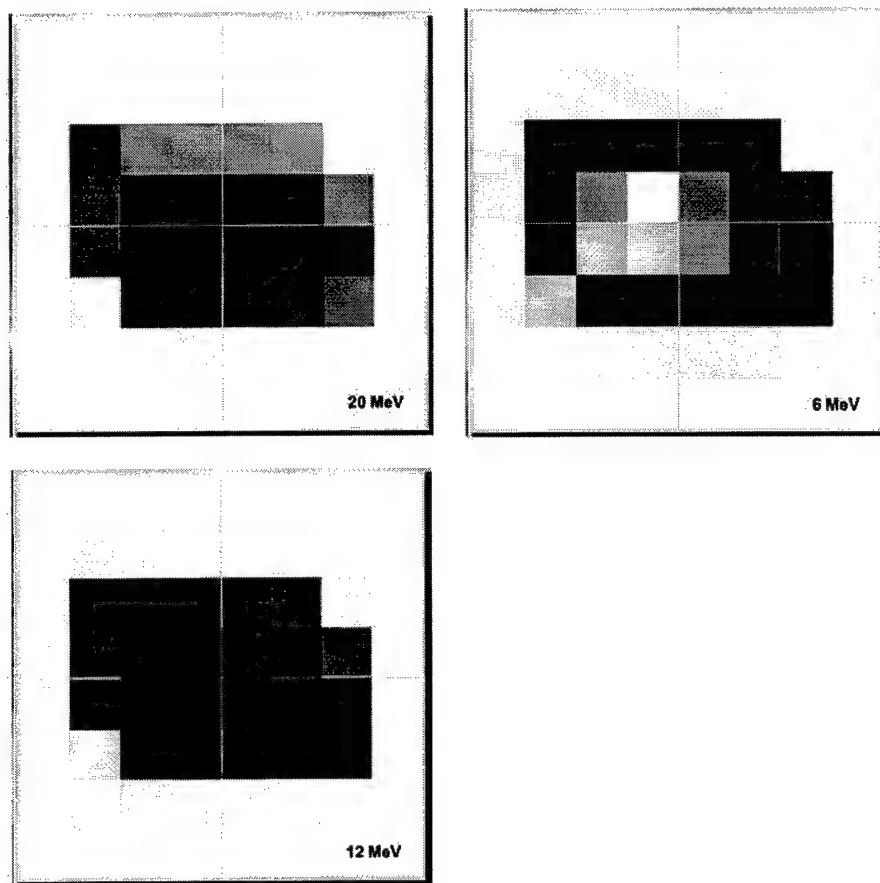


Figure 10. Intensity maps for the three electron beam energies. The beamlet size for each port was  $1 \times 1 \text{ cm}^2$ . Darker beamlets indicate a higher weight than the lighter beamlets and the grey scale for all three maps is in absolute terms.

received a lower dose (10% more volume received 5 Gy and 20% more volume received 2 Gy) compared with tangential photon beams. The clinical significance of the increased lung volume receiving such a low dose needs to be investigated. On the other hand, over  $150 \text{ cm}^3$  of lung received much less dose with MERT compared with tangential photon beams, which could result in reduced lung complications (figure 11(b)). Another clear benefit with MERT is the exclusion of the surrounding normal tissue from the high dose volume (figure 11(b)). Over  $1000 \text{ cm}^3$  of normal tissue received 10–30 Gy less dose in a MERT plan compared with this tangential photon beam plan.

#### 4. Conclusions

In this work, we have investigated the feasibility of modulating both energy and intensity of electron beams for radiotherapy. This was achieved by combining electron beams of different

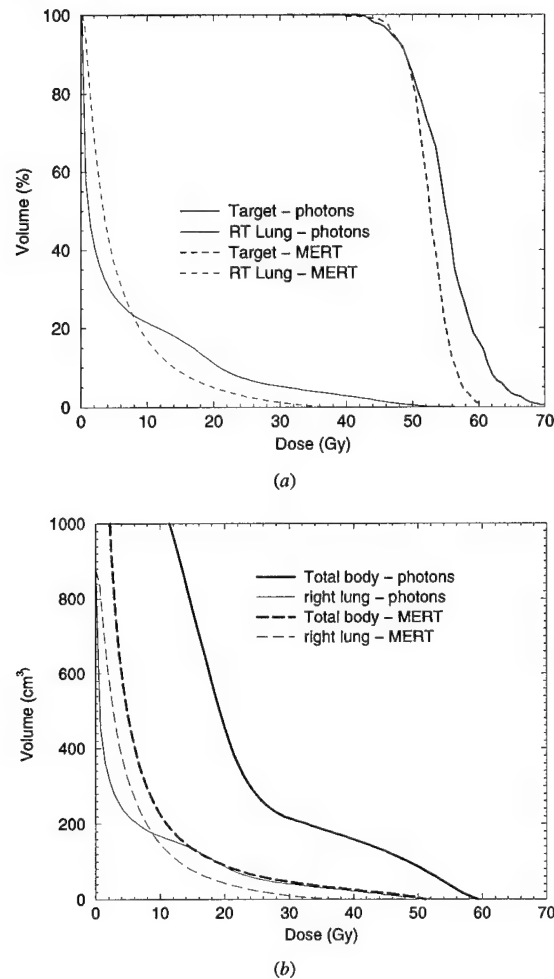


Figure 11. Dose volume histograms (DVH) for the breast treatment plans shown in figure 9: (a) DVH shown as percentage volume for the target (PTV) and the right lung and (b) DVH shown as absolute volume for the right lung and the 'total body' which includes everything inside the external contour.

nominal energies and variable intensity distributions. A prototype electron MLC was built to study the characteristics of MLC-collimated electron beams and the Monte Carlo simulations were used to investigate the effect of MLC leaf material, thickness, shape and location. The beamlet distributions calculated using a 3D electron pencil beam algorithm as implemented in a commercial treatment planning system and the Monte Carlo method were compared for electron beams of different energies, extended air gaps, oblique incidence and heterogeneous geometries. A hypothetical breast case was used to compare the dose distributions using tangential photons and MERT for target coverage (dose homogeneity) and normal tissue sparing (dose reduction in the lung and other surrounding normal tissues).

Our results showed that an electron MLC at the electron cutout location can provide adequate beam collimation for MERT without the need to replace the air in the accelerator head and between the MLC and the phantom with helium. The beam characteristics collimated by an electron MLC are comparable to those collimated by a focused photon MLC. However, the latter requires the accelerator head and between the MLC and the phantom to be filled with helium, which may be impractical for some accelerators because of the major modifications needed to the structure design. An electron MLC can also be used in place of a cutout. The Monte Carlo method can accurately simulate particle transport in cases involving extended air gaps, oblique incidence and heterogeneous anatomy, and is therefore suitable for the beamlet calculation for MERT treatment optimization. Our preliminary results based on a hypothetical breast case demonstrated the potential of MERT for uniform target coverage and normal tissue sparing. To fully explore the potential of MERT, further studies need to be carried out for realistic clinical cases and for other treatment sites such as the head and neck.

#### Acknowledgments

We would like to acknowledge Varian Oncology Systems, Palo Alto, CA, for providing detailed information on the Varian Clinac linear accelerators. We would like to thank our colleagues Fred van den Haak, for making the prototype electron MLC, and Sam Brain, Todd Koumrian, Behrooz Tofighrad and Michael Luxton for help with the computers and software support. This investigation was supported in part by grants CA78331 from the NIH, BC971292, BC990018 and BC990213 from the DOD, Seed Cycle 1 from the RSNA Research and Education Fund, and a consortium agreement with the NumeriX, LLC.

#### References

- AAPM 1983 AAPM TG-21, a protocol for the determination of absorbed dose from high-energy photons and electrons *Med. Phys.* **10** 741
- 1991 AAPM TG-25, Clinical electron beam dosimetry: report of AAPM Radiation Therapy Committee Task Group No. 25 *Med. Phys.* **18** 73–109
- Åsell M, Hyödynmaa S, Gustafsson A and Brahme A 1997 Optimization of 3D conformal electron beam therapy in inhomogeneous media by concomitant fluence and energy modulation *Phys. Med. Biol.* **42** 2083–100
- Bielajew A and Rogers D W O 1987 PRESTA—the parameter reduced electron step algorithm for electron Monte Carlo transport *Nucl. Instrum. Methods B* **18** 165–81
- Bielajew A F, Rogers D W O, Cygler J and Battista J J 1987 A comparison of electron pencil beam and Monte Carlo calculational methods *The Use of Computers in Radiation Therapy* ed I A D Bruinvis (Amsterdam: Elsevier) pp 65–8
- Boesecke R, Doll J, Bauer B, Schlegel W, Pastyr O and Lorenz M 1988 Treatment planning for conformation therapy using a multileaf collimator *Strahlenther. Onkol.* **164** 151–4
- Brewster L, Mohan R, Mageras G, Burman C, Leibel S and Fuks Z 1995 Three dimensional conformal treatment planning with multileaf collimators *Int. J. Radiat. Oncol. Biol. Phys.* **33** 1081–9
- Boyer A L, Geis P B, Grant W, Kendall R and Carol M 1997 Modulated-beam conformal therapy for head and neck tumors *Int. J. Radiat. Oncol. Biol. Phys.* **3** 227–36
- Brahme A 1988 Optimal setting of multileaf collimators in stationary beam radiation therapy *Strahlenther. Onkol.* **164** 343–50
- Chui C S, LoSasso T and Spirou S 1994 Dose calculations for photon beams with intensity modulation generated by dynamic jaw or multileaf collimators *Med. Phys.* **21** 1237–43
- Convery D J and Rosenbloom M E 1992 The generation of intensity-modulated fields for conformal radiotherapy by dynamic collimation *Phys. Med. Biol.* **37** 1359–74
- Cygler J, Battista J J, Scrimger J W, Mah E and Antolak J 1987 Electron dose distributions in experimental phantoms: a comparison with 2D pencil beam calculations *Phys. Med. Biol.* **32** 1073–83
- DeMarco J J, Solberg T D and Smathers J B 1998 A CT-based Monte Carlo simulation tool for dosimetry planning and analysis *Med. Phys.* **25** 1–11

- Ebert M A and Hoban P W 1997 Possibilities for tailing dose distributions through the manipulation of electron beam characteristics *Phys. Med. Biol.* **42** 2065–81
- Faddegon B A, Balogh J, Mackenzie R and Scora D 1998 Clinical considerations of Monte Carlo for electron radiotherapy treatment planning *Radiat. Phys. Chem.* **53** 217–28
- Fraass B A, McShan D L, Kessler M L, Matrone G M, Lewis J D and Weaver T A 1995 A computer-controlled conformal radiotherapy system I: overview *Int. J. Radiat. Oncol. Biol. Phys.* **33** 1139–57
- Hogstrom K R, Mills M D and Almond P R 1981 Electron beam dose calculations *Phys. Med. Biol.* **26** 445–59
- Hyödynmaa S, Gastafsson A and Brahme A 1996 Optimization of conformal electron beam therapy using energy- and fluence-modulated beams *Med. Phys.* **23** 659–66
- ICRU 1984 Radiation dosimetry: Stopping powers for electrons and positrons *ICRU Report 37* (Bethesda, MD: ICRU)
- Jeraj R and Keall P 1999 Monte Carlo-based inverse treatment planning *Phys. Med. Biol.* **44** 1885–96
- Jiang S B 1998 Development of a compensator based intensity modulated radiation therapy system *PhD Thesis* Medical College of Ohio, Toledo, OH
- Jiang S B, Boyer A L and Ma C-M 1999 A hybrid system for IMRT inverse planning and dose verification *Int. J. Radiat. Oncol. Biol. Phys.* **41** 123
- Kapur A 1999 Monte Carlo dose calculations for clinical electron and intensity modulated photon beams in radiotherapy *PhD Thesis* Stanford University, Stanford, CA, USA
- Kapur A, Ma C-M, Mok E and Findley D 1997 Characterization of small field electron beams for radiotherapy using Monte Carlo simulations *Proc. 12th Int. Conf. on the Use of Computers in Radiation Therapy (Salt Lake City, Utah)* (Madison, WI: Medical Physics Publishing) pp 157–8
- Kapur A, Ma C-M, Mok E, Findley D and Boyer A L 1998 Monte Carlo calculations of clinical electron beam output factors *Phys. Med. Biol.* **43** 3479–94
- Karlsson M G, Karlsson M K and Ma C-M 1999 Treatment head design for multileaf collimated high-energy electrons *Med. Phys.* **26** 2125–32
- Karlsson M K, Karlsson M G and Zackrisson B 1998 Intensity modulation with electrons: calculations, measurements and clinical applications *Phys. Med. Biol.* **43** 1159–69
- Kawrakow I, Fippel M and Friedrich K 1996 3D electron dose calculation using a voxel based Monte Carlo algorithm *Med. Phys.* **23** 445–57
- Keall P J and Hoban P 1996 Superposition dose calculation incorporating Monte Carlo generated electron track kernels *Med. Phys.* **23** 479–85
- Kutcher G J, Mageras G S and Leibel S A 1995 Control, correction and modeling of setup errors and organ motion *Semin. Radiat. Oncol.* **5** 134–45
- Leibel S A et al 1992 Three-dimensional conformal radiation therapy at the Memorial Sloan-Kettering Cancer Center *Semin. Radiat. Oncol.* **2** 274–89
- Lief E P, Larsson A and Humm J L 1996 Electron dose profile shaping by modulation of a scanning elementary beam *Med. Phys.* **23** 33–44
- Ling C C et al 1996 Conformal radiation treatment of prostate cancer using inversely-planned intensity-modulated photon beams produced with dynamic multileaf collimation *Int. J. Radiat. Oncol. Biol. Phys.* **35** 731–40
- LoSasso T, Chui C S, Kutcher G J, Leibel S A, Fuks Z and Ling C C 1993 The use of multileaf collimators for conformal radiotherapy of carcinomas of the prostate and nasopharynx *Int. J. Radiat. Oncol. Biol. Phys.* **25** 161–70
- Ma C-M, Mok E, Kapur A and Findley D 1997 Improvement of small-field electron beam dosimetry by Monte Carlo simulations *Proc. 12th Int. Conf. on the Use of Computers in Radiation Therapy (Salt Lake City, Utah)* (Madison, WI: Medical Physics Publishing) pp 159–62
- Ma C-M, Mok E, Kapur A, Pawlicki T A, Findley D, Brain S, Forster K and Boyer A L 1999 Clinical implementation of a Monte Carlo treatment planning system for radiotherapy *Med. Phys.* **26** 2133–43
- Ma C-M and Nahum A E 1993 Calculation of absorbed dose ratios using correlated Monte Carlo sampling *Med. Phys.* **20** 1189–99
- Ma C-M, Reckwerdt P, Holmes M, Rogers D W O and Geiser B 1995 DOSXYZ Users Manual *National Research Council Report PIRS-0509(B)* (Ottawa: NRC)
- Ma L, Boyer A L, Xing L and Ma C-M 1998 An optimized leaf setting algorithm for beam intensity modulation using dynamic multileaf collimators *Phys. Med. Biol.* **43** 1629–43
- Mackie T R, Holmes T W, Reckwerdt P J and Yang J 1995 Tomotherapy: optimized planning and delivery of radiation therapy *Int. J. Imaging Syst. Technol.* **6** 43–55
- Mackie T R et al 1994 The OMEGA project: comparison among EGS4 electron beam simulations, 3D Fermi-Eyges calculations, and dose measurements *Proc. 11th Int. Conf. on the Use of Computers in Radiation Therapy (Manchester, UK)* pp 152–3

- Mageras G S *et al* 1994 Initial clinical experience with computer-controlled conformal radiotherapy using the MM50 microtron *Int. J. Radiat. Oncol. Biol. Phys.* **30** 971–8
- Mah E, Antolak J, Scrimger J W and Pattista J J 1989 Experimental evaluation of a 2D and 3D pencil beam algorithm *Phys. Med. Biol.* **34** 1179–94
- McShan D L, Fraass B A, Kessler M L, Matrone G M, Lewis J D and Weaver T A 1995 A computer-controlled conformal radiotherapy system. II: sequence processor *Int. J. Radiat. Oncol. Biol. Phys.* **33** 1159–72
- Mohan R 1997 Why Monte Carlo? *Proc. 12th Int. Conf. on the Use of Computers in Radiation Therapy* (Salt Lake City, UT) (Madison, WI: Medical Physics Publishing) pp 16–18
- Nelson R, Hirayama H and Rogers D W O 1985 The EGS4 code system *Stanford Linear Accelerator Center Report SLAC-265* (Stanford, CA: SLAC)
- Pawlicki T A, Jiang S B, Deng J, Li J S and Ma C-M 1999 Monte Carlo calculated beamlets for photon beam inverse planning *Med. Phys.* **26** 1064–5
- Powlis W D *et al* 1993 Initiation of multileaf collimator conformal radiation therapy *Int. J. Radiat. Oncol. Biol. Phys.* **25** 171–9
- Rogers D W O and Bielajew A F 1990 Monte Carlo techniques of electrons and photons for radiation dosimetry *Dosimetry of Ionizing Radiation* vol III, ed K Kase, B E Bjarngard and F H Attix (New York: Academic) pp 427–539
- Rogers D W O, Faddegon B A, Ding G X, Ma C-M, Wei J S and Mackie T R 1995 BEAM: a Monte Carlo code to simulate radiotherapy treatment units *Med. Phys.* **22** 503–25
- Shortt K R, Ross C K, Bielajew A F and Rogers D W O 1986 Electron beam dose distributions near standard inhomogeneities *Phys. Med. Biol.* **31** 235–49
- Takahashi S 1965 Conformation radiotherapy-rotation techniques as applied to radiography and radiotherapy of cancer *Acta Radiol. Suppl.* **242** 1–142
- Wang L, Chui C and Lovelock M 1998 A patient-specific Monte Carlo dose-calculation method for photon beams *Med. Phys.* **25** 867–78
- Webb S 1992 Optimization by simulated annealing of three-dimensional conformal treatment planning for radiation fields defined by multi-leaf collimator: II. Inclusion of two-dimensional modulation of x-ray intensity *Phys. Med. Biol.* **37** 1689–704
- 1997 *The Physics of Conformal Radiotherapy: Advances in Technology* (Bristol: Institute of Physics Publishing)
- Yu C X, Symons J M, Du M N, Martinez A A and Wong J W 1995 A method for implementing dynamic photon beam intensity modulation using independent jaws and multileaf collimators *Phys. Med. Biol.* **40** 769–87
- Zackrisson B and Karlsson M 1996 Matching of electron beams for conformal therapy of target volumes at moderate depths *Radiother. Oncol.* **3** 261–70
- Zhang G G, Rogers D W O, Cygler J E and Mackie T R 1999 Monte Carlo investigation of electron beam output factors versus size of square cutout *Med. Phys.* **26** 743–50

# Electron beam modeling and commissioning for Monte Carlo treatment planning

Steve B. Jiang,<sup>a)</sup> Ajay Kapur, and C.-M. Ma

*Department of Radiation Oncology, Stanford University School of Medicine, 300 Pasteur Drive, Stanford, California 94305-5304*

(Received 19 April 1999; accepted for publication 22 October 1999)

A hybrid approach for commissioning electron beam Monte Carlo treatment planning systems has been studied. The approach is based on the assumption that accelerators of the same type have very similar electron beam characteristics and the major difference comes from the on-site tuning of the electron incident energy at the exit window. For one type of accelerator, a reference machine can be selected and simulated with the Monte Carlo method. A multiple source model can be built on the full Monte Carlo simulation of the reference beam. When commissioning electron beams from other accelerators of the same type, the energy spectra in the source model are tuned to match the measured dose distributions. A Varian Clinac 2100C accelerator was chosen as the reference machine and a four-source beam model was established based on the Monte Carlo simulations. This simplified beam model can be used to generate Monte Carlo dose distributions accurately (within 2%/2 mm compared to those calculated with full phase space data) for electron beams from the reference machine with various nominal energies, applicator sizes, and SSDs. Three electron beams were commissioned by adjusting the energy spectra in the source model. The dose distributions calculated with the adjusted source model were compared with the dose distributions calculated using the phase space data for these beams. The agreement is within 1% in most of cases and 2% in all situations. This preliminary study has shown the capability of the commissioning approach for handling large variation in the electron incident energy. The possibility of making the approach more versatile is also discussed. © 2000 American Association of Physicists in Medicine.[S0094-2405(00)03401-5]

**Key words:** electron beam, treatment planning, Monte Carlo simulation, beam commissioning, source modeling

## I. INTRODUCTION

Electron beam radiation therapy is used extensively to treat head and neck cancers to avoid the irradiation of the spinal cord, and to treat chest walls to limit the irradiated volume of lung. The currently available commercial systems for electron treatment planning mostly utilize the Hogstrom algorithm as the dose calculation engine,<sup>1</sup> which is based on Fermi-Eyges theory.<sup>2,3</sup> Due to the inappropriate treatment of electron transport in inhomogeneous phantoms, large discrepancies (10% or more) in the dose distributions have been observed between the current analytical algorithms and measurements or Monte Carlo simulations in some clinical situations where the treatment volumes encompass air cavities and bone.<sup>4-7</sup> Accurate dose calculation is an important factor for the widespread clinical use of electron therapy and the development of new electron therapy techniques, such as electron beam or mixed electron/photon beam intensity modulated therapy, which are expected to improve the conformality of the delivered dose distribution to the target volume for some disease sites.<sup>8-10</sup>

The Monte Carlo method is generally considered to be the most accurate approach for electron dose calculation under all circumstances.<sup>11-16</sup> In particular, Monte Carlo simulation can handle electron multiple scattering in the presence of inhomogeneities (such as bone and air cavity) much more

accurately than any existing analytical dose models. The necessity of accurate electron dose calculation has motivated many efforts to develop Monte Carlo electron beam treatment planning systems.<sup>6,7,17-22</sup> Due to the rapid development of computer technology and the employment of innovative variance reduction techniques, it is expected that treatment planning systems utilizing a Monte Carlo dose engine will begin to serve in routine clinical practice in the next few years.<sup>6,7,20-29</sup>

The commissioning procedure for a Monte Carlo treatment planning system can be different from that for a conventional planning system, since it requires more detailed and accurate clinical beam data.<sup>22</sup> For example, the phase space information (position, direction and energy) is needed to represent particles coming out of the accelerator treatment head. This information is extremely difficult, if not impossible, to acquire experimentally, mainly due to the very high intensity of the therapeutic electron beam.<sup>30</sup> Some researchers tried to extract the phase space information from the limited set of measured dose data (such as depth dose curves and dose profiles) by using a simple beam model.<sup>31</sup> Although the approach may have great potential, at least currently it uses many approximations and the accuracy of the reconstructed phase space cannot be guaranteed. The only method to obtain the accurate electron beam phase space

information is to simulate the accelerator treatment head using the Monte Carlo method.<sup>32-34</sup> An EGS4 Monte Carlo user code, OMEGA BEAM, was developed specifically for this purpose.<sup>34</sup> Using the BEAM code, the accelerator treatment head and electron applicator can be simulated to yield a data file containing the phase space information for tens of millions of particles exiting the treatment head. The phase space data can then be used as input to calculate dose distributions in a patient's CT phantom.<sup>34</sup>

However, direct simulation of the accelerator treatment head using the Monte Carlo method is not a viable commissioning approach for Monte Carlo treatment planning. The beam characteristics are usually different due to variation in accelerator designs and on-site beam tuning. The simulated electron beam phase space for one accelerator may not be used directly for another. It is necessary to simulate each accelerator individually to obtain the phase space information. This fact presents three problems for the clinical acceptance of Monte Carlo treatment planning systems. First, the simulation of the accelerator treatment head for every energy/applicator combination takes much more time than the commissioning of a conventional electron planning system. As estimated by Faddegon *et al.*,<sup>22</sup> even for users with Monte Carlo simulation experience, it takes about two months of CPU time to generate a complete set of beam data for a single accelerator. Second, the storage of the phase space information requires a lot of computer disk space. For each energy/applicator combination, a phase space file is usually pre-calculated and stored in the treatment planning computer. For accurate treatment planning, a phase space file occupies hundreds of megabytes of disk space. This is certainly a substantial burden for the computer resources at most clinical centers. Third, the generation and quality assurance of the phase space data files by simulating the treatment head requires Monte Carlo simulation experience. Therefore, it is a prohibitive task for general users to perform Monte Carlo simulations for their own accelerators.

In this paper, a hybrid approach for commissioning electron beam Monte Carlo treatment planning systems is proposed. This method combines the advantages of the full Monte Carlo simulation and the method of Janssen *et al.*<sup>31</sup> It is based on the assumption that accelerators of the same type have very similar electron beam characteristics and the major difference is the electron incident energy at the exit window due to beam tuning during linac acceptance. By simulating a reference accelerator for a particular type of accelerator using the Monte Carlo BEAM code,<sup>34</sup> a beam model is constructed using the resultant phase space information. The beam model is a simplified implementation of a previously developed multiple source model which can compress the Monte Carlo phase space data by a factor of 1000 or more.<sup>35-37</sup> When commissioning another accelerator of the same type, the energy spectra in the beam model are tuned to match standard measured data such as depth doses and dose profiles. Using this approach, we do not have to simulate every accelerator individually. Only one reference accelerator needs to be simulated for a type of accelerator, and this can be done carefully by someone with Monte Carlo exper-

tise. In this paper, a Varian Clinac 2100C accelerator is chosen as the reference machine. The machine is simulated using the BEAM code<sup>34</sup> and a four-source beam model is established based on the simulated beam phase space information. The accuracy of the Monte Carlo dose distributions calculated with the model is verified. Then, the model based on the reference beam is used to commission three other electron beams. Two beams are also from the reference machine but with incident energies significantly different from that of the reference beam. The third beam is from another Clinac 2100C machine at a different institution.<sup>38</sup> The validity of the proposed commissioning approach is demonstrated by commissioning these three beams.

## II. METHODS AND MATERIAL

### A. Beam modeling

#### 1. General considerations

Beam modeling is the first step in our hybrid commissioning procedure for a Monte Carlo treatment planning system. A beam model for a type of accelerator is established using the Monte Carlo simulated phase space information for the reference beam. The beam data are modeled using the multiple source model developed by Ma *et al.*,<sup>35-37</sup> which is modified in the current work for use in the commissioning procedure. The major modifications of the model are discussed here.

The multiple source model is based on the observation that particles from different components of an accelerator have significantly different energy, angular, and spatial distributions, while the particles from the same component have very similar characteristics.<sup>35-37</sup> Therefore, the particles from different components of an accelerator can be treated as they are from different sub-sources. Each sub-source represents a critical component in the treatment head and its geometrical dimensions are determined by the component dimensions. Each sub-source has its own energy spectrum and planar fluence distribution derived from the simulated phase space data. When the model is used for dose calculation, the incident energy and position of a particle are sampled from the corresponding stored energy spectrum and planar fluence distribution. The incident direction of the particle is reconstructed by sampling the position of the particle on the sub-source and on the phantom surface. The correlation between the particle position and incident angle is naturally retained.

A primary reason to develop the multiple source model was to find a concise way to replace the huge phase space data files generated from Monte Carlo simulations.<sup>35,36</sup> The emphasis of the current work is to develop a clinically practical commissioning procedure for Monte Carlo treatment planning. The multiple source model is simplified to make the commissioning procedure as simple as possible while trying to maintaining dose calculation accuracy under all circumstances of clinical relevance. The number of sub-sources in the model is minimized and only those sub-sources of dosimetric significance are retained. The dependence of the model on the detailed information of accelerators is reduced. Sub-sources are represented by dimensionless geometric ob-

jects, such as points and lines, instead of the actual geometrical shapes and sizes of the treatment head components as used previously.<sup>35,36</sup>

Ma *et al.* established their multiple source model from the Monte Carlo simulated phase space data on the patient surface (at 100 cm SSD) and the last scraper of the electron applicator was included in the model as a sub-source.<sup>35,36</sup> In this work, the treatment head is simulated using the BEAM code down to just above the last scraper of the electron applicator,<sup>34</sup> where the patient specific cutout is inserted. The last scraper, as well as the field-defining cutout, are simulated together with the patient CT phantom when performing Monte Carlo treatment planning dose calculations. The advantage of this method is that the beam model is patient independent. However, this approach, compared to that of Ma *et al.*,<sup>35,36</sup> requires more careful beam modeling since an air gap between the last scraper and patient surface is not included in the original BEAM simulation.

In the present paper, the beam modeling approach is applied to a Varian Clinac 2100C machine at Stanford Medical Center, which is chosen as the reference machine to build beam models. At first, a very detailed model for each beam is used as the starting point. All the critical components of the treatment head are modeled as sub-sources. With this model, the phase space information of the electron beam can be precisely reconstructed and the dose distribution in a water phantom can be accurately calculated. Then, the number of sub-sources is gradually reduced while maintaining the accuracy in dose distribution calculation. We find that a point electron source with the energy spectrum obtained from the Monte Carlo simulation is able to give a reasonably accurate depth-dose curve, which is consistent with the previous observation.<sup>36</sup> By adding another point photon source, the bremsstrahlung tail in the depth dose distribution can be reproduced accurately. However, it is found that the penumbra at the phantom surface generated with this two point source model is sharper compared to that generated with the full phase space data. In order to get the dose profiles correct, we find that, in addition to the two point sources, two square ring electron sources (which emit electrons isotropically) are needed to represent electrons scattered from the applicator scrapers. (The term *square ring* is used here to represent the edge of a square.) Therefore, the beam model should include four sub-sources: a point electron source for direct electrons (which do not interact with the beam defining system) and electrons scattered from the primary collimator, movable jaws and shieldings, a point photon source for all contaminant photons, and two square ring electron sources for electrons scattered from the first two scrapers of the electron applicator (the third also last scraper is not included in the model).

As described previously, beam modeling consists of two steps, namely, beam representation and beam reconstruction.<sup>35,36</sup> In beam representation, parameters in the model are extracted from the simulated phase space file. In the current simplified model, these parameters include the positions and relative intensities of the sub-sources, the energy spectra for particles inside and outside the field for each

sub-source, and the planar fluence distributions on the scoring plane (directly above the last scraper) for each sub-source. Beam reconstruction is performed when using the model for dose calculations. The phase space information for each particle, including the energy, position and direction, is reconstructed from the scored source parameters.

## 2. Beam representation

The positions of the virtual electron and photon point sources can be determined using a method described in Ref. 36, which is analogous to the pinhole method.<sup>39</sup> A thin annular aperture is selected on the scoring plane and phase space particles are allowed to pass through the aperture and form an image at a distance below the scoring plane. Ray lines drawn through the center of the aperture and the peak of the aperture image form a virtual focal spot, which is adopted as the position of the point source. This pinhole method is very effective for the photon point source. However, we find that for electrons, this method is only applicable to high energy beams. For lower energy beams, e.g., 6 MeV, the virtual SSD determined with this method is greatly overestimated and dependent on the radius of the thin annular aperture on the scoring plane. This is due to the fact that the in-air multiple scattering of low energy electrons is significant. To overcome this problem we performed another Monte Carlo simulation of the accelerator treatment head by replacing the intervening air with vacuum. Then, based on the new phase space data, this pinhole method can be used to generate the correct position for the virtual electron point source, which is independent of the sampling radius. The effect of in-air multiple scattering is taken into account during beam reconstruction by adding a perturbation to the electron incident direction, as discussed later.

Two square ring sources of electrons are located at the corresponding positions of the two applicator scrapers. The sides of the square rings correspond to the actual openings of the scrapers.

The energy spectrum for each sub-source is derived from the simulated phase space data. It was found that the mean energy of the electrons is relatively uniform inside the field as well as outside the field. The change of mean energy with the distance from the central axis is more like a step function.<sup>36</sup> Therefore, in the current model, each sub-source has two different energy spectra, one for electrons inside and the other for electrons outside the treatment field. Parameters stored in the model are the minimum and maximum energies, number of energy bins as well as the relative fluence for each energy bin. The minimum and maximum energies correspond to the cutoff energies (ECUT or PCUT) and the incident energy used in the accelerator simulation. The number of bins is determined by the desired resolution. For example, if we want the uncertainty in the calculated depth of 50% dose,  $R_{50}$ , to be less than 1%, the uncertainty in the peak position of the energy spectrum should be within 1% and therefore the bin width should be smaller than 1% of the peak energy. For the 12 MeV beam, we used 128 bins and then the bin width is less than 0.1 MeV. This bin width is

also found to be small enough to represent the peak width of the energy spectrum, which has a significant effect on the slope of the depth dose fall-off.

The planar fluence distribution for each sub-source is also derived from the simulated phase space data and recorded on the scoring plane using a grid scheme. Within each pixel of the grid, the planar fluence is assumed to be uniform. The dimension of a pixel is dependent on field size, usually from 1 to 3 mm. Parameters used to represent the planar fluence distribution include the treatment field dimension, the number of pixels and the relative intensity of each pixel, for each sub-source. It has been found that in general, the mean energy varied from position to position in the treatment field by less than 10% for a given sub-source.<sup>36</sup> Thus, it is reasonable to store and then sample the particle energy and position independently.

The angular distributions are not scored explicitly. They are reconstructed during the dose calculation, as described in the next section.

Finally, the simulated phase space information is represented with a set of parameters for each sub-source. The resultant source parameter file is much smaller (about 100 kilobytes) than the original phase space file (>100 megabytes).

### 3. Beam reconstruction

When performing dose calculation in a patient's CT phantom, the source parameter file is used to reconstruct the phase space information (energy, position and direction) of every incident particle. The beam reconstruction process consists of the following steps:

- (1) Determine from which particular sub-source a particle originates by sampling from the relative source intensity of each sub-source.
- (2) Determine the position on the sub-source (excluding point sources) where the particle is emitted.
- (3) Sample the particle position on the scoring plane from the fluence pattern for the sub-source.
- (4) Sample the particle energy from the energy spectrum for the given sub-source based on the particle position (inside or outside the treatment field).
- (5) Determine the particle incident angle by connecting the position on the sub-source from where the particle is emitted and the position of the particle on the scoring plane.
- (6) Add in-air perturbation on the particle direction if it is an electron.

The sampling from the relative source intensity distribution is done by a table-look-up method.<sup>35</sup> All the sub-sources are in turn numbered from 1 to  $N$  (here  $N=4$  for accelerators with designs similar to the Varian Clinac 2100C machine) and the relative intensity of the  $i$ th sub-source is  $p_i$  ( $i=1, \dots, N$ ). The accumulative source intensity for the  $i$ th sub-source,  $P_i (= \sum_{j=1}^i p_j)$ , is multiplied by a large integer  $M$ . The value of  $M$  is determined according to the desired sampling precision of the relative source intensity. For ex-

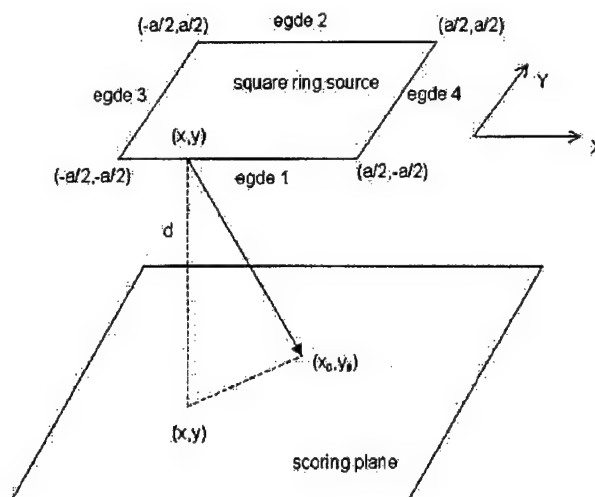


FIG. 1. A diagram for illustrating the sampling algorithm from a square ring source. The origin of the coordinate system is at the center of the square ring.

ample,  $M=1000$  corresponds to the precision of 0.1% in sampling from the relative source intensity distribution. Then, a one dimensional array of  $M$  elements is prepared by assigning value  $i$  to array elements from  $INT(MP_{i-1})$  to  $INT(MP_i)$ , where the operator  $INT$  returns the integer part of a real number. During the beam reconstruction, a random integer number  $K$  between 1 and  $M$  is generated and the value of the  $K$ th array element is the sub-source number where the particle is emitted. Such a table-look-up method is of very high sampling speed and efficiency. Its speed is also independent of the number of sub-sources. The sampling precision is usually adequate as long as an large enough array is used.

According to the energy spectra on the scoring plane, the bin number in which the particle energy falls is also sampled using the table-look-up method. An additional uniform sampling is done within the given energy bin to make the particle energy continuous.

The same table-look-up method is also used to sample the pixel number corresponding to a particle position on the scoring plane. Another sampling is performed uniformly to determine the particle's coordinates within the chosen pixel.

For the point sources, the incident angle of the particle is determined by constructing a ray line from the point source to the position of the particle on the scoring plane. For the square ring electron sources, we need to determine where the electron comes from on the ring. This is done in two steps. First, we determine from which edge of the square ring the electron is emitted. Second, we determine from where on the chosen edge the electron comes.

As illustrated in Fig. 1, a square ring of size  $a \times a$  is located above the scoring plane at a distance  $d$ . We assume that the square ring edge emits electrons uniformly and isotropically. Under this approximation, the probability for an electron on the scoring plane to come from a point on the ring is proportional to the inverse square of the distance be-

tween the points on the ring and plane. This approximation greatly simplifies the sampling process. It is found that the angular distribution of the scattered electrons reconstructed based on the fluence distribution on the scoring plane and the emitting position on the square ring source is reasonably accurate, although electrons scattered from the applicator scraper mainly correspond to electrons incident on the vertical face of the scraper and are dominantly forward directed.<sup>40</sup> Furthermore, the dose profile at the patient surface is greatly influenced by electrons scattered from the last scraper or cut-outs, which are not included in the source model but will be accurately simulated with the patient CT phantom.

For an electron at position  $(x_0, y_0)$  on the scoring plane (see Fig. 1), the probability for it to have come from the  $i$ th edge is given as

$$p'_i(x_0, y_0) \sim \frac{1}{C_i} \left[ \arctan\left(\frac{x_0 + a/2}{C_i}\right) - \arctan\left(\frac{x_0 - a/2}{C_i}\right) \right] \text{ for } i=1,2, \quad (1)$$

$$p'_i(x_0, y_0) \sim \frac{1}{C_i} \left[ \arctan\left(\frac{y_0 + a/2}{C_i}\right) - \arctan\left(\frac{y_0 - a/2}{C_i}\right) \right] \text{ for } i=3,4, \quad (2)$$

where

$$C_1 = \sqrt{(y_0 + a/2)^2 + d^2}, \quad (3)$$

$$C_2 = \sqrt{(y_0 - a/2)^2 + d^2}, \quad (4)$$

$$C_3 = \sqrt{(x_0 + a/2)^2 + d^2}, \quad (5)$$

$$C_4 = \sqrt{(x_0 - a/2)^2 + d^2}. \quad (6)$$

Using the probabilities given above, the edge from which the electron has come can be sampled. Then, the position  $(x, y)$  on the chosen edge is further sampled. For edges 1 and 2,

$$x = x_0 - C_i \cdot \tan \left[ (1 - \xi) \cdot \arctan\left(\frac{x_0 + a/2}{C_i}\right) + \xi \cdot \arctan\left(\frac{x_0 - a/2}{C_i}\right) \right] \quad i=1,2, \quad (7)$$

$$y = \begin{cases} -a/2 & \text{for } i=1 \\ a/2 & \text{for } i=2 \end{cases}, \quad (8)$$

and for edges 3 and 4,

$$x = \begin{cases} -a/2 & \text{for } i=3 \\ a/2 & \text{for } i=4 \end{cases} \quad (9)$$

$$y = y_0 - C_i \cdot \tan \left[ (1 - \xi) \cdot \arctan\left(\frac{y_0 + a/2}{C_i}\right) + \xi \cdot \arctan\left(\frac{y_0 - a/2}{C_i}\right) \right] \quad i=3,4, \quad (10)$$

where  $\xi$  is a random number uniformly distributed from 0 to 1.

After the electron position on the square ring is determined, the connection of this position to the position on the scoring plane gives the electron's incident direction, which needs to be additionally perturbed to address the in-air multiple scattering.

In a previous implementation of this model, the effect of electron multiple scattering in air as well as other materials on its path to the scoring plane was taken into account by sampling the electron perturbation angle from a Monte Carlo simulated angular distribution.<sup>36</sup> This angular distribution was stored while performing the Monte Carlo simulation for the accelerator and only included electrons falling into a small region (e.g., of 1 cm radius) around beam central axis. In the current work, the effect of in-air multiple scattering is considered more accurately using the Fermi-Eyges theory.<sup>2,3</sup> The effect of other materials is considered by adding a parameter to the standard deviation of the angular distribution. The Fermi-Eyges theory is a well-known small-angle theory and can predict the multiple scattering effect of megavoltage electrons in air or other heavier materials as long as the electron effective pathlengths are small.<sup>41,42</sup>

Assume that an electron initially travels along the  $z$  axis. According to the Fermi-Eyges theory, the distributions for the projections of the polar angle,  $\theta$ , on the  $x-z$  plane,  $\theta_x$ , and on the  $y-z$  plane,  $\theta_y$ , are both Gaussian after electrons travel a distance, and are given as<sup>3,42</sup>

$$f(\theta_x) = \frac{1}{\sqrt{2\pi}\sigma_{\theta_x}} \exp\left(-\frac{\theta_x^2}{2\sigma_{\theta_x}^2}\right), \quad (11)$$

$$f(\theta_y) = \frac{1}{\sqrt{2\pi}\sigma_{\theta_y}} \exp\left(-\frac{\theta_y^2}{2\sigma_{\theta_y}^2}\right), \quad (12)$$

where  $\sigma_{\theta_x}$  and  $\sigma_{\theta_y}$  are the standard deviations for each Gaussian distribution, respectively. In a homogeneous material, and without the presence of an electromagnetic field, both standard deviations should be the same, so we let  $\sigma = \sigma_{\theta_x} = \sigma_{\theta_y}$ . Under the small-angle approximation

$$\theta^2 = \theta_x^2 + \theta_y^2, \quad (13)$$

therefore the polar angle  $\theta$  obeys a radial Gaussian distribution while the azimuthal angle  $\phi$  is uniformly distributed in  $[0, 2\pi]$ . Hence the sampling method for these two angles is given as follows:

$$\theta = \sigma \sqrt{-2 \ln \xi_1}, \quad (14)$$

$$\phi = 2\pi \xi_2, \quad (15)$$

where  $\xi_1$  and  $\xi_2$  are random numbers uniformly distributed in  $[0, 1]$ .

According to the Fermi-Eyges theory,  $\sigma$  can be calculated as<sup>3,42</sup>

$$\sigma^2 = A_0 - A_1^2/A_2, \quad (16)$$

where

$$A_i = \frac{1}{2} \int_0^l K(l-t)^i dt, \quad i=0,1,2. \quad (17)$$

Here,  $K$  is the electron linear scattering power and  $l$  is the distance at which electrons travel. The electron linear scattering power can be fitted well using a simple formula proposed by Werner *et al.*:<sup>43</sup>

$$K(E) = \alpha E^{-\beta}. \quad (18)$$

Using this formula we fitted the linear scattering power data in air supplied by ICRU Report 35<sup>44</sup> and found that  $\alpha = 3.329 \times 10^{-3} \text{ rad}^2/\text{cm}$  and  $\beta = 1.638$ .  $E$  is the electron energy in MeV and sampled from the energy spectrum at the scoring plane. The energy loss of electrons in air is usually very small and can be ignored when they travel from the virtual source to the scoring plane. The mean energy loss of 6 MeV electrons after traveling 100 cm in air is about 4% of its initial energy (estimated using the stopping power) and it is about 2% for 20 MeV electrons. Therefore  $\sigma$  can be given as

$$\sigma^2 = \frac{1}{8} K(E)l, \quad (19)$$

which is a function of electron energy and the distance between the virtual source and the position on scoring plane. During beam reconstruction, according to the sampled electron energy, positions on the scoring plane and on the virtual source,  $\sigma$  can be calculated. Then using Eqs. (14) and (15)  $\theta$  and  $\phi$  are sampled and a perturbation is added to the electron's incident direction.

The perturbation caused by in-air multiple scattering can be directly calculated using Eq. (19) for electrons from the squaring ring sources. For direct electrons, there are other accelerator components in their paths from the virtual point source to the scoring plane in addition to the intervening air, such as the exit window, scattering foil, monitor chamber, mirror and protection window. The effect of these materials on electron angular distribution has been mainly included in the determination of the virtual electron point source position. We also need to take into account the angular perturbation caused by these materials. If we know precisely the material and thickness of these parts, we can calculate their effect on  $\sigma$ , as done by Keall and Hoban.<sup>41</sup> However, it is usually difficult for users to know this information about their accelerator when commissioning a Monte Carlo treatment planning system. Therefore, we introduce a factor  $k$  to account for the effect of these materials. For direct electrons,  $\sigma$  is then given as

$$\sigma^2 = \frac{1}{8} K(E)lk. \quad (20)$$

The factor  $k$  is determined by fitting the angular distribution calculated using Fermi-Eyes theory to that simulated with the Monte Carlo method for direct electrons. The introduction of  $k$  factor provides a potentially tunable parameter in the source model.

#### 4. Model verification

The four-source model is verified dosimetrically by comparing the dose distributions in a water phantom calculated

using the model with those calculated using the full phase space data. Dose distributions are calculated for various combinations of three electron energies (6, 12, and 20 MeV), three applicator sizes ( $6 \times 6$ ,  $10 \times 10$ , and  $20 \times 20 \text{ cm}^2$ ), and two SSDs (100 cm and 120 cm).

The measurement of electron beam applicator factors (defined as the ratio of the open field dose in water at  $d_{\max}$  for a given applicator to that of the reference applicator, typically the  $10 \times 10$  or  $15 \times 15 \text{ cm}^2$ , for the same beam energy) is done during accelerator commissioning for all energy/cone combinations. Therefore, the applicator factors will be supplied by the user when performing the model commissioning. Cutout factors (defined as the ratio of the dose in water at  $d_{\max}$  for a blocked field to that of the open field for the same applicator and beam energy) are patient specific and not always easy to measure accurately for all clinical situations. Therefore, the model should be able to calculate cutout factors. To demonstrate this, we compare the model calculated cutout factors with those measured and calculated by Kapur *et al.* using a full Monte Carlo simulation.<sup>45</sup>

#### B. Beam commissioning

The four-source model which is built using a Varian Clinac 2100C accelerator as the reference machine can be used to reconstruct electron beams from other Clinac 2100C accelerators by tuning the energy spectra in the model.

For accelerators with exactly the same design, the major different is the electron incident energy due to the on-site tuning to suit the user. This energy approximately corresponds to the maximum energy of all the stored energy spectra in the source model. It is found that the energy spectra for all sub-sources are very similar for different accelerators of the same type. When the incident energy is changed, the energy spectra can be approximated as stretched or compressed along the energy axis accordingly. The depth dose curve is very sensitive to the electron incident energy and therefore used to adjust the maximum energy,  $E_{\max}$ , in the model. The relationship between the incident energy,  $E_{\text{in}}$ , and  $R_{50}$  has been studied by simulating the reference accelerator using a  $10 \times 10 \text{ cm}^2$  cone and 100 cm SSD with various incident energies. Then, the variation of  $E_{\text{in}}$  as a function of the variation of  $R_{50}$  is established for this type of accelerator. This relationship is used as a guide to tune the maximum energy in the model to commission a clinical beam.

The proposed commissioning approach can be summarized as follows:

- (1) Chose an accelerator as the reference machine for all other accelerators of the same design, and carefully perform full Monte Carlo simulations for the electron beams of various nominal energies from the reference machine with  $10 \times 10 \text{ cm}^2$  applicator.
- (2) Build the source models for the simulated beams based on the Monte Carlo phase space data, perform Monte Carlo dose calculation in water for 100 cm SSD, and record the maximum energy,  $E_{\max}^{(\text{ref})}$ , in the model and the  $R_{50}^{(\text{ref})}$  value for each beam.

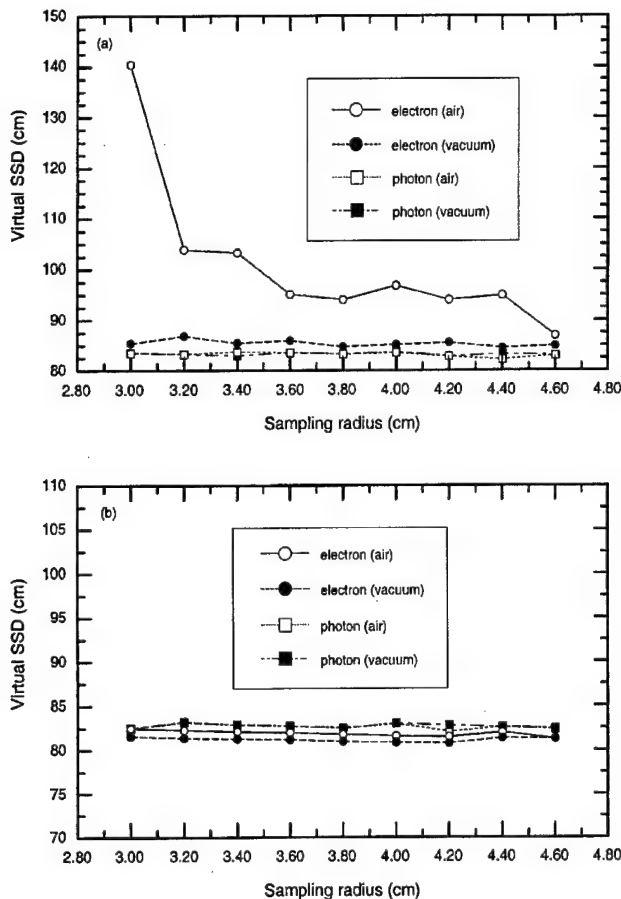


FIG. 2. Effects of intervening air and sampling radius on virtual SSD (defined here as the distance from the point source to the scoring plane) for the electron point source determined with the pinhole method. (a) 6 MeV; (b) 20 MeV.

- (3) For the beam to be commissioned, find the  $R_{50}^{(mea)}$  value of the measured depth-dose curve in water for  $10 \times 10 \text{ cm}^2$  applicator and 100 cm SSD.
- (4) Select the reference beam which has the same or closest nominal energy as the commissioning beam. Let  $i=0$ ,  $E_{\max}^{(i)} = E_{\max}^{(ref)}$ , and  $R_{50}^{(i)} = R_{50}^{(ref)}$ .
- (5) Calculate  $\Delta R_{50}^{(i)} = R_{50}^{(i)} - R_{50}^{(mea)}$ . If  $\Delta R_{50}^{(i)} \leq \epsilon$ , where  $\epsilon$  is the pre-set convergence tolerance, stop iteration and use  $E_{\max}^{(i)}$  as the maximum energy in the source model for the commissioning beam; otherwise, go to the next step.
- (6) According to the relationship between  $\Delta E_{\text{in}}$  and  $\Delta R_{50}$ , calculate  $\Delta E^{(i)}$  using  $\Delta R_{50}^{(i)}$  and then calculate  $E_{\max}^{(i+1)} = E_{\max}^{(i)} - \Delta E^{(i)}$ .
- (7) Calculate the dose distribution using the source model with  $E_{\max}^{(i+1)}$  and find the corresponding  $R_{50}^{(i+1)}$ .
- (8) Let  $i \leftarrow i+1$ ; go back to step 5.

The first two steps only need to be done once for all accelerators of the same design. The convergence tolerance,  $\epsilon$ , is set by the user, usually according to the estimated measurement error in  $R_{50}$ . For example,  $\epsilon=1 \text{ mm}$  is good enough in most

clinical situations. The iteration process converges very fast; usually only two or three iterations are needed even for  $\epsilon$  much smaller than 1 mm.

The commissioning approach has been applied to three electron beams, A, B, and C. The reference beam is the same for all three beams, which is from the reference Clinac 2100C accelerator with  $E_{\text{in}}=12.0 \text{ MeV}$ . Beam A and beam B are also from the reference machine but with  $E_{\text{in}}$  as 9.0 MeV and 15.0 MeV, respectively. These two beams are used to mimic two clinical beams of the same nominal energy as the reference beam but with significantly different incident energies. Of course, in reality, the electron incident energy will not be tuned so much ( $\pm 3 \text{ MeV}$ ). These two beams are used as extreme cases to test the commissioning approach. Beam C is a 9 MeV electron beam from another Clinac 2100C accelerator. The dose distributions for beam C are taken from the published data.<sup>38</sup>

### III. RESULTS AND DISCUSSION

Figure 2 shows the effects of intervening air and sampling radius on the electron and photon virtual SSD determined with the pinhole method for 6 MeV and 20 MeV beams. It can be seen that for photons and high energy electrons (20 MeV) effects of intervening air and sampling radius on the positions of virtual point sources are negligible. However, for low energy electrons (6 MeV), these effects are significant. Therefore, to obtain the accurate virtual electron point source position for low energy beams, the phase space simulated without intervening air should be used.

Figure 3 shows the comparison between the angular distributions for direct electrons in 6, 12 and 20 MeV beams calculated with the Fermi-Eyges theory and the Monte Carlo method. We can see that, in general, the fitted angular distributions based on the Fermi-Eyges theory match well with those calculated with the Monte Carlo simulation. We also notice that at large angles the Fermi-Eyges theory slightly

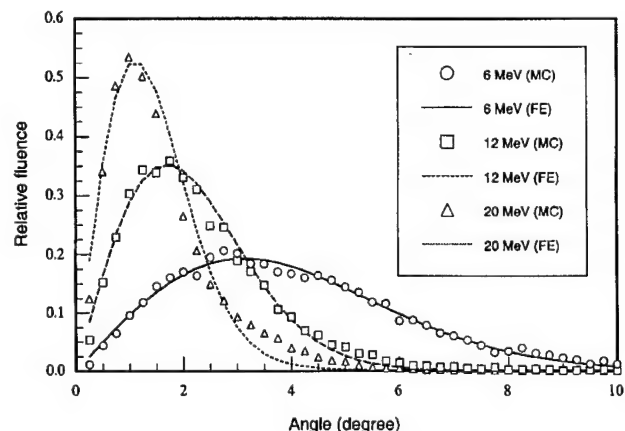


FIG. 3. Angular distributions for direct electrons calculated using the Fermi-Eyges theory and the Monte Carlo method. Beam energies are 6 MeV, 12 MeV and 20 MeV. The fitted  $k$  factor is 1.540 for 6 MeV, 1.501 for 12 MeV and 1.571 for 20 MeV. Each distribution is normalized to have unit area under the curve.

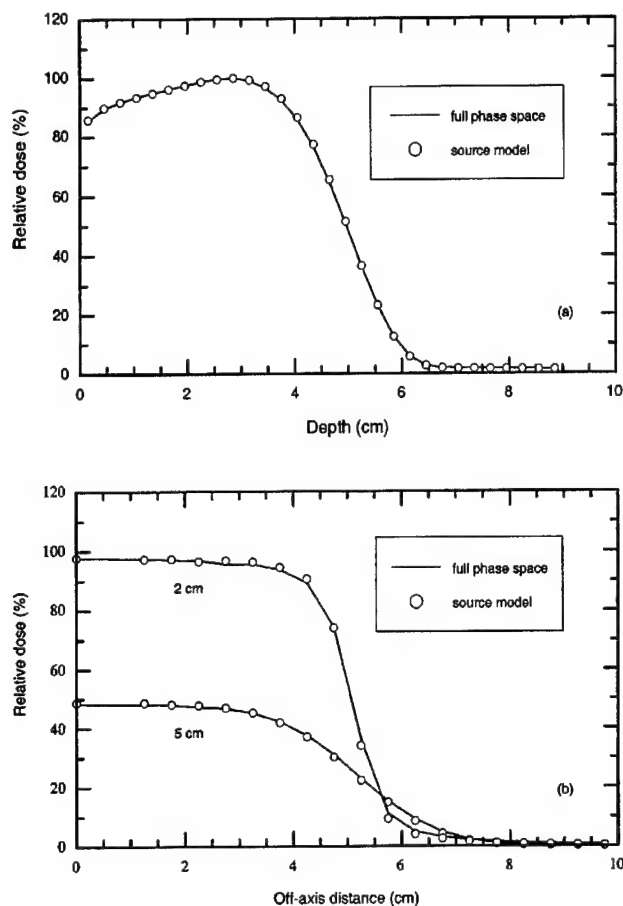


FIG. 4. Dose distributions in water for 12 MeV electron beam with  $10 \times 10 \text{ cm}^2$  applicator at 100 cm SSD, calculated with full phase space data and source model: (a) Depth-dose distributions; (b) dose profiles at depths of 2 cm and 5 cm. Curves are normalized to the dose at  $d_{\text{max}}$ .

underestimates electron fluence due to the fact that it is a small-angle theory. We found that the small discrepancy does not have any significant effect on the final dose distributions. Therefore, the Fermi-Eyges theory with the fitted  $k$  factor can be used to account for the angular perturbations of electrons on their way from the source to the scoring plane.

The four-source model was tested by comparing the dose distributions calculated by the model with those calculated by full phase space data for various combinations of three electron energies (6, 12, and 20 MeV), three applicator sizes ( $6 \times 6$ ,  $10 \times 10$ , and  $20 \times 20 \text{ cm}^2$ ), and two SSDs (100 cm and 120 cm). For all the cases tested, the agreement of 1%–2%/1–2 mm has been achieved. Figure 4 shows the comparison for a 12 MeV beam with a  $10 \times 10 \text{ cm}^2$  cone at 100 cm SSD. Figure 5 gives the depth-dose curves and dose profiles for 20 MeV beam with  $6 \times 6 \text{ cm}^2$  cone at 120 cm SSD, calculated with both the source model and full phase space data. All the curves in Figs. 4 and 5 are normalized to the doses at  $d_{\text{max}}$ . The Monte Carlo uncertainty is always less than 0.5% and therefore not shown on the curves. In both figures the agreement between the full Monte Carlo simulations and the source model calculations is better than 1%/1 mm. Keep in

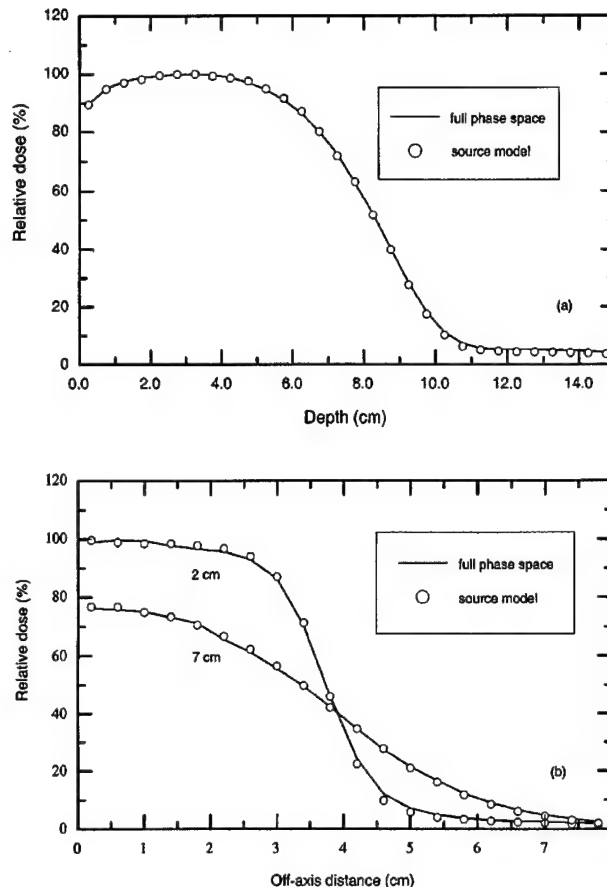


FIG. 5. Dose distributions in water for 20 MeV electron beam with  $6 \times 6 \text{ cm}^2$  applicator at 120 cm SSD, calculated with full phase space data and source model: (a) Depth-dose distributions; (b) dose profiles at depths of 2 cm and 7 cm. Curves are normalized to the dose at  $d_{\text{max}}$ .

mind that 20 cm air gap is rarely used in actual clinical situations. Therefore, we have demonstrated that the simplified four-source model can be used for accurate dose calculations even for extreme cases (such as very large extended SSDs).

The capability of the model for calculating the relative beam output was also tested. Table I shows cutout factors for various square inserts in a  $10 \times 10 \text{ cm}^2$  applicator for 6, 12 and 20 MeV electron beams. It is found that the cutout factors calculated with the four-source model are within about  $\pm 2\%$  compared to the measured values except for one case where we see 2.5% difference. This is at about the same accuracy level as the full Monte Carlo simulation and considered to be acceptable for clinical use.

The relationship between  $E_{\text{in}}$  and  $R_{50}$  for the reference accelerator with a  $10 \times 10 \text{ cm}^2$  cone and 100 cm SSD is shown in Fig. 6. A linear relationship was found and fitted as

$$E_{\text{in}} = 2.597R_{50} + 0.633. \quad (21)$$

It gives the relationship between the variation in the incident energy and the variation in  $R_{50}$  as

$$\Delta E_{\text{in}} = 2.597\Delta R_{50}. \quad (22)$$

TABLE I. The electron cutout factors for various square inserts in  $10 \times 10 \text{ cm}^2$  applicator for 6, 12, and 20 MeV beams calculated with the source model and the full phase space data and compared with the measurement of Kapur *et al.* (Ref. 45). The values in parenthesis indicate the difference of the data calculated with the source model or the full phase space from the measured data.

Energy (MeV)	Insert ( $\text{cm}^2$ )	Cutout factor		
		Source model	Full phase space	Measurement
6	2×2	0.803 (2.5%)	0.765 (−1.3%)	0.778
	3×3	0.930 (0.3%)	0.923 (−0.4%)	0.927
	4×4	0.970 (−1.8%)	0.982 (−0.6%)	0.988
	8×8	1.002 (−0.1%)	1.005 (−0.2%)	1.003
12	2×2	0.881 (−0.8%)	0.861 (−2.8%)	0.889
	3×3	0.908 (−2.0%)	0.930 (0.2%)	0.928
	4×4	0.942 (−2.1%)	0.956 (−0.7%)	0.963
	8×8	0.999 (0.8%)	1.002 (1.1%)	0.991
20	2×2	0.963 (−1.1%)	0.957 (−1.9%)	0.976
	3×3	0.989 (−0.4%)	0.968 (−2.5%)	0.993
	4×4	0.993 (−1.8%)	0.993 (−1.8%)	1.011
	8×8	0.999 (−0.5%)	0.993 (−1.1%)	1.004

Equation (22) is used for tuning the maximum energy in the source model to match the measured depth dose curves when commissioning a clinical beam.

Figure 7 shows the dose distributions for the reference beam, beam A, and beam B with the applicator size of  $10 \times 10 \text{ cm}^2$  and SSD of 100 cm. All the curves are normalized to the dose at  $d_{\text{max}}$ . The statistical uncertainty ( $1\sigma$ ) in all the Monte Carlo dose calculations was kept to be smaller than 0.5%, therefore, the error bars are smaller than the symbol size and not shown on the curves. The maximum energy in the source model was adjusted to 8.87 MeV to match the dose distributions of the beam A ( $E_{\text{in}}=9.0 \text{ MeV}$ ) and to 15.17 MeV to match the dose distributions of the beam B ( $E_{\text{in}}=15.0 \text{ MeV}$ ). The difference between the depth-dose curves calculated by the adjusted models and the full Monte Carlo simulation is always less than 0.5% for both beam A and beam B. For dose profiles, the difference is usually less than 1% except that in the shoulder region for beam B the difference is about 2%.

Figure 8 shows the dose distributions for the reference beam and beam C with the applicator size of  $10 \times 10 \text{ cm}^2$  and SSD of 100 cm. Again, the curves are normalized to the dose at  $d_{\text{max}}$  and the Monte Carlo uncertainty is lower than 0.5%. In this case, the maximum energy in the source model was adjusted to 11.25 MeV. The dose distributions calculated by the source model with the adjusted maximum energy agree very well (1%/1 mm) with the published data.<sup>38</sup>

Table II gives  $E_{\text{in}}$  and  $R_{50}$  for the reference and Monte Carlo simulated beams, and  $E_{\text{max}}$  and  $R_{50}$  for the adjusted source models. For the reference beam,  $E_{\text{max}}$  was directly obtained from the full Monte Carlo simulation. For beam C,  $E_{\text{in}}$  is unknown. In this study, we set  $\epsilon=0.01 \text{ cm}$ . Therefore, the  $R_{50}$ 's calculated using the adjusted source model match with the full Monte Carlo simulation to within 0.01 cm. Of course, we will not use such a small  $\epsilon$  in real clinical applications since it is much smaller than the measurement uncertainty in  $R_{50}$ . Here, we just want to demonstrate the capa-

bility of the method to reproduce  $R_{50}$  accurately.

We have applied the commissioning approach to electron beams from a Clinac 2300C/D accelerator in our institution. The reference machine is still the same Clinac 2100C accelerator. These two machines are sufficiently similar to each other in treatment head geometry. Their dosimetric characteristics are very close to each other due to the beam tuning during linac acceptance. Therefore, it is not surprising to see that the dose distributions calculated with the adjusted source model agree well (within 1%–2% or 1–2 mm) with the measured data.

These preliminary results have shown that the proposed hybrid commissioning approach can be used for accelerators of the same design to account for the dosimetric variations mainly caused by the on-site tuning of the electron incident energy. The capability of the approach to handle large variation in the electron incident energy has been demonstrated. It is believed that for most clinical accelerators of the same type, their treatment head designs are exactly the same or at least very similar, therefore the dosimetric difference can usually be traced back to the difference in the electron incident energy. Therefore, the current approach should be applicable in most clinical situations. In the future work, the method will be evaluated under more critical conditions, such as small field sizes, extended SSD, and heterogeneous phantoms.

The general idea proposed here should also work for other types of accelerators, although we have selected the Varian Clinac 2100C accelerators in the current study. For each type of accelerator, a reference machine should be carefully simulated using the Monte Carlo method. A source model, which may consist of a different number of sub-sources, can be established based on the simulated data. Then, the maximum energy in the model can be adjusted to commission electron beams from other accelerators of the same type.

In some situations, the proposed commissioning approach may not be directly applicable. For example, the measured

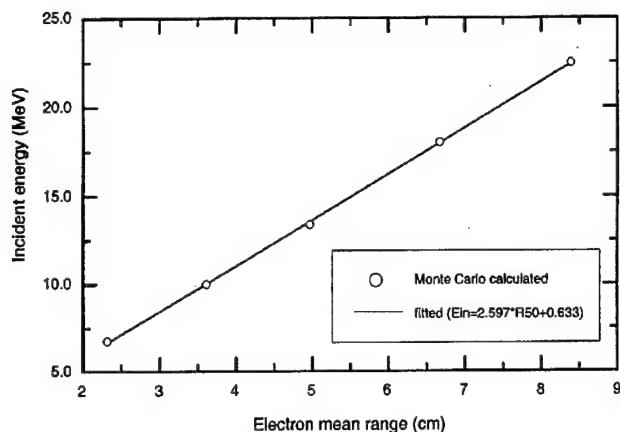


FIG. 6. The relationship between electron incident energy at accelerator exit window ( $E_{in}$ ) and the depth of 50% dose ( $R_{50}$ ) for electron beams from the reference accelerator with  $10 \times 10 \text{ cm}^2$  applicator and 100 cm SSD. Symbols are calculated with Monte Carlo simulation of the accelerator treatment head. Solid line is the fitted result with formula  $E_{in} = 2.597R_{50} + 0.633$ .

dose distributions used for commissioning more or less contain measurement errors, depending on the measurement techniques and the experience of the person who performs the measurements. Since only the maximum energy is the adjustable parameter in the current source model, our approach may not be able to exactly match the measured data. Occasionally, an accelerator used in the clinic may differ from its original design in addition to the electron incident energy. Some parts in the accelerator treatment head may be replaced with nonstandard ones. In this case, we can always perform a full Monte Carlo simulation for this unique accelerator and build its own source model. Alternatively, we can make the present approach more versatile to handle those situations. More parameters in the source model other than the maximum energy, such as the relative intensity of each sub-source, the  $k$  factor for in-air perturbation for the direct electrons, and the field size, can be adjusted to match the measured dose distributions. For example, the adjustment of the relative intensity of the photon source will ensure a good match to the bremsstrahlung tail in the depth-dose curve. If some of the materials in the paths of direct electrons, such as the scattering foil, monitor chamber or mirror, are different from those used in the reference accelerator, the adjustment of the  $k$  factor can yield a better estimation of the electron angular perturbation. The adjustment of the field size in the source model should recover the measurement error in the width of the dose profiles (e.g., errors of the order of about 1 mm are not rare in a clinical situation). In summary, the introduction of more adjustable parameters in the source model will make the current commissioning approach more powerful. This possibility will be investigated in our future study.

#### IV. CONCLUSIONS

A hybrid commissioning approach based on a multiple source model has been proposed for Monte Carlo treatment planning. It has been demonstrated that a simplified four-

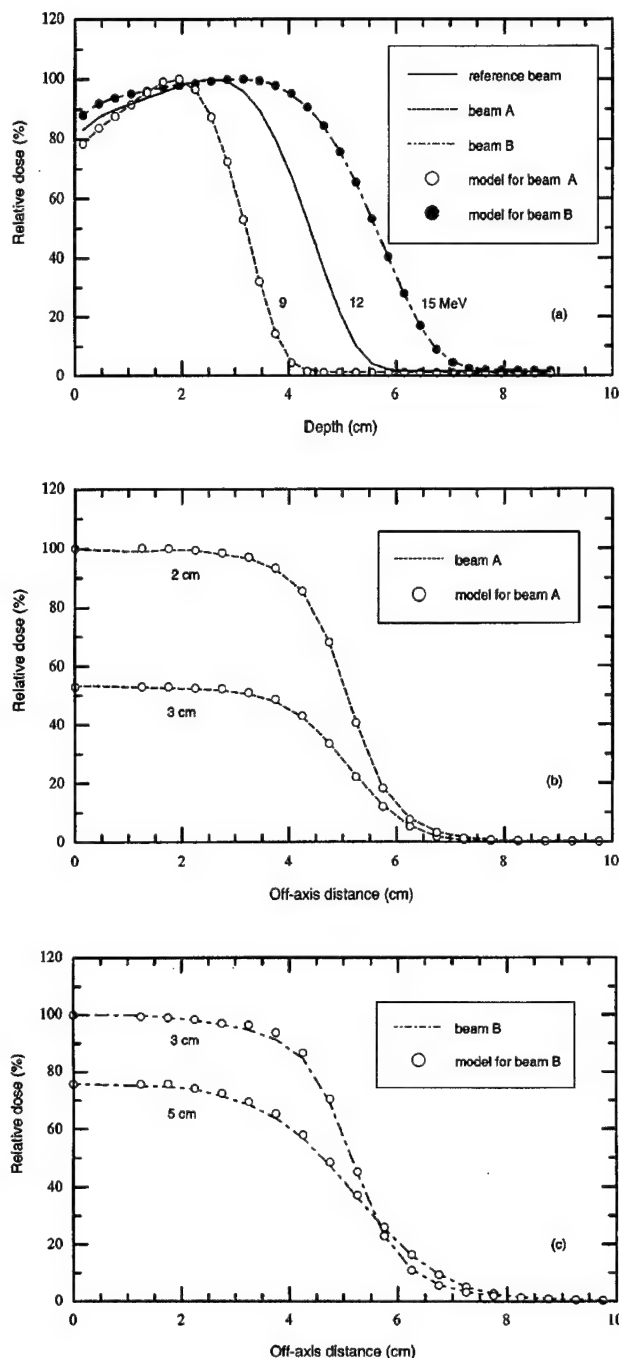


FIG. 7. Dose distributions in water for electron beams from the reference accelerator with  $10 \times 10 \text{ cm}^2$  applicator and at 100 cm SSD. The reference beam has the electron incident energy of 12.0 MeV. A source model was built based on the Monte Carlo simulation of the reference beam. The maximum energy of the energy spectra in the model was adjusted to 8.87 MeV to match the beam A (with  $E_{in} = 9.0 \text{ MeV}$ ) and 15.17 MeV to match the beam B (with  $E_{in} = 15.0 \text{ MeV}$ ). Lines are dose distributions from the full Monte Carlo simulations. Symbols are data calculated by the source model with adjusted maximum energies. All data are normalized to the doses at  $d_{max}$ . (a) Depth-dose distributions; (b) dose profiles at depths of 2 cm and 3 cm for beam A; (c) dose profiles at depths of 3 cm and 5 cm for beam B.

source model can be used to generate accurate Monte Carlo dose distributions for electron beams from Varian Clinac 2100C accelerators. The model includes a point electron source for direct electrons and electrons scattered from pri-

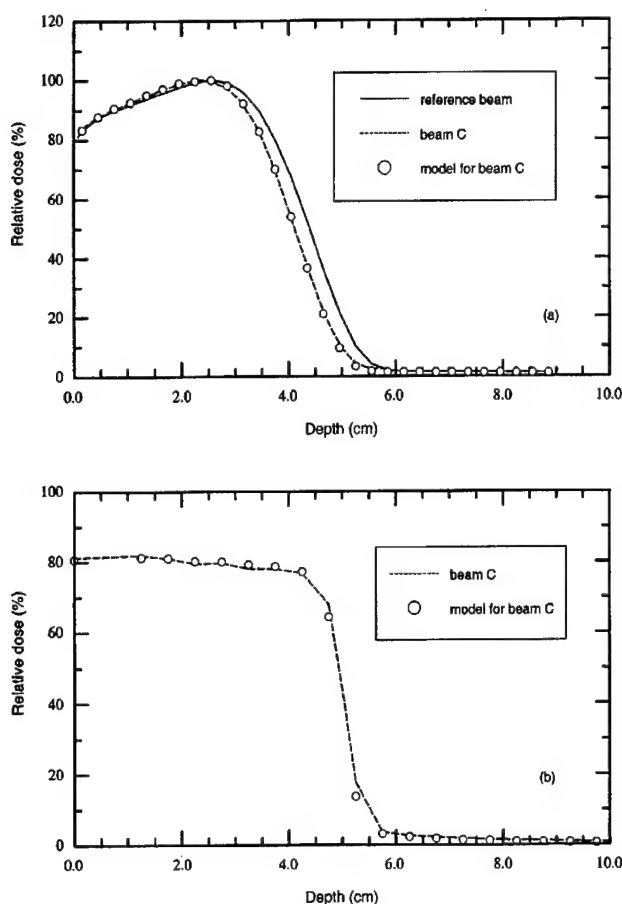


FIG. 8. Dose distributions in water for electron beams with  $10 \times 10 \text{ cm}^2$  applicator and at 100 cm SSD. The reference beam (solid line) is from a Clinac 2100C accelerator with  $E_{in} = 12.0 \text{ MeV}$ . The dose distributions for beam C (dashed lines) is taken from the published data for a 9 MeV beam from another Clinac 2100C accelerator with type III applicator (Ref. 38). A source model built based on the Monte Carlo simulation of the reference beam is used to match beam C by adjusting the maximum energy to 11.25 MeV (open circles). All data are normalized to the dose at  $d_{max}$ . (a) Depth-dose distributions; (b) dose profiles at depth of 0.1 cm.

mary collimator and jaws, a point photon source for all contaminant bremsstrahlung photons, and two square ring electron sources representing electrons scattered from two scrapers (other than the last scraper) of the Varian electron applicator (type III). It was found that the position of the virtual point source can be determined accurately using the pinhole method for photons in all cases and electrons in high energy beams. For low energy beams, we should use the Monte Carlo phase space data which are obtained by simulating the treatment head with the intervening air replaced by vacuum. We also found that the in-air perturbation on the electron incident direction can be properly accounted for using the Fermi-Eyges model. The source model which was built based on the simulated phase space data for the reference accelerator can be used for other accelerators of the same type, by simply adjusting the energy spectra in the model. The capability of this commissioning approach for handling large variation in the electron incident energy has been demonstrated.

TABLE II. Some parameters for the full Monte Carlo simulations and the adjusted source models.  $E_{in}$  is the electron incident energy at the exit window in the simulation.  $E_{max}$  is the maximum energy in the source model.  $R_{50}$  is the depth of 50% dose of the depth dose curve in water for  $10 \times 10 \text{ cm}^2$  applicator and 100 cm SSD. A source model was built based on the full Monte Carlo simulation of the reference beam. For beams to be commissioned (A, B, and C),  $E_{max}$  in the model was adjusted to match the corresponding  $R_{50}$  from the Monte Carlo simulation.

Beam tested	MC simulation		Source model	
	$E_{in}$ (MeV)	$R_{50}$ (cm)	$E_{max}$ (MeV)	$R_{50}$ (cm)
Reference	12.0	4.397	12.00	4.397
Beam A	9.0	3.197	8.87	3.192
Beam B	15.0	5.622	15.17	5.624
Beam C	unknown	4.116	11.25	4.119

## ACKNOWLEDGMENTS

The authors are grateful to the referees, Drs. Art Boyer, Alan Nahum, Alex Bielajew, David Findley, Gary Luxton, Ed Mok, Todd Pawlicki, and Frank Verhaegen for useful comments on the manuscript. The authors would also like to thank Dr. Sam Brain, Todd Koumian, and Behrooz Tofighrad for computer support, Dr. Dave Rogers and his OMEGA/BEAM team at the National Research Council of Canada for the Monte Carlo simulation system, and Eva Papiez for supplying some measured data. The work was supported in part by the U.S. Army breast cancer research program (BC971292), NCI Grant No. CA78331 and a consortium agreement with the Numerix Cooperation.

<sup>a</sup>Corresponding author. Tel: (650)498-4074, Fax: (419)498-4015, E-mail: stevej@reyes.stanford.edu

<sup>1</sup>K. R. Hogstrom, M. D. Mills, and P. R. Almond, "Electron beam dose calculations," *Phys. Med. Biol.* **26**, 445-459 (1981).

<sup>2</sup>E. Fermi, in B. Rossi and K. Greisen, "Cosmic-ray theory," *Rev. Mod. Phys.* **13**, 265-268 (1941).

<sup>3</sup>L. Eyges, "Multiple scattering with energy loss," *Phys. Rev.* **74**, 1534-1535 (1948).

<sup>4</sup>J. Cygler, J. J. Battista, J. W. Scrimger, E. Mah, and J. Antolak, "Electron dose distributions in experimental phantoms: A comparison with 2D pencil beam calculations," *Phys. Med. Biol.* **32**, 1073-1086 (1987).

<sup>5</sup>E. Mah, J. Antolak, J. W. Scrimger, and J. J. Battista, "Experimental evaluation of a 2D and a 3D electron pencil beam algorithm," *Phys. Med. Biol.* **34**, 1179-1194 (1989).

<sup>6</sup>I. Kawrakow, M. Fippel, and K. Friedrich, "3D electron dose calculation using a voxel based Monte Carlo algorithm (VMC)," *Med. Phys.* **23**, 445-457 (1996).

<sup>7</sup>C. M. Ma, E. C. Mok, A. Kapur, T. Pawlicki, D. O. Findley, S. Brain, K. Forster, and A. L. Boyer, "Clinical implementation of a Monte Carlo treatment planning system," *Med. Phys.* **26**, 2133-2143 (1999).

<sup>8</sup>M. A. Ebert and P. W. Hoban, "Possibilities for tailoring dose distributions through the manipulation of electron beam characteristics," *Phys. Med. Biol.* **42**, 2065-2081 (1997).

<sup>9</sup>M. G. Karlsson, M. Karlsson, and B. Zackrisson, "Intensity modulation with electrons: calculations, measurements and clinical applications," *Phys. Med. Biol.* **43**, 1159-1169 (1998).

<sup>10</sup>M. Åsell, S. Hyödynmaa, S. Söderström, and A. Brahme, "Optimal electron and combined electron and photon therapy in the phase space of complication-free cure," *Phys. Med. Biol.* **44**, 235-252 (1999).

- <sup>11</sup> A. E. Nahum, "Monte Carlo electron transport simulation II: Application to dose planning," in *The Computation of Dose Distributions in Electron Beam Radiotherapy*, edited by A. E. Nahum (Umeå University, Umeå, Sweden, 1985), pp. 319–340.
- <sup>12</sup> T. M. Jenkins, W. R. Nelson, A. Rindi, A. E. Nahum, and D. W. O. Rogers, *Monte Carlo Transport of Electrons and Photons* (Plenum, New York, 1988).
- <sup>13</sup> T. R. Mackie, "Applications of the Monte Carlo method in radiotherapy," in *Vol. III of Dosimetry of Ionizing Radiation*, edited by K. Kase, B. Bjärngard, and F. H. Attix (Academic, New York, 1990), 541–620.
- <sup>14</sup> D. W. O. Rogers and A. F. Bielajew, "Monte Carlo techniques of electron and photon transport for radiation dosimetry," in *Vol. III of The Dosimetry of Ionizing Radiation*, edited by K. R. Case, B. E. Bjärngard, and F. H. Attix (Academic, New York, 1990), pp. 427–539.
- <sup>15</sup> D. W. O. Rogers, "The role of Monte Carlo simulation of electron transport in radiation dosimetry," *Int. J. Appl. Radiat. Isot.* **42**, 965–974 (1991).
- <sup>16</sup> P. Andreo, "Monte Carlo techniques in medical radiation physics," *Phys. Med. Biol.* **36**, 861–920 (1991).
- <sup>17</sup> C. Manfredotti, U. Nastasi, R. Ragona, and S. Anglesio, "Comparison of three dimensional Monte Carlo simulation and the pencil beam algorithm for an electron beam from a linear accelerator," *Nucl. Instrum. Methods Phys. Res. A* **255**, 355–359 (1987).
- <sup>18</sup> C. Manfredotti, U. Nastasi, R. Marchisio, C. Ongaro, G. Gervino, R. Ragona, S. Anglesio, and G. Sannazzari, "Monte Carlo simulation of dose distribution in electron beam radiotherapy treatment planning," *Nucl. Instrum. Methods Phys. Res. A* **291**, 646–654 (1990).
- <sup>19</sup> A. A. al-Beteri and D. E. Raeside, "Optimal electron-beam treatment planning for retinoblastoma using a new three-dimensional Monte Carlo-based treatment planning system," *Med. Phys.* **19**, 125–135 (1992).
- <sup>20</sup> H. Neuenschwander, T. R. Mackie, and P. J. Reckwerdt, "MMC—A high-performance Monte Carlo code for electron beam treatment planning," *Phys. Med. Biol.* **40**, 543–574 (1995).
- <sup>21</sup> P. J. Keall and P. W. Hoban, "Super-Monte Carlo: A 3-D electron beam dose calculation algorithm," *Med. Phys.* **23**, 2023–2034 (1996).
- <sup>22</sup> B. Faddegon, J. Balogh, R. Mackenzie, and D. Scora, "Clinical considerations of Monte Carlo for electron radiotherapy treatment planning," *Radiat. Phys. Chem.* **53**, 217–227 (1998).
- <sup>23</sup> C. M. Ma and A. E. Nahum, "Calculation of absorbed dose ratios using correlated Monte Carlo sampling," *Med. Phys.* **20**, 1189–1199 (1993).
- <sup>24</sup> M. A. Holmes, T. R. Mackie, W. Sohn, P. J. Reckwerdt, T. J. Kinsella, A. F. Bielajew, and D. W. O. Rogers, "The application of correlated sampling to the computation of electron beam dose distributions in heterogeneous phantoms using the Monte Carlo method," *Phys. Med. Biol.* **38**, 675–688 (1993).
- <sup>25</sup> A. F. Bielajew, "Monte Carlo modeling in external electron-beam radiotherapy—Why leave it to chance?," in *Proceedings of The 11th International Conference on The Use of Computers in Radiation Therapy*, edited by A. R. Hounsell, J. M. Wilkinson, and P. C. Williams (Manchester, UK, 1994), pp. 2–5. North Western Medical Physics Department, Christie Hospital NHS Trust.
- <sup>26</sup> R. Mohan, "Why Monte Carlo?" in *Proceedings of The 12th International Conference on The Use of Computers in Radiation Therapy*, edited by D. D. Leavitt and G. Starkschall, Salt Lake City, Utah (Medical Physics Publishing, Madison, 1997), pp. 16–18.
- <sup>27</sup> C. L. Hartmann-Siantar, P. M. Bergstrom, W. P. Chansler, L. Chase, L. J. Cox, T. P. Daly, D. Garrett, S. M. Hornstein, R. K. House, E. I. Moses, R. W. Patterson, J. A. Rathkopf, and A. S. von Wittenau, "Lawrence Livermore National Laboratory's PEREGRINE project," in *Proceedings of the 12th International Conference on the Use of Computers in Radiation Therapy*, edited by D. D. Leavitt and G. Starkschall, Salt Lake City, Utah (Medical Physics Publishing, Madison, 1997), pp. 19–22.
- <sup>28</sup> J. J. DeMarco, T. D. Solberg, and J. B. Smathers, "A CT-based Monte Carlo simulation tool for dosimetry planning and analysis," *Med. Phys.* **25**, 1–11 (1998).
- <sup>29</sup> L. Wang, C. S. Chui, and M. Lovelock, "A patient-specific Monte Carlo dose-calculation method for photon beams," *Med. Phys.* **25**, 867–878 (1998).
- <sup>30</sup> J. O. Deasy, P. R. Almond, and M. T. McEllistrem, "Measured electron energy and angular distributions from clinical accelerators," *Med. Phys.* **23**, 675–684 (1996).
- <sup>31</sup> J. J. Janssen, E. W. Korevaar, L. J. van Battum, P. R. M. Storchi, and H. Huizenga, "Clinical electron beam dose calculations with the Phase Space Evolution model," in *Proceedings of the 12th International Conference on the Use of Computers in Radiation Therapy*, edited by D. D. Leavitt and G. Starkschall, Salt Lake City, Utah (Medical Physics Publishing, Madison, 1997), pp. 195–196.
- <sup>32</sup> M. Udale, "A Monte Carlo investigation of surface doses for broad electron beams," *Phys. Med. Biol.* **33**, 939–954 (1988).
- <sup>33</sup> M. Udale-Smith, "Monte Carlo calculations of electron beam parameters for three Philips linear accelerators," *Phys. Med. Biol.* **37**, 85–105 (1992).
- <sup>34</sup> D. W. O. Rogers, B. A. Faddengon, G. X. Ding, C. M. Ma, J. We, and T. R. Mackie, "BEAM: A Monte Carlo code to simulate radiotherapy treatment units," *Med. Phys.* **22**, 503–524 (1995).
- <sup>35</sup> C. M. Ma and D. W. O. Rogers, "Beam characterization: a multiple-source model," Technical Report PIRS 509d, National Research Council of Canada, Ottawa, Canada, 1995.
- <sup>36</sup> C. M. Ma, B. A. Faddegon, D. W. O. Rogers, and T. R. Mackie, "Accurate characterization of Monte Carlo calculated electron beams for radiotherapy," *Med. Phys.* **24**, 401–416 (1997).
- <sup>37</sup> C. M. Ma, "Characterization of computer simulated radiotherapy beams for Monte-Carlo treatment planning," *Radiat. Phys. Chem.* **53**, 329–344 (1998).
- <sup>38</sup> G. X. Ding and D. W. O. Rogers, "Energy spectra, angular spread and dose distributions of electron beams from various accelerators used in radiotherapy," Technical Report PIRS 0439, National Research Council of Canada, Ottawa, Canada, 1995.
- <sup>39</sup> AAPM TG-25, "Clinical electron beam dosimetry: Report of AAPM Radiation Therapy Committee Task Group No. 25," *Med. Phys.* **18**, 73–109 (1991).
- <sup>40</sup> M. A. Ebert and P. W. Hoban, "A Monte Carlo investigation of electron-beam applicator scatter," *Med. Phys.* **22**, 1431–1435 (1995).
- <sup>41</sup> P. J. Keall and P. W. Hoban, "Calculating the angular standard deviation of electron beams using Fermi-Eyges theory," *Phys. Med. Biol.* **41**, 1511–1515 (1996).
- <sup>42</sup> S. B. Jiang, Z. M. Luo, and K. M. Ayyangar, "Incorporation of the electron energy-loss straggling into the Fermi-Eyges equation," *Radiat. Phys. Chem.* **53**, 477–482 (1998).
- <sup>43</sup> B. L. Werner, F. M. Khan, and F. C. Deibel, "A model for calculating electron beam scattering in treatment planning," *Med. Phys.* **9**, 180–187 (1982).
- <sup>44</sup> ICRU 35, "Radiation Dosimetry: Electron Beams with Energies Between 1 and 50 MeV," International Commission on Radiation Units and Measurements, Bethesda, MA, 1984.
- <sup>45</sup> A. Kapur, C. M. Ma, E. C. Mok, D. O. Findly, and A. L. Boyer, "Monte Carlo calculations of electron beam output factors for a medical linear accelerator," *Phys. Med. Biol.* **43**, 3479–3494 (1998).

# Monte Carlo and experimental investigations of multileaf collimated electron beams for modulated electron radiation therapy

Michael C. Lee,<sup>a)</sup> Steve B. Jiang, and C.-M. Ma

*Department of Radiation Oncology, Stanford University School of Medicine, Stanford, California 94305-5304*

(Received 17 November 1999; accepted for publication 2 October 2000)

Modulated electron radiation therapy (MERT) has been proposed as a means of delivering conformal dose to shallow tumors while sparing distal structures and surrounding tissues. Conventional systems for electron beam collimation are labor and time intensive in their construction and are therefore inadequate for use in the sequential delivery of multiple complex fields required by MERT. This study investigates two proposed methods of electron beam collimation: the use of existing photon multileaf collimators (MLC) in a helium atmosphere to reduce in-air electron scatter, and a MLC specifically designed for electron beam collimation. Monte Carlo simulations of a Varian Clinac 2100C were performed using the EGS4/BEAM system and dose calculations performed with the MCDOSE code. Dose penumbras from fields collimated by photon MLCs both with air and with helium at 6, 12, and 20 MeV at a range of SSDs from 70 to 90 cm were examined. Significant improvements were observed for the helium based system. Simulations were also performed on an electron specific MLC located at the level of the last scraper of a  $25 \times 25$  cm<sup>2</sup> applicator. A number of leaf materials, thicknesses, end shapes, and widths were simulated to determine optimal construction parameters. The results demonstrated that tungsten leaves 15 mm thick and 5 mm wide with unfocused ends would provide sufficient collimation for MERT fields. A prototype electron MLC was constructed and comparisons between film measurements and simulation demonstrate the validity of the Monte Carlo model. Further simulations of dose penumbras demonstrate that such an electron MLC would provide improvements over the helium filled photon MLC at all energies, and improvements in the 90–10 penumbra of 12% to 45% at 20 MeV and 6 MeV, respectively. These improvements were also seen in isodose curves when a complex field shape was simulated. It is thus concluded that an MLC specific for electron beam collimation is required for MERT. © 2000 American Association of Physicists in Medicine. [S0094-2405(00)01612-6]

**Key words:** modulated electron radiation therapy (MERT), IMRT, EGS4 Monte Carlo, multileaf collimator (MLC)

## I. INTRODUCTION

In recent years, intensity modulated radiation therapy (IMRT) with photon beams has been used to deliver highly conformal doses to target areas while sparing neighboring tissues. However, because of the need for electron buildup, photon fields provide low surface doses and are thus not well suited to the treatment of shallow tumors. Additionally, due to the highly penetrating nature of the photon beams, some scenarios present an unavoidable accompanying risk to distal structures during photon treatments. Therefore shallow tumors are often treated with megavoltage electron beams. The rapid depth-dose fall-off associated with electron beams allows delivery of therapeutic doses to the target areas while sparing distal tissues. This makes electron beam therapy ideal for treatment of the head and neck and the chest wall. However, presently electron beam techniques offer only limited conformity in the depth direction.

One proposed treatment modality that overcomes this limitation is modulated electron radiation therapy (MERT).<sup>1–7</sup> In a MERT treatment, lateral dose conformity and uniformity may be achieved by intensity modulation,

while conformity in the depth direction may be improved through use of different energies. This technique may be extremely valuable for treatment of curved surfaces, such as irradiation of the intact breast, shallow head and neck tumors, and irradiation of targets located on the extremities.

However, before MERT can be used in a clinical setting, a new system of electron beam collimation must be developed. The present system of lead alloy (Cerrobend) cutouts and boluses are not practical for the rapid delivery of the intensity distributions required in MERT. As with photon IMRT, a multileaf collimator (MLC) may provide a solution to the field shaping and intensity modulation problem. It has been proposed that scanned beam systems, alone or in conjunction with existing photon MLCs can provide adequate collimation.<sup>8</sup> In his work, Brahme further suggests that “fourth-generator” clinical accelerators may be filled with helium, thereby significantly reducing in-air electron scatter and making the photon MLC a practical system for electron beams. Indeed, a number of studies have been conducted utilizing scanned beam systems (MM50, Scanditronix Medical AB, Uppsala, Sweden) in a clinical setting to improve

dose distributions.<sup>3,5</sup> Jansson *et al.* have demonstrated that a scattering foil accelerator (MM22, Scanditronix Medical AB, Uppsala, Sweden) and its intrinsic MLC can be used to generate matched photon and electron fields to improve dose distributions in breast cancer therapy.<sup>9</sup>

Despite these successes, the use of the photon MLC with electrons has key limitations. Experimental work by Klein *et al.* has shown that in a standard Varian Clinac 2100C (Varian Oncology Systems, Palo Alto, CA), a source-to-surface distance (SSD) of 70 cm is necessary to provide a clinically acceptable field when using the photon MLC.<sup>10</sup> Indeed, beams collimated by a photon MLC were shown to be inferior to applicator fields in penumbra and uniformity and furthermore could not be adequately matched to photon fields. Monte Carlo simulations by Karlsson *et al.* have shown that for a 9 MeV beam from a Varian Clinac 2100C/D, a reduction of the 80–20 fluence penumbra from 18 mm to 11 mm could be achieved by replacing the treatment head air with helium (including the use of a helium filled balloon between the accelerator and patient) and/or moving the MLC at least 11 cm towards the patient.<sup>5</sup> Thus, this work focuses on developing an electron specific MLC (eMLC) located at the same level as a Cerrobend cutout, typically 40 cm or more closer to the patient than the photon MLC. Such a system could have the additional benefit of being backwards-compatible with existing accelerators and also being more generally accessible than scanned beam systems.

In order to have an eMLC system that may be used for MERT, several issues must be considered. While any beamlet distribution may be used during inverse planning, dose conformity will improve if the field edges are sharpened. To this end, it is desirable to have a system that provides the smallest penumbra possible and be able to provide maximum ability to resolve narrow fields. Furthermore, as with photon IMRT, a larger number of monitor units must be delivered relative to conventional treatments, and so both photon and electron leakage must be reduced. It has been shown by Ma *et al.* that if such a system is developed, intensity-modulated electron fields may be delivered.<sup>7</sup>

This study utilizes a combination of Monte Carlo simulations and film measurements to compare a helium/photon MLC based system, an air/photon MLC based system, and an electron specific MLC located near the phantom surface. It has been demonstrated that traditional analytical dose calculation algorithms, such as the 3D pencil beam<sup>11</sup> are limited in their use with small irregular electron fields,<sup>12–14</sup> and therefore Monte Carlo simulations were chosen for treatment head modeling and dose calculations. The EGS4/BEAM<sup>15,16</sup> and MCDOSE<sup>17</sup> systems were employed to simulate different MLC systems and calculate dose in homogeneous water phantoms. These simulations allowed comparisons of the proposed collimation systems. Recommendations with regard to eMLC design and construction are also presented on the basis of the Monte Carlo simulations.

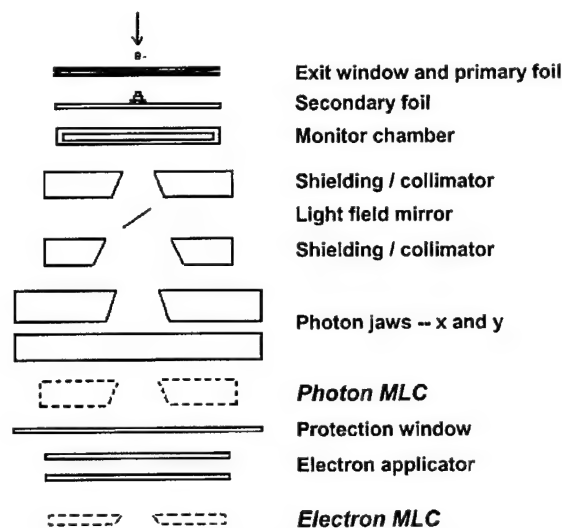


FIG. 1. Schematic of a Varian Clinac 2100C treatment head used in the BEAM simulation. Also shown are the two collimation systems proposed for electron beams.

## II. MATERIALS AND METHODS

### A. Monte Carlo simulation of the photon MLC

Electron beam simulations of a Varian Clinac 2100C (Varian Oncology Systems, Palo Alto, CA) were performed using the EGS4/BEAM code.<sup>15,16</sup> Vendor supplied geometries were used in the component-wise simulation, and a schematic of the simulation model is displayed in Fig. 1. The simulation code and geometry employed have been previously shown to provide agreement with measured data of better than 2% in transverse profiles and depth dose curves for the three nominal energies simulated: 6, 12, and 20 MeV.<sup>18</sup> Phase space files were obtained below the photon jaws. The photon jaws were set according to the manufacturer specifications for a 25×25 cm<sup>2</sup> applicator. These phase space files were then used as the sources for simulating various MLCs.

In the first set of simulations, the particles in the first phase space were transported through a photon MLC open to 10×10 cm<sup>2</sup> projected, the protective window and an appropriate thickness of air to the desired SSD. The photon MLC in this study was an idealized MLC with tungsten leaves of the same geometry as the Varian 52 leaf MLC (~7 cm thick, ~55 cm downstream of the target), with ends and sides always focused to the source regardless of leaf position (i.e., double focused). The MLC was set to project to an exact 10×10 cm<sup>2</sup> field at the SSD of interest (measured here from the photon target to the phantom surface). No attempt was made to simulate the number and width of the leaves of any existing accelerator. In all cases, interleaf leakage (i.e., tongue and groove effect) was ignored. Simulations were performed beginning with the aforementioned phase space source, through the photon MLC, the protective window, and through an appropriate thickness of air to the SSD of interest.

For each energy, two phase space files were generated, one in which the ambient atmosphere of the treatment head

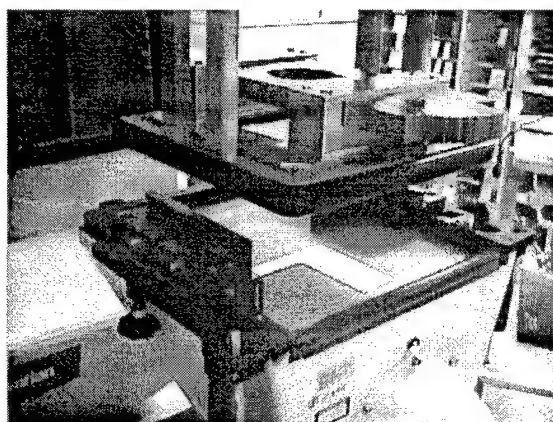


FIG. 2. Prototype electron MLC used for Monte Carlo simulations and film measurements. The MLC consists of 30 pairs of manually set steel leaves, and is designed to mount in the cutout position of a 25×25 cm<sup>2</sup> Varian applicator.

was air (density =  $1.205 \times 10^{-3}$  g cm<sup>-3</sup>), and one in which it was replaced with helium (density =  $1.663 \times 10^{-4}$  g cm<sup>-3</sup>). In the case of helium filled accelerators, the atmosphere of the air gap was also replaced with He, to simulated the use of helium bags. The walls of the bag were not simulated, as it was believed that ~0.01 cm Mylar would have a trivial impact on dose distributions. In all cases, phase space files were obtained at the SSD of interest (70, 75, 80, 85, 90 cm nominal SSD) and used for dose calculations.

This and all subsequent Monte Carlo simulations were performed on various elements of a suite of 22 Pentium Pro (200 MHz) CPUs and 10 Pentium III CPUs (450 MHz), all running EGS4, BEAM, and MCDOSE under the Linux operating system. In general, simulations were performed in parallel and the phase space files (or dose files) statistically combined to give improved performance. All simulations utilized an electron cutoff (ECUT) of 0.7 MeV total energy and a photon cutoff of 10 keV, below which all remaining energy was deposited on the spot. It has been documented that an ECUT of 0.7 MeV, corresponding to a residual continuous-slowing-down approximation range in water of <0.5 mm, is sufficient for most dosimetric purposes.<sup>16</sup> PRESTA extensions were employed for step length calculations.<sup>19</sup> The number of initial electron histories ranged from  $150 \times 10^6$  for 6 MeV to  $50 \times 10^6$  for 20 MeV.

Dose calculations were performed using the above generated phase space files using the EGS4/MCDOSE code.<sup>17</sup> Homogeneous water phantoms were simulated with voxels 3 mm along the profiled axis, and 15 mm in the orthogonal in-plane direction, and 2 mm along the direction in axis. Statistical error was less than 1% ( $1\sigma$ ) in all dose calculations.

## B. Electron MLC design considerations

### 1. Material and leaf thickness

A number of different prototypes for eMLCs were simulated. First, under the assumption that a minimal distance

TABLE I. Simulated penumbras of a 10×10 cm<sup>2</sup> field collimated by different MLC systems. The 6 MeV beam penumbra was calculated at 0.75 cm depth, the 12 MeV beam at 2.0 cm, and the 20 MeV beam at 3.0 cm depth. The ideal MLC is built out of 1.5 cm thick tungsten located at the level of the last scraper, while the prototype MLC is 2.54 cm thick steel located 3.0 cm above the last scraper.

Energy	Gas	MLC	SSD	Dose penumbra			
				Absolute (mm)		Relative to ideal eMLC	
				80/20	90/10	80/20	90/10
6 MeV	air	photon	70	18.5	30.7	2.28	2.33
			75	23.9	38.7	2.95	2.93
			80	29.0	46.7	3.58	3.54
			85	33.2	52.3	4.10	3.96
			90	37.6	60.0	4.64	4.55
	He	photon	80	17.3	27.6	2.14	2.09
			85	19.8	32.5	2.44	2.46
			90	22.3	35.1	2.75	2.66
	air	ideal e-	100	8.1	13.2	1.00	1.00
	air	proto. e-	100	12.0	19.3	1.48	1.46
12 MeV	air	photon	70	10.9	18.8	1.31	1.38
			75	14.0	23.1	1.69	1.70
			80	16.5	26.0	1.99	1.91
			85	19.0	30.3	2.29	2.23
			90	22.0	35.0	2.65	2.57
	He	photon	80	11.3	18.6	1.36	1.37
			85	12.7	20.5	1.53	1.51
			90	13.9	22.8	1.67	1.68
	air	ideal e-	100	8.3	13.6	1.00	1.00
	air	proto. e-	100	9.8	17.1	1.18	1.26
20 MeV	air	photon	70	10.5	17.4	1.21	1.20
			75	11.7	18.9	1.34	1.30
			80	13.1	22.3	1.51	1.54
			85	14.2	23.1	1.63	1.59
			90	16.0	26.3	1.84	1.81
	He	photon	80	10.0	16.5	1.15	1.14
			85	10.7	17.5	1.23	1.21
			90	11.3	18.6	1.30	1.28
	air	ideal e-	100	8.7	14.5	1.00	1.00
	air	proto. e-	100	10.3	18.4	1.18	1.27

between the MLC and the treatment surface was optimal,<sup>8,12</sup> simulations were performed with the MLCs completely replacing the last scraper of a 25×25 cm<sup>2</sup> applicator (i.e., with the back surface at approximately 95 cm from the photon target). Different materials and thicknesses were simulated, and phase space files obtained immediately at the back surface of the MLC. A total of five construction materials were considered in this investigation: zinc (density = 7.14 g cm<sup>-3</sup>), steel (8.06 g cm<sup>-3</sup>), copper (8.93 g cm<sup>-3</sup>), lead (11.34 g cm<sup>-3</sup>), and tungsten (19.30 g cm<sup>-3</sup>). The copper, zinc, lead, and tungsten MLCs were limited to 1.5 cm in thickness, and the steel MLC was 2.0 cm in thickness. Analysis of phase space fluence and energy spectra was performed using the BEAMDP software.<sup>20</sup> Based on fluence leakage profiles, 1.5 cm tungsten was selected as the optimal leaf thickness and material and used in the following sections.

### 2. Leaf width

Simulations were performed to examine the optimal leaf width. The overall width of the MLC and the number of

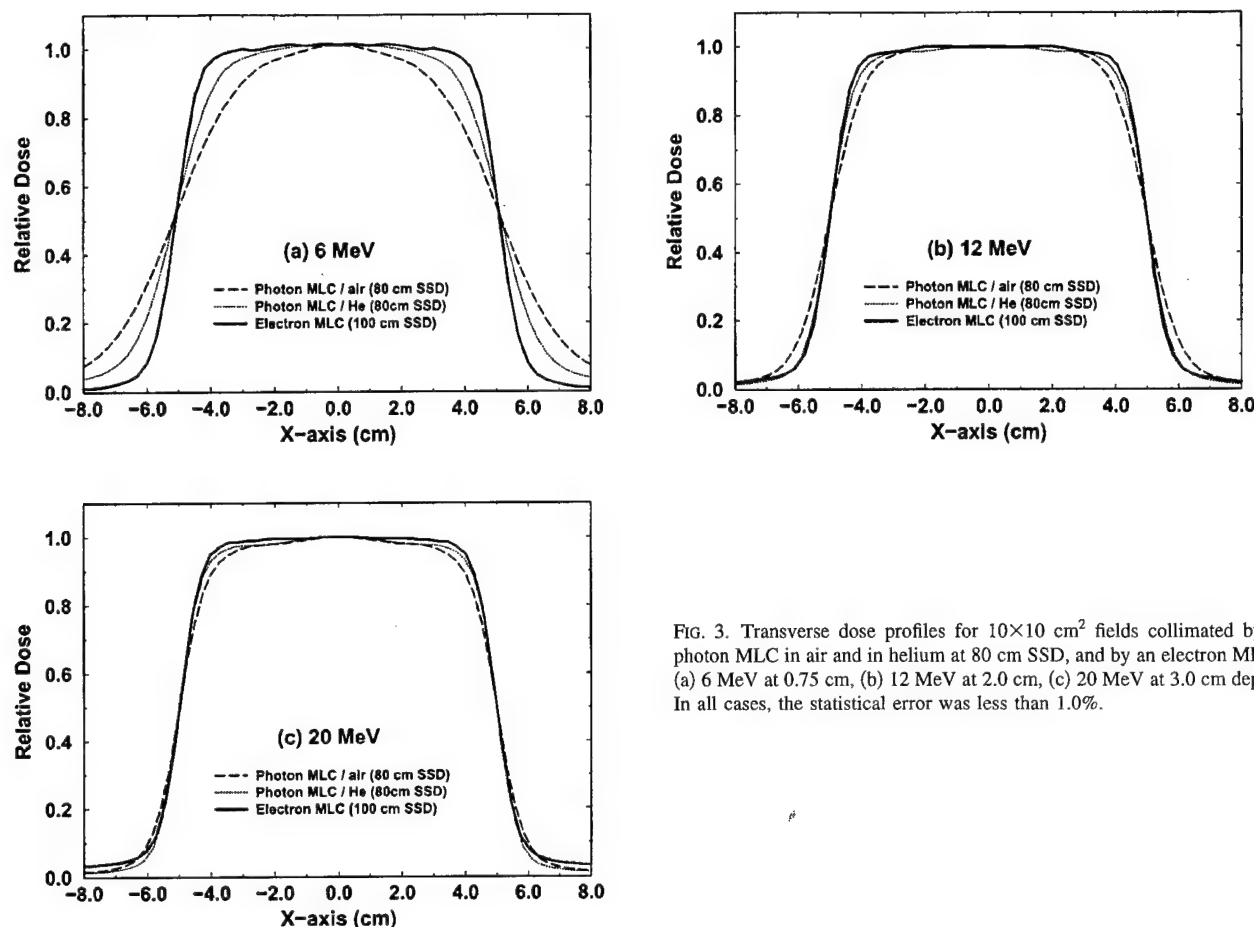


FIG. 3. Transverse dose profiles for  $10 \times 10$  cm<sup>2</sup> fields collimated by a photon MLC in air and in helium at 80 cm SSD, and by an electron MLC. (a) 6 MeV at 0.75 cm, (b) 12 MeV at 2.0 cm, (c) 20 MeV at 3.0 cm depth. In all cases, the statistical error was less than 1.0%.

leaves and their positions were adjusted so that a single leaf of varying width was inserted in the first off-axis position of a  $20 \times 20$  cm<sup>2</sup> field. Electron beams of 6 and 20 MeV electron beam were simulated through this collimator and the resulting phase space files were used for a dose calculation. The geometry for the dose calculation utilized  $2 \times 40 \times 2$  mm<sup>3</sup> in the region from  $x = -3$  cm to 3 cm, and  $5 \times 40 \times 2$  mm<sup>3</sup> in the remaining in-field region. Additionally, the same single leaf simulation was performed for a photon MLC based on the dimensions of the intrinsic MLC in the Varian Clinac 2100C.

### 3. Leaf end shape

Additional BEAM simulations were performed to examine the effect of leaf shape of the eMLC. Two simulations were performed at each of two energies, 6 and 20 MeV. In one case, the leaf ends and sides were focused to the photon target, and in the second case, the ends and sides of the 1.5 cm thick tungsten leaves were parallel to the beam axis. The phase space at 100 cm SSD was analyzed using BEAMDP and used for dose calculations.

### C. Prototype electron MLC

Based on the results of the theoretical study, a prototype of an eMLC was designed and built. A view of the prototype eMLC is shown in Fig. 2, and the design information is

summarized here. The MLC comprised two sets of 30 leaves, each leaf 2.54 cm (1") in thickness and 0.48 cm (3/16") in width. Both ends and sides were designed to be parallel with the beam axis, i.e., unfocused. Leaf positions could be set manually and allowed a maximum opening of  $14.2 \times 15.9$  cm<sup>2</sup> with complete leaf over run allowed. The MLC was designed to fit into the cutout mounting frame in the last scraper of a  $25 \times 25$  cm<sup>2</sup> applicator from a Varian Clinac 2100C linear accelerator.

The geometry of this prototype was simulated using the EGS4/BEAM simulation package and phase space files were obtained for a representative set of leaf positions shown in Fig. 11(d). A dose calculation was then performed using MCDOSE on a homogeneous water phantom composed of  $3 \times 3 \times 2$  mm<sup>3</sup> voxels.

The MLC was then installed onto the treatment head and film (Kodak X-omat V, Eastman Kodak Company, Rochester, NY) measurements were taken at the surface and at 2 cm depth in solid water. Measurements were taken at energies of 6, 12, 20 MeV at an SSD of 100 cm. The film was scanned using a Vidar scanning system and the RIT315 software package (Radiological Imaging Technology, Colorado Springs, CO) was then used to generate isodose distributions for comparison with the simulated dose results.

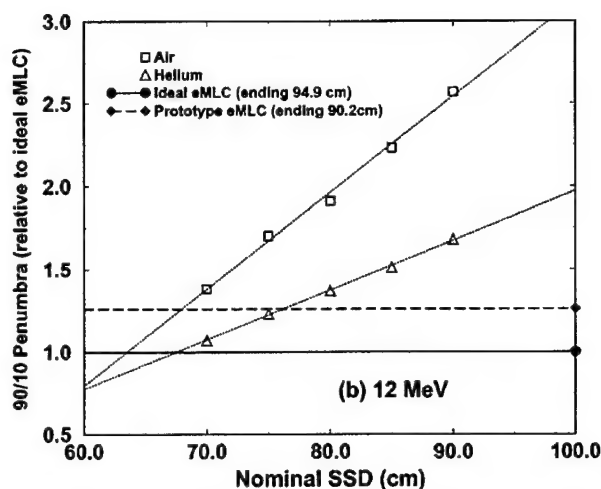
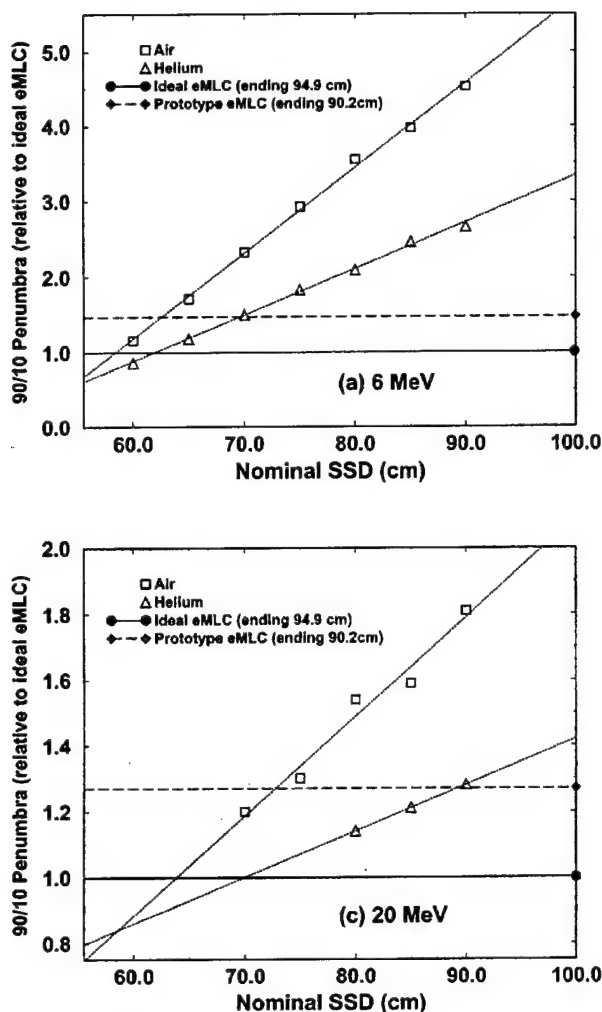


Fig. 4. Plot of 90–10 penumbra size as a function of SSD for  $10 \times 10$  cm<sup>2</sup> fields collimated by a photon MLC in air and in helium, the ideal electron MLC, and the prototype electron MLC. All data are normalized to the ideal electron MLC penumbra. (a) 6 MeV, (b) 12 MeV, (c) 20 MeV.

Additionally, a BEAM simulation and dose calculation were performed with the photon MLC in a helium atmosphere using these same leaf positions (projected).

### III. RESULTS AND DISCUSSION

#### A. Electron beams collimated with the photon MLC

Collimation of electron beams with a photon MLC was simulated by using the standard BEAM component module for the MLC, and the resulting phase space files used to calculate dose in a homogeneous water phantom. The 80–20 and 90–10 penumbras, defined by the lateral distance between isodose curves along the major axes, were computed and are displayed in Table I. As expected, at all energies, there is a substantial difference in the penumbra width between the helium gas systems and the normal air-filled treatment heads. For a 6 MeV beam at 80 cm SSD and a depth of 0.75 cm, the improvement in the 90–10 penumbra was 40.9%. However, as a consequence of reduced in-air scatter of high energy electrons, the effect was much less pronounced at higher energies: for a 20 MeV beam at 3.0 cm depth and 80 cm SSD, the 90–10 penumbra was reduced by 26.0%. Similar results in both beam penumbra reduction and

energy dependence are seen for the 80–20 penumbras. Representative profiles at 80 cm SSD are shown in Fig. 3. The changes in 90–10 penumbras can be seen in Fig. 4.

#### B. Design considerations for an electron MLC

In order to compare the photon MLC and the eMLC, it was necessary to develop a model of an ideal eMLC. Three key design parameters were investigated:

- (i) leaf material and thickness;
- (ii) leaf width;
- (iii) leaf end shape (focusing).

The effect of these parameters on dose distributions and electron and photon transmission were examined through Monte Carlo simulations of the treatment head and MLC and dose distributions calculated in homogeneous water phantoms.

##### 1. Leaf material and thickness

Preliminary studies were performed in which 20 MeV electrons were simulated through the treatment head and a  $25 \times 25$  cm<sup>2</sup> applicator, and incident upon proposed eMLC designs. The primary concern was leakage: though the leaves

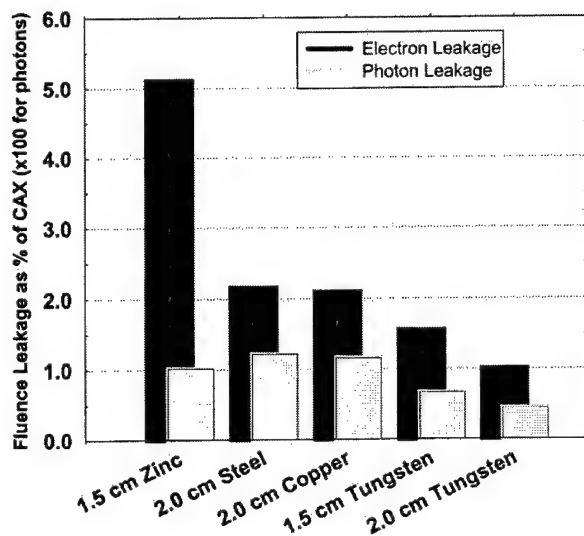


FIG. 5. Monte Carlo simulated fluence for electrons and photons for a 20 MeV electron field. Photon and electron leakage at a point 3 cm outside the field are shown, expressed as a percentage of central axis fluence. Note that for photons, the true value is the value shown  $\times 100$ .

themselves were thick enough to stop direct passage of all electrons, there was a concern regarding production of bremsstrahlung and secondary electrons, especially with regard to electrons interacting in the leaf ends and adding a contaminant dose in the penumbral region. To study this effect, the eMLC was set to define a  $10 \times 10$  cm<sup>2</sup> field within the  $25 \times 25$  cm<sup>2</sup> applicator and the electron and photon fluence studied using the BEAM system.

The electron leakage, scored 3 cm outside of the  $10 \times 10$  cm<sup>2</sup> field, is shown in Fig. 5. The 1.5 cm thick tungsten MLC exhibited a background electron leakage of 1.5% of the central axis fluence, while both the steel and copper models exhibited greater than 2.0% leakage. Additionally, by examining the profiles at the field edge, it was observed that tungsten leaves resulted in a steeper drop at the field edge, corresponding to a reduction in the passage of large angle electrons through the leaf ends. While increasing the tungsten leaf thickness to 2.0 cm reduces background electron fluence to less than 1% of the central axis fluence, this modest improvement may not sufficiently offset the added weight and the associated cost.

The production of bremsstrahlung photons by the interaction of high energy electrons in the leaves was also considered. As seen in Fig. 5, as expected on the basis of the material bremsstrahlung production cross sections, tungsten again exhibits the best fluence profile, presenting less than half the photon leakage of the copper or steel MLCs. The conjecture that both photon and electron leakage is almost entirely due to bremsstrahlung and not direct leakage was supported by the use of the BEAM code "latch bit" settings to track particle interactions, as seen in Fig. 6. As expected, 1.5 cm tungsten is sufficient to stop most incident photons, and these direct photons account for only 15% of the total leakage. Also, in Fig. 7 it can be seen that the energy of the

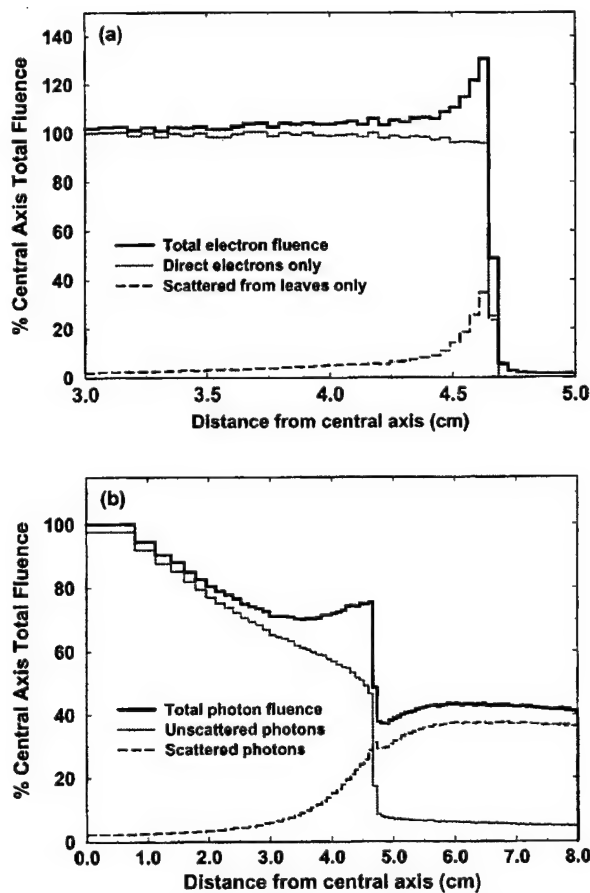


FIG. 6. Monte Carlo simulated (a) electron and (b) photon planar fluence at the edge of a  $10 \times 10$  cm<sup>2</sup> field collimated by a 1.5 cm thick tungsten MLC, separated into particles that interacted in the leaves, and those that did not. The fluence was scored at the back surface of the eMLC.

photons escaping the tungsten leaves is higher than that of the photons from the copper or steel leaves (5.3 MeV versus 4.3 MeV). The ordering of the energies is as expected based on the ordering of the effective atomic numbers of the materials. However, even though the photons are more energetic, the overall photon energy fluence from the tungsten leaves remains significantly below that of the other materials. Furthermore, contaminant photon dose generally scales with the cube of the incident electron energy.<sup>21</sup> As this simulation was performed with an initial electron energy of 20 MeV, it is expected that this photon dose effect will rapidly become trivial as the energy is reduced. Based on this information, the 1.5 cm thick tungsten leaf design was chosen as the model of what we hereafter refer to as the "ideal" eMLC.

## 2. Leaf width

Further Monte Carlo studies were performed to analyze the leaf width that provides the highest degree of resolution while optimizing the number of leaves so as to reduce inter-leaf leakage, mechanical complexity, and cost. A simulation was performed with a single leaf inserted into a  $20 \times 20$  cm<sup>2</sup> field. The dose profile at  $d_{\max}$  was examined and the mini-

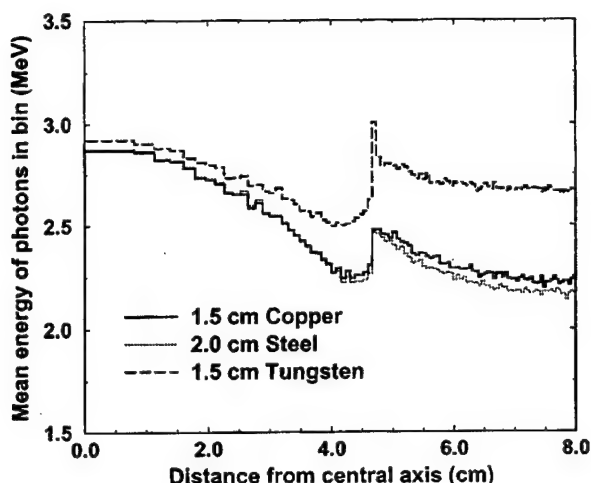


FIG. 7. Mean energy of photons in the presence of a copper, steel, and tungsten MLC set to a  $10 \times 10$  cm<sup>2</sup> field with an incident electron energy of 20 MeV. The energy was scored at the back surface of the eMLC.

imum of the resulting dose “valley” was considered. As seen in Fig. 8 and Table II, the dose reduction as a function of leaf width can be well approximated by a decaying exponential. Using the “worst-case scenario,” an energy of 6 MeV, it was found that a leaf width of 8.8 mm projected to 100 cm SSD, or 8.6 mm at the level of the MLC, would produce a dose reduction of 50%. As expected, the leaf width corresponding to a 50% reduction for the high energy 20 MeV beam was much smaller, and a dose reduction of 50% could be achieved by a leaf width of 4.9 mm projected, or 4.8 mm at the MLC.

Additionally, the full width of the region where the dose was less than 50% and the full width of the region where the dose was less than 75% are displayed in Table II. At 20

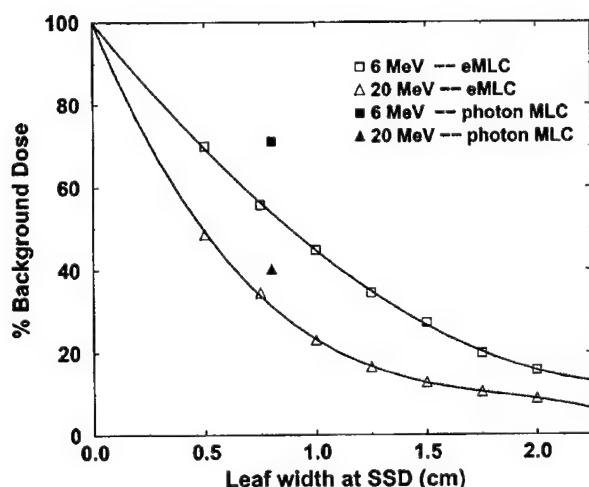


FIG. 8. Dose reduction as a function of leaf width. A Monte Carlo simulation was performed in which a single leaf was inserted a  $20 \times 20$  cm<sup>2</sup> field and dose profiles computed. The plotted points represented the dose minimum as a percentage of background dose for various leaf widths. The two solid points represent the leaves of the intrinsic MLC of a Varian Clinac 2100C at 6 and 20 MeV at 80 cm SSD.

TABLE II. Achievable resolution for a (a) 6 MeV field at  $d_{\max}$ . Parameters from simulated single leaf dose profiles at  $d_{\max}$ . A single leaf of a given width was entered into a  $20 \times 20$  cm<sup>2</sup> 6 MeV field generated by an idealized electron MLC. (b) Achievable resolution for a 20 MeV field at  $d_{\max}$ . \* indicates that this dose was not passed, i.e., the dose reduction from a single leaf was less than 50% of the background dose.

		Width at % background dose	
Projected width at SSD (cm)	Dose at minimum (% background)	75% dose (cm)	50% dose (cm)
(a) 6 MeV			
0.50	70.0	0.77	*
0.75	55.7	1.49	*
1.00	44.8	1.88	0.60
1.25	34.5	2.08	1.16
1.50	27.3	2.48	1.45
1.75	19.9	2.81	1.81
2.00	15.7	3.02	2.04
Varian MLC 0.80 cm at 80 cm SSD (with He)	71.0	1.11	*
(b) 20 MeV			
0.50	48.6	0.87	0.08
0.75	34.5	1.22	0.67
1.00	23.1	1.50	0.96
1.25	16.5	1.75	1.19
1.50	12.8	2.05	1.52
1.75	10.5	2.31	1.79
2.00	8.9	2.54	2.04
Varian MLC 0.80 cm at 80 cm SSD (with He)	40.3	1.44	0.67

MeV, it is seen that at an eMLC leaf width of 1 cm, the 50% full width is approximately equal to the leaf width. A similar trend is noted beyond the 1.25 cm leaf width at 6 MeV.

Based on these findings, we conclude that a leaf width of less than 10 mm at 100 cm SSD is not useful for defining the shape of a low energy field, and leaves of less than 5 mm are not useful for defining the field shape at any energies. In order to provide maximum utility at both high and low energies, a 5 mm leaf width was chosen as the ideal leaf width for the eMLC. Individual leaves can then be used at high energies to provide maximum resolution, while multiple leaves may be moved together to define fields at lower energies.

For comparison, identical simulations were performed to simulate the leaves of a Varian 52-leaf multileaf collimator, with a leaf width projected at isocenter of 10 mm, using a helium filled accelerator (and air gap) at 80 cm nominal SSD. The results are also shown in Fig. 8 and Table II. It can be seen in Fig. 8 that at 20 MeV, the eMLC and photon MLC the difference in dose reduction for a projected leaf width of 8 mm is only 5%. However, at 6 MeV, a significant difference can be observed between the eMLC and Varian MLC systems, and it can be seen that for a given projected leaf width, the eMLC provides a superior level of resolution.

### 3. Leaf end shape

In contrast with observed results regarding photon MLC leaf shapes, simulations performed in this study demon-

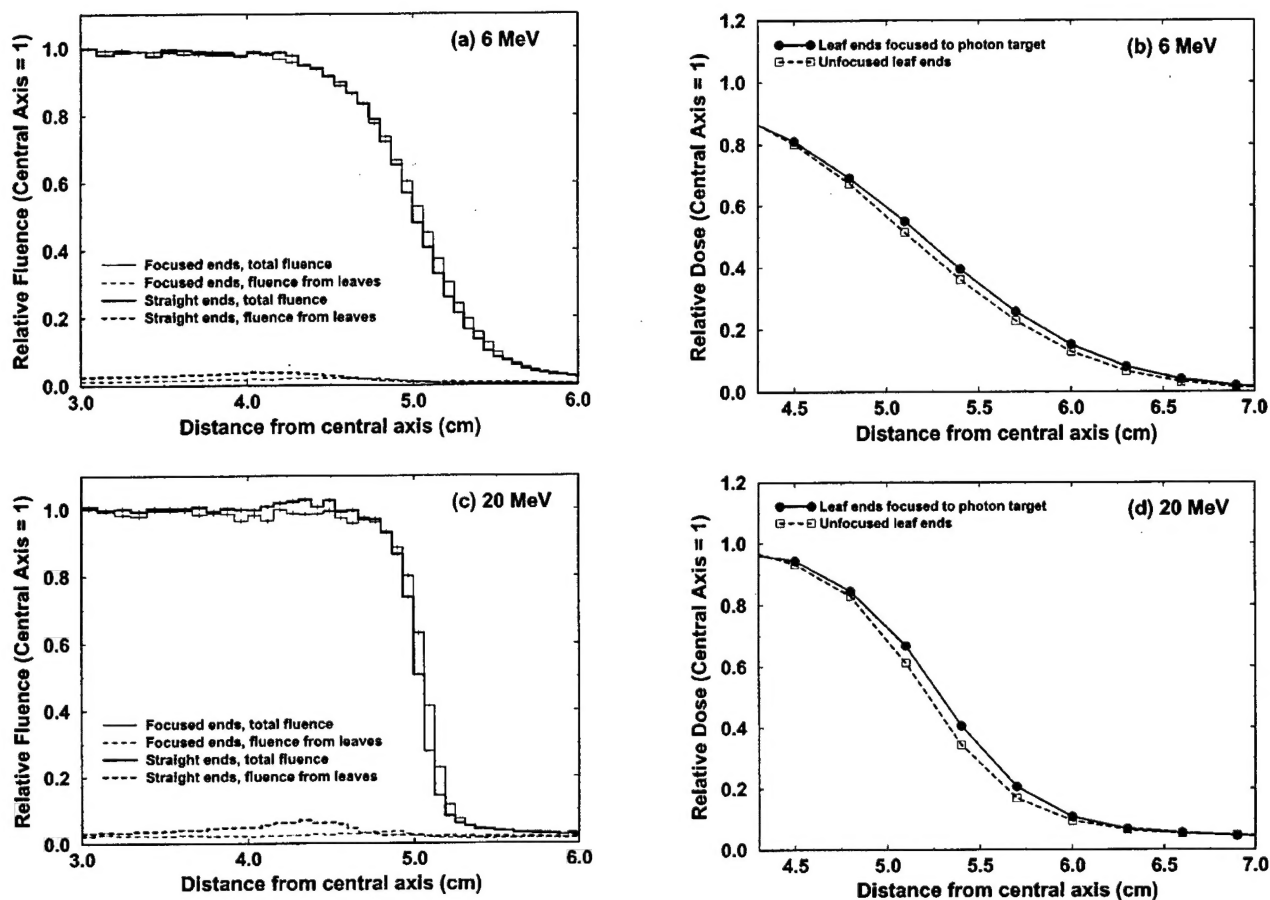


FIG. 9. Effect of leaf end shape on electron fluence and dose distribution. (a) 6 MeV fluence, (b) corresponding 6 MeV dose at 1 cm depth, (c) 20 MeV fluence, (d) corresponding 20 MeV dose at 3 cm depth. Latch bit settings were used to separate the 100 cm SSD fluence into the total fluence and fluence from electrons scattered from the leaves.

strated that focused leaf ends did not provide any benefit at all at either high or low energies. Indeed, unfocused leaf ends provided a "horn" effect at the edge of the fields which actually improved beam penumbras, as seen in Fig. 9. This eliminates the additional complexity required focusing, as well as the issue of choosing a focal point that would be useful for a range of electron energies.

### C. Prototype electron MLC: Measurements and Monte Carlo simulations

Based on previous experiences, it was believed that Monte Carlo calculations could accurately calculate the dose distributions from the MLC, and that the Monte Carlo method could be used for MERT calculations. However, it was necessary to demonstrate that the Monte Carlo method remains valid for the more complex geometry of the eMLC. Monte Carlo simulations were used to generate isodose curves for fields collimated by the prototype eMLC and compared with film measurements taken using the actual prototype installed on an accelerator located at the Stanford University Medical Center. Isodose curves for the measured and Monte Carlo 20 MeV fields normalized to the in-plane maximum at 3 cm depth in solid water are displayed in Fig. 10. The agreement between the measured and simulated data is

excellent at all energies, with deviations falling within 2 mm at 3 cm depth for 12 and 20 MeV and 1.5 cm depth for 6 MeV. It is therefore concluded that the Monte Carlo method is capable of simulating the isodose distribution from an eMLC in homogeneous media.

### D. Comparison of electron MLC and photon MLC

Having established a computer model of the eMLC and verified the validity of the model using film measurements and a prototype eMLC, it was possible to compare the dose distributions from the eMLC and the photon MLC.

#### 1. Penumbra comparison

Calculations were performed to compare the dose penumbras from  $10 \times 10$  cm<sup>2</sup> fields collimated by the eMLC to those from the photon MLC. As shown in Table I and Figs. 4 and 5, even when compared to a photon MLC in the presence of helium, using the ideal eMLC results in reductions in the  $10 \times 10$  cm<sup>2</sup> 90–10 penumbra ranging from 12.1% at 20 MeV to as much as 44.6% at 6 MeV. However, the absolute change from 20 MeV was only 2 mm. Extrapolating from the existing data points, one can calculate the SSD required for the penumbra from the photon MLC to match the eMLC, as

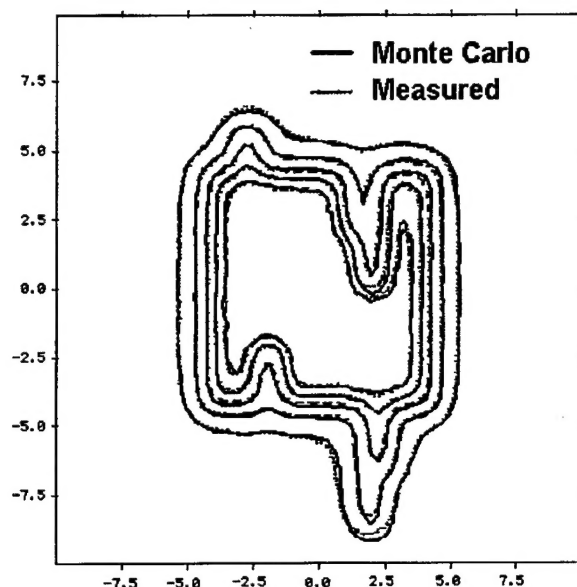


FIG. 10. Isodose curves for an arbitrary leaf pattern at 20 MeV, normalized to in-plane maximum. The plane displayed is orthogonal to the incident beam direction (beam eye view). The curves represent the 90%, 80%, 60%, 30%, and 10% isodose surfaces at a depth of 3 cm. The solid line represents the Monte Carlo results while the broken line represents the film measurements. With only a few small regions as exceptions, the two sets of curves are indistinguishable.

shown in Table III. It was determined that the required SSDs to match at 90–10 for 6, 12, and 20 MeV are, respectively, 65.5, 68.0, 69.8 cm. In a standard air atmosphere, the required SSDs are all less than 65 cm, which is clearly unachievable in any practical system. However, it was observed that at 80 cm SSD in the presence of helium, the photon MLC provided a sharper penumbra than the prototype eMLC at 20 MeV. Extrapolating from the helium penumbra data, it can be seen that at 6, 12, and 20 MeV, the required SSD to match the *prototype* eMLC are 68.5, 76.6, and 89.3 cm.

When comparing the photon and eMLC, it is crucial to note the difference in leakage dose. From Figs. 3(a), 3(b), and 3(c), it can be seen that at 6 and 12 MeV, the two MLCs provide comparable background doses, with the difference at 12 MeV representing less than 1% of the central axis dose.

TABLE III. SSDs required for a photon MLC to match the ideal electron MLC and the prototype electron MLC. These calculations are based on a linear interpolation of the penumbra data shown in Table I and Fig. 4.

Energy (MeV)	eMLC	SSD required for photon MLC to match electron MLC penumbras (cm)			
		Air		Helium	
		80/20	90/10	80/20	90/10
6	ideal	59	58	61	61
	prototype	63	62	69	69
12	ideal	65	64	68	68
	prototype	68	68	74	77
20	ideal	64	64	70	70
	prototype	70	73	82	89

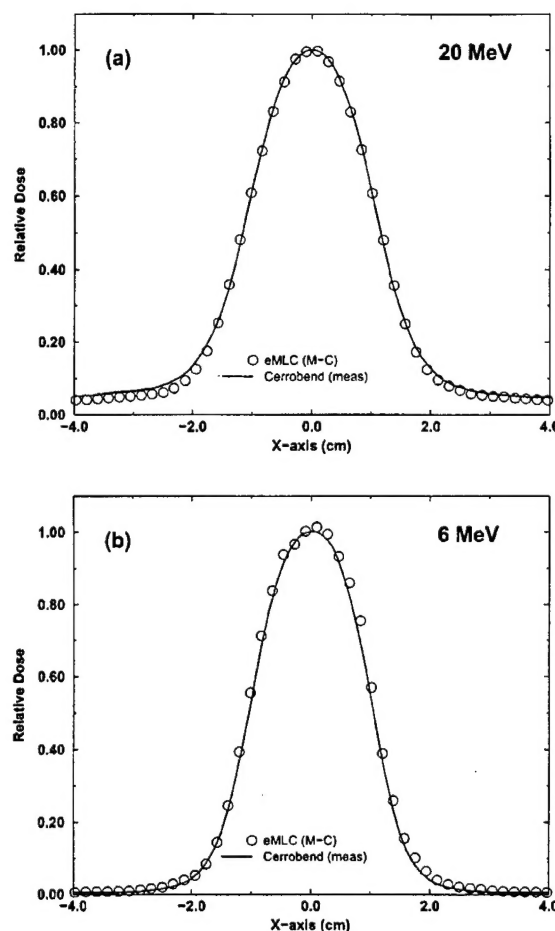


FIG. 11. Profiles obtained for  $2 \times 2$  cm<sup>2</sup> fields defined by Cerrobend cutouts and by the electron MLC. (a) 20 MeV at 4 cm depth, (b) 6 MeV at 1 cm depth.

However, at 20 MeV, the leakage from the significantly thinner eMLC is more than twice that from the photon MLC (approximately 2%). This leakage dose still compares favorably to the 5% leakage seen at 20 MeV with 1.5 cm of Cerrobend cutout mounted in the  $25 \times 25$  cm<sup>2</sup> scraper. However, it is imperative that any MERT treatment planning system using an eMLC account for this leakage dose and reduce the number of monitor units to be delivered.

For comparison with a well-understood system, simulations of a  $2 \times 2$  cm<sup>2</sup> field defined by the ideal eMLC were performed and the dose distributions compared with measured profiles for a  $2 \times 2$  cm<sup>2</sup> Cerrobend field in a  $6 \times 6$  cm<sup>2</sup> applicator. Because the collimators are positioned identically with respect to the phantom surface, the penumbras were identical, as seen in Fig. 11. The leakage at 6 MeV was negligible in both the cutout and the eMLC, while the leakage at 20 MeV was greater in the case of the cutout. The same result was found for other field sizes, and similarly, using the photon MLC to define electron fields compares equally unfavorably with both cutouts and the electron specific MLC.

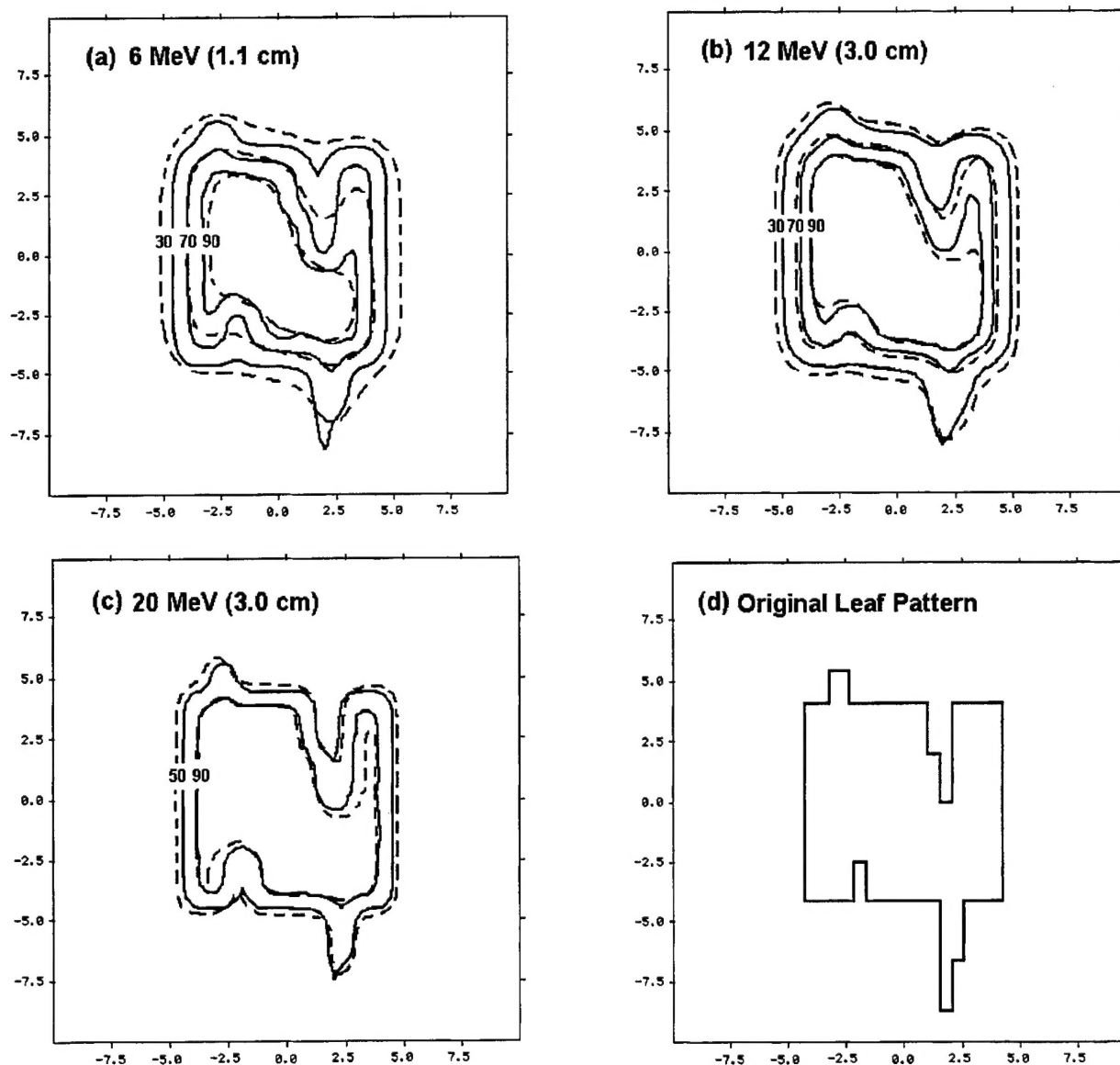


FIG. 12. Isodose curves for an arbitrary leaf pattern. Solid lines represent a 1.5 cm thick tungsten electron MLC at the last scraper level and dashed lines represent a photon MLC in the presence of helium at 80 cm SSD. (a) 6 MeV at 1.1 cm, (b) 12 MeV at 3.0 cm, (c) 20 MeV at 3.0 cm, (d) original leaf pattern, projected to the phantom surface.

## 2. Isodose curve comparison

In Fig. 12, the Monte Carlo simulated isodose curves for an electron field collimated by an idealized eMLC and an equivalent field collimated by a photon MLC with He are shown. The original leaf pattern is displayed in Fig. 12(d). In all cases, the fields were normalized such that the 90% isodose curves coincided for the open field portion ( $y = -1.0$  cm), effectively “prescribing dose to an isodose curve.” In all cases, the penumbras differed according to the trends described earlier: in particular, when 90% isodose curves are matched, the photon MLC collimated field exhibited 30% and 70% dose regions that were uniformly larger than those from the eMLC. More significant, however, is the ability to resolve narrow fields. In particular, focusing on the upper right portion of the fields, as displayed, it can be seen

that at both 6 and 12 MeV, the photon MLC is unable to fully resolve either the partially closed leaves or the open leaves at upper-right most corner. A much smaller but visible effect is observed at 20 MeV.

Based on these results, it is therefore concluded that at all energies, the eMLC is more faithful to the original leaf pattern than the photon MLC. However, as predicted by the leaf width simulations, even with the eMLC, leaf widths of less than 1 cm do not result in any appreciable improvement in resolution, especially at low energies.

Simulations were also performed with the photon MLC in air, and with the prototype eMLC. In all cases, the photon MLC in air performed worse in terms of resolution and penumbra when compared to the helium MLC, and likewise with the prototype when compared to the idealized eMLC.

#### IV. CONCLUSIONS

It has been demonstrated through the use of Monte Carlo simulations that the in-air scattering of the electron beam makes the photon MLC a poor choice for generating complex shapes needed for intensity modulated electron therapy. This is partially ameliorated by filling the treatment head with helium and placing a helium filled balloon between the patient surface and the treatment head. Indeed, for such a system, at 12 and 20 MeV at an SSD of 80 cm, the isodose curves are within 3 mm of the equivalent eMLC field. If accurate commissioning data is available for these helium-filled accelerator and accurate dose calculation algorithms are employed, it is believed that highly accurate MERT plans can be delivered and the quality of treatment will not differ significantly from an eMLC delivered plan. However, at 6 MeV the isodose curves are no longer comparable, and adding helium to the beam axis atmosphere does not improve the situation.

An electron specific multileaf collimator placed at the cut-out level of an electron applicator was then studied. Monte Carlo simulations were used to investigate construction and design considerations and on the basis of these simulations, it was concluded that an eMLC constructed of tungsten leaves of 15 mm thickness and 5 mm width, would be minimally sufficient for use in intensity modulated electron beam therapy. This MLC would optimally be part of a specially designed electron applicator, although experiments have indicated that an MLC designed as an applicator accessory also provides significant improvement in dose penumbras and field resolution when compared to the photon MLC. Additionally, it has been demonstrated that Monte Carlo simulations provide an accurate means of calculating dose distributions from such a collimation system.

#### ACKNOWLEDGMENTS

We thank our colleagues at Stanford: Art Boyer, Gary Luxton, Todd Pawlicki, Jun Deng, and Jinsheng Li, for helpful discussions of this work, and Professor Byong-yong Yi of Asan Medical Center, University of Ulsan, College of Medicine in Seoul, Korea for discussions regarding the prototype electron MLC. This work was supported in part by Grants Nos. BC971292 and BC990213 from the US Department of Defense, CA 78331 from the NIH, and the NIH Training Grant No. 5T32GM08294-11.

<sup>a)</sup> Author to whom correspondence should be addressed: Department of Radiation Oncology, 300 Pasteur Drive, Stanford, CA 94305-5304. Electronic mail: mclee@reyes.stanford.edu

<sup>1</sup> E. P. Lief, A. Larsson, and J. L. Humm, "Electron dose profile shaping by modulation of a scanning elementary beam," *Med. Phys.* **23**, 33-44 (1996).

<sup>2</sup> S. Hyödynmaa, A. Gustafsson, and A. Brahme, "Optimization of conformal electron beam therapy using energy- and fluence-modulated beams," *Med. Phys.* **23**, 659-666 (1996).

<sup>3</sup> B. Zackrisson and M. Karlsson, "Matching of electron beams for con-

formal therapy of target volumes at moderate depths," *Radiother. Oncol.* **39**, 261-270 (1996).

<sup>4</sup> M. Åsel, S. Hyödynmaa, A. Gustafsson, and A. Brahme, "Optimization of 3D conformal electron beam therapy in inhomogeneous media by concomitant fluence and energy modulation," *Phys. Med. Biol.* **42**, 2083-2100 (1997).

<sup>5</sup> M. K. Karlsson, M. G. Karlsson, and B. Zackrisson, "Intensity modulation with electrons: calculations, measurements and clinical applications," *Phys. Med. Biol.* **43**, 1159-1169 (1998).

<sup>6</sup> M. G. Karlsson, M. K. Karlsson, and C.-M. Ma, "Treatment head design for multileaf collimated high-energy electrons," *Med. Phys.* **26**, 2125-2132 (1999).

<sup>7</sup> C.-M. Ma, T. Pawlicki, M. C. Lee, S. B. Jiang, J. Li, J. Deng, B. Yi, E. Mok, G. Luxton, and A. L. Boyer, "Energy- and intensity-modulated electron beams for radiotherapy," *Phys. Med. Biol.* **45**, 2293-2311 (2000).

<sup>8</sup> A. Brahme, "Design principles and clinical possibilities with a new generation of radiation therapy equipment," *Acta Oncol.* **26**, 403-412 (1987).

<sup>9</sup> T. Jansson, H. Lindman, K. Nygård, C. V. Dahlgren, A. Montelius, S. Öberg-Kreuger, S. Asplund, and J. Berg, "Radiotherapy of breast cancer after breast-conserving surgery: an improved technique using mixed electron-photon beams with a multileaf collimator," *Radiother. Oncol.* **46**, 83-89 (1997).

<sup>10</sup> E. E. Klein, Z. Li, and D. A. Low, "Feasibility study of multileaf collimated electrons with a scattering foil based accelerator," *Radiother. Oncol.* **46**, 189-196 (1996).

<sup>11</sup> K. R. Hogstrom, M. D. Mills, and P. R. Almond, "Electron beam dose calculations," *Phys. Med. Biol.* **26**, 445-459 (1981).

<sup>12</sup> A. F. Bielajew, D. W. O. Rogers, J. Cygler, and J. J. Battista, "A comparison of electron pencil beam and Monte Carlo calculational methods," in *The Use of Computers in Radiation Therapy*, edited by I. A. D. Bruinvis *et al.* (Elsevier Science, New York, 1987), pp. 65-68.

<sup>13</sup> T. R. Mackie, P. J. Reckwerdt, C. M. Wells, J. N. Yang, J. O. Deasy, M. Podgorsak, M. A. Holmes, D. W. O. Rogers, G. X. Ding, B. A. Faddegon, C.-M. Ma, A. F. Bielajew, and J. Cygler, "The OMEGA project: comparison among EGS4 electron beam simulations, 3D Fermi-Eyges calculations, and dose measurements," *Proceedings of the XIth International Conference on the use of Computers in Radiation Therapy, Manchester, UK* (Medical Physics Publishing, Madison, 1994), pp. 152 and 153.

<sup>14</sup> C.-M. Ma, E. Mok, A. Kapur, T. Pawlicki, D. Findley, S. Brain, K. Forster, and A. L. Boyer, "Clinical implementation of a Monte Carlo treatment planning system for radiotherapy," *Med. Phys.* **26**, 2133-2143 (1999).

<sup>15</sup> W. R. Nelson, H. Hirayama, and D. W. O. Rogers, "The EGS4 Code System," SLAC-Report-265, Stanford Linear Accelerator Center, 1985.

<sup>16</sup> D. W. O. Rogers, B. A. Faddegon, G. X. Ding, C.-M. Ma, J. Wei, and T. R. Mackie, "BEAM: A Monte Carlo code to simulated radiotherapy treatment units," *Med. Phys.* **22**, 503-524 (1995).

<sup>17</sup> C.-M. Ma, J. S. Li, T. Pawlicki, S. B. Jiang, and J. Deng, "MCDOSE—A Monte Carlo dose calculation tool for radiation therapy treatment planning," *Proceedings of the XIII International Conference on the Use of Computers in Radiotherapy*, edited by W. Schlegel and T. Bortfeld (Springer, Heidelberg, Germany), pp. 123-125.

<sup>18</sup> A. Kapur, C.-M. Ma, E. Mok, D. Findley, and A. L. Boyer, "Monte Carlo calculations of clinical electron beam output factors," *Phys. Med. Biol.* **44**, 3479-3494 (1998).

<sup>19</sup> A. Bielajew and D. W. O. Rogers, "PRESTA—the parameter reduced electron step algorithm for electron Monte Carlo transport," *Nucl. Instrum. Methods Phys. Res. B* **18**, 165-181 (1987).

<sup>20</sup> C.-M. Ma and D. W. O. Rogers, "BEAMDP Users Manual," National Research Council Report No. PIRS-0509(C), NRC, Ottawa, Canada 1995.

<sup>21</sup> ICRU Report No. 35, "Radiation dosimetry: Electron beams with energies between 1 and 50 MeV," Bethesda, 1984.